Topological analysis of the metal-metal bond: A tutorial review

Christine Lepetit, Pierre Fau, Katia Fajerwerg, Myrtil L. Kahn, Bernard Silvi

Topological analysis of the metal-metal bond: a tutorial review

Christine Lepetit[a,b], Pierre Fau[a,b], Katia Fajerwerg[a,b], Myrtil L. Kahn[a,b], Bernard Silvi[c,*]

[a] *CNRS, LCC (Laboratoire de Chimie de Coordination), 205, route de Narbonne, BP 44099, F-31077 Toulouse Cedex 4, France.*
[b] *Université de Toulouse, UPS, INPT, F-31077 Toulouse Cedex 4, i France*
[c] *Sorbonne Universités, UPMC, Univ Paris 06, UMR 7616, Laboratoire de Chimie Théorique, case courrier 137, 4 place Jussieu, F-75005 Paris, France*

Abstract

This contribution explains how the topological methods of analysis of the electron density and related functions such as the electron localization function (ELF) and the electron localizability indicator (ELI-D) enable the theoretical characterization of various metal-metal (M-M) bonds (multiple M-M bonds, dative M-M bonds). Examples are taken in both bulk metals, alloys and molecular complexes. Metallic bonds as well as weak partially covalent M-M interactions, are described and characterized unambiguously combining AIM (atoms in molecules) and ELF/ELI-D topological analysis.

Keywords: Electron Density, Chemical Bonding, Topological Analysis, Quantum Theory of Atoms in Molecules, Electron Localization Function, Electron localizability indicator, Source Function, Metal-metal bond.

Contents

*Corresponding author
Email address: christine.lepetit@lcc-toulouse.fr (Christine Lepetit)

1. Introduction

Among the 88 metallic elements, 20 belong to the main groups, 40 to the transition periods, 14 to the lanthanides and 14 to the actinides offering a potentially large panel of metal-metal (M-M) bonding situations. M-M bonding is encountered in a wide variety of molecular compounds or crystalline systems such as bulk metals, alloys, superconducting materials, Zintl-Klemm phases. Although compounds featuring M-M bonds are known for many decades, the chemistry of M-M bonds is still a hot topic as attested by several reviews dedicated to recent advances in both main group and transition element chemistry [1–5]. Compounds with homometallic or heterometallic extended metal atom chains (EMACs) are considered as potential molecular wires [3, 6, 7].

For a given metal, the M-M interatomic distance can be modulated by a suitable choice of the number and the nature of the ligands which implies specific synthesis approaches. The evidence by X-ray crystallography of a very short Re-Re distance in the $[ReCl_8]^{2-}$ dianion [5, 8, 9] identified later as a quadruple bond [10] is a significant landmark in inorganic chemistry. It opened the way of a rich chemistry of multiple M-M bonding in bimetallic complexes[8–10] as illustrated by the Cr-Cr distances ranging from 1.7056 Å[11] to 2.498 Å in the bulk metal and even to 2.612 Å[12]. The wealth and diversity of M-M bonding across the transition element series has no equivalent in rare-earth metals, but recent compounds involving heavy main group elements such as Sn, Pb, Sb or Bi complexes [13–15] challenges the long-held assumption that multiple bonds are stable only between first-row elements.

The interpretation of the bonding requires at least pieces of information concerning the geometry, the charge density, the spin state of the metallic centres and the curvature of the energy hypersurface at the equilibrium. These data can be either obtained by experimental techniques such as single-crystal X-Ray Diffraction (XRD), X-Ray photoelectron spectroscopy (XPS), vibrational, Nuclear Magnetic Resonance (NMR), Electron Spin Resonance (ESR), Electron spectroscopy for chemical analysis (ESCA), electronic spectroscopies [12, 16] or by quantum mechanical calculations. Which are the pieces of information available by experiment?

1. M-M distance from XRD analysis;
2. Electron density maps: X-ray scattering, incorrectly termed as “experimental densities” fit of promolecular density;
3. Number of interacting metal atoms from NMR coupling constants or ESR hyperfine structures;

4. Bond strength from Raman M-M force constants, from $\delta \rightarrow \delta^*$ electronic transitions or from X-ray photoelectron spectroscopy XPS (δ bond only [17]);

5. Oxidation state from NMR and XPS [18, 19] or from electrochemical measurements;

6. Enhanced photoluminescence because of LMMCT excited states (electronic spectroscopy).

Molecular M-M bonding is primarily characterized by the intermetallic distance in the crystal structure. A M-M interaction is anticipated when the intermetallic distance is shorter than the sum of van der Waals radii (and comparable to the sum of covalent radii) of the metal atoms. Pt(II)-Pt(II) bonding was indeed assumed in switchable platinum tweezers on the basis of intermolecular Pt-Pt distances of 3.21 Å shorter than twice the van der Waals radii of Pt, namely 3.44 Å (covalent radii of Pt 1.4 Å) [20]. The intermetallic distance criterion should however be taken with care, because molecular charge, bridging ligands, symmetry or crystal packing forces may significantly influence the M-M contacts and rule out any quantitative relationship between the M-M distance and bond strength [21].

Besides short intermetallic distances, M-M bonding exhibit unique spectroscopic signatures. Nuclear Magnetic Resonance signatures of M-M bonding are:

1. A downfield shift of the NMR signal of either the metal nuclei or a proximal nuclei of the ligands with non-zero nuclear spin, that are strongly affected by the M-M bonding [22]. A strongly deshielded resonance of δ = 1142.3 ppm in the ^{199}Hg NMR spectrum was assigned to the $[Hg{-}Hg]^{2+}$ unit [22, 23]. ^{1}H NMR chemical shift of methylene protons by as much as 3.5 ppm was reported in $d^{10}{-}d^{10}$ bimetallics [21].

2. Large ^{1}J(M,M) or ^{1}J(M,^{13}C) coupling constants. In a trinuclear silver-carbene complex with three short Ag–Ag distances (av. 2.724 Å), the ^{13}C NMR signal for the carbon atoms of the N-heterocyclic carbene ligand shows all the expected $^{1}J(^{107,109}\mathrm{Ag},^{13}\mathrm{C})$ couplings which are compatible with significant interactions between the three silver atoms [24].

3. Electron Spin Resonance may be used for open-shell polymetallic complexes: the intramolecular antiferromagnetic coupling of two Cu(II) centres was evidenced by the characteristic half-field ESR signal [25]. The number of bonded metal atoms may be also evidenced through the hyperfine structure of the ESR signal of the radical formed upon oxidation of the polynuclear complex [21, 26].

4. M-M bond strength from infrared and Raman spectroscopy: although difficult to detect, the low frequency Raman M-M stretching and corresponding force constant may be used to estimate the M-M bond strength. Aurophilic interactions have been therefore reported significantly stronger (ν(Au-Au) = 88 cm^{-1}, force constan f = 0.449 mdyn Å^{-1}) than argentophilic interactions in cyclic diphosphine dinuclear dicationic complexes of comparable M-M distance (ν(Ag-Ag) = 80 cm^{-1}, force constant f = 0.203 mdyn Å^{-1}) [16])

5. M-M bonding studies using electronic spectroscopy: in tetrathiomolybdatorhodium(I) monoanionic complexes, the maximum absorption band was found to involve a charge transfer ν(Rh→Mo) electronic transition, the wavelength of which correlates linearly both with Tolman's electronic parameter of the phosphite ligands and the calculated HOMO-LUMO gap of the complexes [27]. The red-shifted photoluminescence observed in bi- and polynuclear silver complexes was assigned to Ligand to Metal Charge transfer (LMCT) emissions perturbed by the short Ag-Ag contacts (LMMCT electronic transitions) [16]. Delta-bonding electrons should manifest a $\delta \rightarrow \delta^*$ transitions, which can indirectly probe the M-M bond strength [28]. For example $\delta^2 \rightarrow \delta\delta^*$ transitions in quadruply bonded complexes are well-known, but reports of $\delta^4 \rightarrow \delta^3\delta^*$ transitions in quintuply bonded species are missing [21]. Upon oxidation of the polynuclear complex, a mixed-valence complex may be formed. Depending on the strength of the coupling of the metal centres, an intervalence charge transfer absorption band in the near-infrared range, signature of the class of the mixed-valence complex may be observed [26].

The bonding between two or more metallic elements is described in physics and in chemistry by several simple models. Bulk metals and alloys are currently explained by the band structure theory and implies the closure of the energetic gap between the valence and conduction bands [29, 30]. This combined energetic-orbital picture is related to the reciprocal space representation of the crystal. In the absence of a direct space representation, the metallic bond is rather difficult to include in any general chemical theory of the bonding. For example, G. N. Lewis has not considered

the metallic bond in his classical textbook [31] while Pauling describes it as a partial covalent bond between nearest neighbour atomic centres [32]. This covalent description has been more recently advocated by Anderson *et al*. [33] and by L. C. Allen and J. Capitani [34] in order to remove the metallic bond from the vocabulary of Chemistry. The simplest model, the jellium model, describes a bulk metal or alloy as a periodic array of positively charged ions embedded in a uniform homogeneous gas. The interstitial-electron model (IEM) has been developed in the generalized-valence-bond method by Mo and Goddard [35] for lattice dynamics in close-packed structures which considers orbitals centred in the tetrahedral site at equilibrium, but able to shift position adiabatically under lattice vibrations.

The bonding in molecular polymetallic complexes is usually interpreted in the framework of the Molecular Orbital (MO) theory. A very detailed survey has been written by Mc Grady [36]. In addition to standard σ and π bonds, δ bonds have to be considered in the case of transition metals [37] as well as ϕ-OMs for lanthanides and actinides. The MO analysis provides bond orders which can formally reach 6 for an approximate single determinant wave function but which are lowered when a more accurate description of the bond, using a bonding orbital and its anti-bonding counterpart, is considered [38].

An example of application of MO analysis may be found in the report about the mixed-valence tri-Zinc complex, [LZnZnZnL] (L = bulky amide) bearing a linear chain of two-coordinate zinc atoms [39]. NBO and NPA analyses of the compounds revealed that their Zn-Zn bonds have a significant covalent Zn-Zn σ-bonding character (Wiberg bond index of the Zn-Zn σ-bonding WBO = 0.68).

M-M bonds may be first classified into supported or unsupported interactions depending on the absence or presence of a bridging ligand between the metal atoms [36].

Table 1: Formal bond orders and electronic configuration of the M-M bond resulting from two interacting metal centres in D_{4h} symmetry.

Interaction type	Formal bond order	Electronic configuration
$d^1 - d^1$	Single bond	σ^2
$d^2 - d^2$	Double bond	$\sigma^2\pi^2$
$d^3 - d^3$	Triple bond	$\sigma^2\pi^4$
$d^4 - d^4$	Quadruple bond	$\sigma^2\pi^4\delta^2$
$d^5 - d^5$	Triple bond	$\sigma^2\pi^4\delta^2\delta^{*2}$
$d^6 - d^6$	Double bond	$\sigma^2\pi^4\delta^2\delta^{*2}\pi^{*2}$
$d^7 - d^7$	Single bond	$\sigma^2\pi^4\delta^2\delta^{*2}\pi^{*4}$
$d^8 - d^8$	No-bond	$\sigma^2\pi^4\delta^2\delta^{*2}\pi^{*4}\sigma^{*2}$

In molecular systems, three classes of M-M bonding may be further derived from an orbital diagram restricted to *d* orbitals interactions and electron countings in a square-planar ligand field. as shown by Figure 1:

– *Covalent multiple M-M bonding.* It is the most common type of M-M bonding. Formal bond orders up to four may be derived by filling the *d* orbitals with one electron coming from each metal centre (Table 1). The quadruple M-M bond related to a $\sigma^2\pi^4\delta^2$ electronic configuration is obtained for the optimum $d^4 - d^4$ interaction. Generally σ-bonding plays by far the dominant role, while π and δ components are of lesser importance [36]. Similarly to charge-shift bonds, such M-M bonds are indeed at the borderline of the electron-shared and electron-unshared interactions [40].

– *Dative M-M bonding.* One metal uses a filled *d* orbital lone pair to coordinate to an empty orbital of a second metal more unsaturated [41].

– *Weak M-M interactions due to symmetry.* Based on the above MO diagram, $d^8 - d^8$ systems shouldn't have any M-M bonding due to the filling of all the M-M antibonding orbitals, which cancels out the M-M bonding orbitals (Table 1). However, few bi- or polymetallic d^8 complexes do show the presence of weak M-M interactions. For example, the rhodium and iridium tetrakis(phenylisocyanide) $[M(CNPh_4]^+$ complexes form oligomeric M-M bonded stacks both in solution and in the solid-state [42]. Because of symmetry, molecular orbital interaction

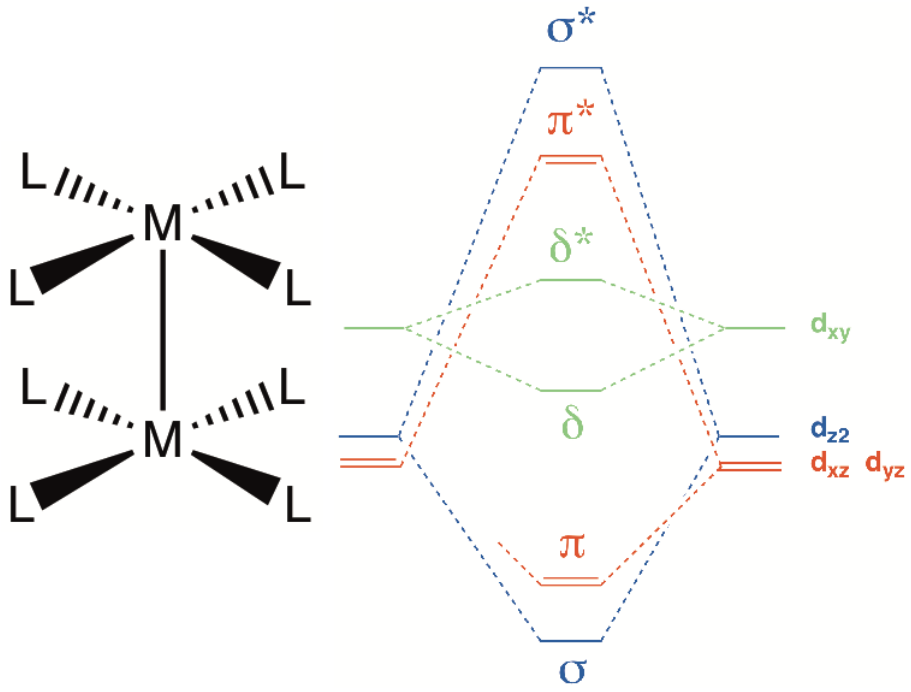

Figure 1: Molecular diagram restricted to d orbitals for two interacting metal centres in D_{4h} symmetry.

between both d_{z^2} orbitals of the metal centres with the p_z and π^* orbitals of the isocyanide ligand pushes the filled orbitals down in energy [43]. This generates a weak M-M bond, strong enough, however, to allow these complexes to form M-M bonds even in solution. Non-covalent weak attractive $d^{10} - d^{10}$ interactions, referred to as metallophilic interactions are also well-known in homo-or heterometallic transition element clusters and have been reviewed recently [16, 44].

The MO interpretation provides quantum chemical explanations for the understanding of the bonding in polymetallic compounds. Though this method has proved its efficiency in both predictive and interpretative purposes, it has a constitutive epistemological weakness because it mostly relies on the interpretation of the approximate wave function in terms of its atom related components rather than upon observable quantities. As pointed out by Coulson [45]: "This epistemological difficulty is mostly due to the weakness of interpretative methods that give a physical significance to quantities, such as molecular orbitals or valence bond structures, appearing as intermediates during the course of solution of the many-body Schrödinger equation". In another approach, no more than quantum mechanics interpretative postulates is required and no approximation is considered in the principles. Theories derived accordingly should [46] "provide the mathematical bridge between the chemical intuition and wave mechanics, which may be considered as a theoretical justification of the main chemical ideas." Several interpretative methods have been developed in this spirit: the loge theory [46–50], the Quantum Theory of Atoms in Molecules (QTAIM)[51–62], the topological analysis of the electron localization function(ELF) [63–67] and of the electron localizability indicator (ELI) [68–70] as well as the determination of maximum probability domains [71–73] and the determination of the electron number probability distribution functions [74–77]. Among these different methods, only those based on the topological analysis of gradient dynamical systems, namely QTAIM, ELF and ELI-D analyses, have been applied so far to compounds involving M-M bonds. The aim of this tutorial review is to show how these topological analyses provide pieces of information which help to understand the M-M bonding. A first section provides a detailed presentation of the QTAIM and ELF/ELI-D methods of analysis, it is followed by three section describing the applications to a specific class of compound: bulk metals and alloys, M-M two centre bonds in molecular systems, multicentre polymetallic bonds in molecular systems and small aggregates. Each of these sections is divided in three subsections according to the chemical composition of

the investigated compounds (*i.e.* main group elements, transition element, lanthanides and actinides, heterometallic systems). For each subsection an example will be discussed in a detailed tutorial fashion.

2. AIM and ELF analysis overview

The term Quantum Chemical Topology (QCT) has been introduced by Popelier and Aicken [78] to encompass the study of various molecular vector fields by topological tools belonging to the mathematical theory of dynamical systems. It has mostly been applied not only to the electron density in the framework of the Quantum Theory of Atoms in Molecules [58, 61, 79–83] but also to other scalar fields such as those of the Laplacian of the electron density [84], of the Becke and Edgecombe electron localization function [64, 85], of the source function [86–90], of the Electron Localization Indicator (ELI-D) [68–70], of the Fukui function [91] and non-scalar fields [92]. Since these methods share a common mathematical background and vocabulary, it appears useful to us to present the common features before considering the aims and possibilities of the QTAIM and ELF approaches which is the subject of this review. The dynamical system theory is a branch of mathematics which deals with the analysis of the behaviour of vector fields bound on manifolds. Inspired by classical mechanics, it had been pioneered by Poncarsé, Lyapunov at the end of the XIX$^{\text{th}}$ and by Birkhoff at the beginning of the XX$^{\text{th}}$, it has been further developed in its contemporary presentation in the 1960s and 1970s by mathematicians like Peixotto, Abraham, Palis, Smale [93–95]. The catastrophe theory of René Thom is an example of a very fruitful branch of the dynamical system theory [96]. A practical example of application of the dynamical system has been given a long time before the development of the mathematical theory by the partition of land made in hydrology in terms of drainage basins limited by watersheds. The mathematical vocabulary used in the dynamical system and consequently in QCT is given in appendix A.

2.1. Population analysis based on dynamical system partitioning

The dynamical system theory provides a partition of real space occupied by a molecule or a crystal in terms of space-filling non-overlapping basins. The evaluation of the properties associated with a given basin is conceptually straightforward provided the relevant density of property is available. In quantum mechanics the density of property is defined as:

$$\rho_A(\mathbf{r}) = \int \hat{A}(\mathbf{r},\mathbf{p})F(\mathbf{r},\mathbf{p})d\mathbf{p} \tag{1}$$

where $\hat{A}(\mathbf{r},\mathbf{p})$ is a one electron operator and $F(\mathbf{r},\mathbf{p})$ the joint distribution of position and momentum. Although it is not possible to define the joint distributions in quantum mechanics, it is possible to introduce a so-called phase-space quasi distributions, such as the Wigner function [97], in order to get an expression which yields the proper expectation value of the operator when integrated over all space. The quasi distributions are built up from correspondence rules but, in general, do not fulfill the requirement of uniqueness [98]. For an operator which only depends upon the position coordinates they are expressed as the product of this operator and the electron density function, *i.e.*

$$\rho_A(\mathbf{r}) = A(\mathbf{r})\rho(\mathbf{r}) \tag{2}$$

Basin properties, $\langle\hat{A}\rangle_{\Omega_I}$, are calculated by integrating the densities of property over the volume of the basin labelled by Ω_I:

$$\langle\hat{A}\rangle_{\Omega_I} = \int_{\Omega_I} \rho_A(\mathbf{r})d\mathbf{r} \tag{3}$$

The partition in spin components is achieved considering the α and β spin electron density instead of the total density. The α population (Eq. 4), β population (Eq. 5), total population (Eq. 6) and integrated spin density (Eq. 7) are given

below:

$$\bar{N}^{\alpha}[\Omega_I] = \int_{\Omega_I} \rho^{\alpha}(\mathbf{r}) d\mathbf{r} \tag{4}$$

$$\bar{N}^{\beta}[\Omega_I] = \int_{\Omega_I} \rho^{\beta}(\mathbf{r}) d\mathbf{r} \tag{5}$$

$$\bar{N}[\Omega_I] = \bar{N}^{\alpha}[\Omega_I] + \bar{N}^{\beta}[\Omega_I] = \int_{\Omega_I} \rho(\mathbf{r}) d\mathbf{r} \tag{6}$$

$$\langle S_z \rangle_{\Omega_I} = \frac{1}{2}\left(\bar{N}^{\alpha}[\Omega_I] - \bar{N}^{\beta}[\Omega_I]\right) \tag{7}$$

The electrostatic multipoles of basins are defined as the negative integral over volume of the product of electron density distribution and a multipole operator $Q_l^m(\mathbf{r} - \mathbf{r}_c)$, here expressed on the basis of the spherical harmonics:

$$\langle Q_l^m \rangle_{\Omega_I} = -\int_{\Omega_I} Q_l^m(\mathbf{r} - \mathbf{r}_c)\rho(\mathbf{r}) d\mathbf{r} \tag{8}$$

Except for the unipole ($l = 0$), the multipole operators are origin dependent. As a general rule, the origin is taken at the attractor of the basin.

The generalization to two-electron properties is done by substituting one-electron densities by pair functions, the integration is then performed over the same basin volume or over two basins. Particularly interesting are the pair populations:

$$\bar{\Pi}^{\alpha\beta}[\Omega_I, \Omega_J] = \int_{\Omega_I}\int_{\Omega_J} \pi^{\alpha\beta}(\mathbf{r}, \mathbf{r}') d\mathbf{r} d\mathbf{r}' \tag{9}$$

$$\bar{\Pi}^{\alpha\alpha}[\Omega_I, \Omega_J] = \int_{\Omega_I}\int_{\Omega_J} \pi^{\alpha\alpha}(\mathbf{r}, \mathbf{r}') d\mathbf{r} d\mathbf{r}' \tag{10}$$

$$\bar{\Pi}^{\beta\beta}[\Omega_I, \Omega_J] = \int_{\Omega_I}\int_{\Omega_J} \pi^{\beta\beta}(\mathbf{r}, \mathbf{r}') d\mathbf{r} d\mathbf{r}' \tag{11}$$

$$\bar{\Pi}[\Omega_I, \Omega_J] = \int_{\Omega_I}\int_{\Omega_J} \pi(\mathbf{r}, \mathbf{r}') d\mathbf{r} d\mathbf{r}' \tag{12}$$

The populations are averaged values which can be expressed as the expectation value of the population operator [99].

$$\hat{N}[\Omega_I] = \sum_i^N \hat{y}(\mathbf{r}_i) \qquad \text{with} \qquad \hat{y}(\mathbf{r}_i) \begin{cases} \hat{y}(\mathbf{r}_i) = 1 & \mathbf{r}_i \in \Omega_I \\ \hat{y}(\mathbf{r}_i) = 0 & \text{otherwise} \end{cases}$$

where N is the number of electrons of the system. The eigenvalues of the population operator belong to the series of integer $0, \ldots, N$ and represent all the accessible numbers of electrons within Ω_I. The eigenvalues of the population operators of ithe different basins spanning the entire space are correlated since they also obey the closure relation

$$\sum_I N[\Omega_I] = N \tag{13}$$

which enables to carry out a statistical analysis of the basins populations through the definition of a covariance matrix [100]. The covariance operator is a matrix operator whose elements are deduced from the classical expression of the

covariance:

$$\widehat{\sigma^2}(\Omega_I, \Omega_I) = \hat{N}[\Omega_I]\hat{N}[\Omega_I] - \bar{N}[\Omega_I]^2 = \hat{\Pi}[\Omega_I, \Omega_I] + \hat{N}[\Omega_I] - \bar{N}[\Omega_I]^2 \quad (14)$$

$$\widehat{\sigma^2}(\Omega_I, \Omega_J) = \hat{N}[\Omega_I]\hat{N}[\Omega_J] - \bar{N}[\Omega_I]\bar{N}[\Omega_J] = \hat{\Pi}[\Omega_I, \Omega_J] - \bar{N}[\Omega_I]\bar{N}[\Omega_J] \quad (15)$$

the expectation value of which

$$\langle\sigma^2(\Omega_I, \Omega_I)\rangle = \bar{\Pi}[\Omega_I, \Omega_I] + \bar{N}[\Omega_I](1 - \bar{N}[\Omega_I]) \quad (16)$$

$$\langle\sigma^2(\Omega_I, \Omega_J)\rangle = \bar{\Pi}[\Omega_I, \Omega_J] - \bar{N}[\Omega_I]\bar{N}[\Omega_I] \quad (17)$$

provide a measure of the delocalization of the electrons among the basins. Moreover, the covariance matrix element operators as well as their expectation values satisfy:

$$\sum_J \widehat{\sigma^2}(\Omega_I, \Omega_J) = 0 \quad (18)$$

$$\sum_J \langle\sigma^2(\Omega_I, \Omega_J)\rangle = 0 \quad (19)$$

as a consequence of Eq. 13

2.2. The QTAIM method

The Quantum Theory of Atoms in Molecules (QTAIM), which has been developed since 1972 by Richard F. W. Bader and his coworkers, relies on the partition of the position space in terms of the basins of the attractors of the density gradient field $\nabla\rho(\mathbf{r})$. The motivation is to be found in the papers published in 1972 [101] and 1973 [102] where the kinetic energy integrated over fragments bounded by zero-flux surfaces of the density function, $S(\Omega; \mathbf{r}_s)$, is shown to have a definite value. This follows from the general expression of the kinetic energy density:

$$T(\mathbf{r}) = T_s(\mathbf{r}) + a\nabla^2\rho(\mathbf{r}) \quad (20)$$

where $T_s(\mathbf{r})$ is the definite positive kinetic energy and a an arbitrary multiplicative constant. The condition for a definite integrated kinetic energy density is that the integral of $\nabla^2\rho(\mathbf{r})$ vanishes, which happens when the integration is performed over the whole space or, according to the divergence theorem, if the bounding surface is a zero flux surface:

$$\int_\Omega \nabla^2\rho(\mathbf{r})d\mathbf{r} = \oint_S \mathbf{n}(\mathbf{r}) \cdot \nabla\rho(\mathbf{r})d\mathbf{s} = 0 \quad (21)$$

where $\mathbf{n}(\mathbf{r})$ denotes a unit vector normal to $S(\mathbf{r})$ at point $\mathbf{r}$. The virial theorem provides a simple relationship between the kinetic, $\langle\hat{T}\rangle$, and potential, $\langle\hat{V}\rangle$ energies of a quantum system. For a molecule at its equilibrium geometry:

$$-2\langle\hat{T}\rangle = \langle\hat{V}\rangle \quad (22)$$

It is possible to derive an analogous equation for a subsystem Ω, provided its kinetic energy has a definite value, in other words that eq. 21 be satisfied. In the case:

$$E(\Omega) = -\int_\Omega T_s(\mathbf{r})dr \quad (23)$$

The domain energy is therefore defined in each fragment Ω such as a local variational principle holds enabling the virial and hypervirial theorems to be proved [103]. Collard and Hall [104] recognized the basins of the attractors of $\nabla\rho(\mathbf{r})$ in the fragments provided by the virial partitioning. The QTAIM is rooted on firm mathematical and quantum mechanical foundations, it provides an acknowledged theoretical framework for the study of the chemical bonding giving access to both rigorous qualitative and quantitative information. Being based on an observable quantity, this theory applies to both experimental and calculated densities.

2.2.1. The QTAIM basins

Large maxima of the charge density are located at the nuclear positions $\mathbf{R}_A$, and therefore these points are only ω-limits for the trajectories of $\nabla\rho(\mathbf{r})$. In this sense, they are attractors of the gradient field, although they are not critical points as the nuclear cusp condition makes $\nabla\rho(\mathbf{R}_A)$ not defined. The stable manifold of the nuclear attractors are the *atomic basins*. Non-nuclear attractors (NNAs) occur in metal clusters [105–108] and bulk metals [109] at their equilibrium geometry and between homonuclear groups at internuclear distances far away from the equilibrium geometry [110].

In the QTAIM approach, an atom is defined as the union of a nucleus and of its atomic basin. It is either limited by zero-flux surfaces, the interatomic separatrices, or extends to infinity. It is therefore an open system bounded by its zero-flux surfaces for which a Lagrangian formulation of quantum mechanics [58, 61, 62, 81, 111, 112] enables the derivation of many theorems such as the atomic force theorem:

$$m\int_{\Omega}\frac{\partial\mathbf{J}(\mathbf{r})}{\partial t}d\mathbf{r}=\int_{\Omega}d\mathbf{r}\int\Psi^{*}(-\nabla\hat{V})\Psi d\tau'+\oint\overleftrightarrow{\sigma}(\mathbf{r})\cdot\mathbf{n}(\mathbf{r})dS(\mathbf{r}) \tag{24}$$

the atomic virial theorem:

$$m\int_{\Omega}\mathbf{r}\cdot\frac{\partial\mathbf{J}(\mathbf{r})}{\partial t}d\mathbf{r}=2T(\Omega)+\int_{\Omega}d\mathbf{r}\int\Psi^{*}(-\mathbf{r}\cdot\nabla\hat{V})\Psi d\tau'+\oint\mathbf{r}\cdot\overleftrightarrow{\sigma}(\mathbf{r})\cdot\mathbf{n}(\mathbf{r})dS(\mathbf{r}) \tag{25}$$

In the latter equation, $T(\Omega)$ is the kinetic energy of the atom, $\mathbf{J}(\mathbf{r})$ the current density:

$$\mathbf{J}(\mathbf{r})=-\frac{\imath\hbar}{2m}\int\left\{\Psi^{*}\nabla\Psi-\Psi\nabla\Psi^{*}\right\}d\tau' \tag{26}$$

and $\overleftrightarrow{\sigma}(\mathbf{r})$ the stress tensor density:

$$\overleftrightarrow{\sigma}(\mathbf{r})=\frac{\hbar^{2}}{4m}\int\left\{(\nabla\nabla\Psi^{*})\Psi-\nabla\Psi^{*}\nabla\Psi-\nabla\Psi\nabla\Psi^{*}+\Psi^{*}\nabla\nabla\Psi\right\}d\tau' \tag{27}$$

In a molecule, an atom has parts which extend to infinity. It is bounded by the interatomic surfaces inside the molecule and unbounded outside.

2.2.2. Bond path, molecular graph and definition of the molecular structure

The connectivity of the critical points of the electron density gradient field provides a characterization of its topology and of the molecular structure.There are four types of critical points in $\mathbb{R}^3$ summarized in Table 2. Instead of the index I_P a couple of integers (r, s), the rank and the signature, is used to characterize the critical points in the QTAIM framework. The rank is the number of non-zero eigenvalues of the Hessian matrix and the signature is the algebraic sum of their signs. A critical point is connected by the trajectories belonging to its unstable manifold to

Table 2: Critical points of the charge density gradient field. Index I_P, rank r, signature s. The dimensionality of the stable and unstable manifolds are respectively $3 - I_P$ and I_P.

	I_P	(r, s)	stable manifold
attractor (peak)	0	(3,-3)	basin
bond critical point (pass)	1	(3,-1)	separatrix
ring critical point (pale)	2	(3,+1)	separatrix
cage critical point (pit)	3	(3,+3)	empty

critical points of the lower indexes. A critical point of index 1 is called *bond critical point* (BCP). It is connected to two attractors as the dimension of its unstable manifold, the *bond path*, is also 1. The index of a *ring critical point*

(RCP) is 2. It is connected to at least three attractors and BCPs, whereas critical points of index 3, the *cage critical points* are connected to four or more non coplanar attractors.

The bond paths are the lines of maximum density linking the neighbouring atoms. Keith *et al*. have demonstrated the structural homeomorphism between the negative of the virial field $\mathcal{V}(\mathbf{r})$ and the electron density [113]. Both have their attractors located at the nuclear position, which are linked by pairs of trajectories to BCPs [114]. Exceptions to this rule have been evidenced for piano-stool complexes, such as $(\eta^3\text{-}C_3H_3)Co(CO)_3$, in which the region between the metal centre and the carbocyclic ligand is characterized by a very flat density [115].

A molecular graph is defined as the set of the unstable manifolds of the index 1 critical points of the charge density gradient field, in other words the set of the bond paths linking each BCP to its associated nuclei. Within a given structural stability domain (SSD), all molecular graphs have the same topology and are therefore equivalent; they form an equivalence class called molecular structure [116].

2.2.3. The QTAIM population analysis

The integration of the electron density over the atomic basins provides the atomic population, $\bar{N}(A)$, and the atomic charge, $Q(A)$, by subtracting the atomic population from the atomic number, $Q(A) = Z_A - \bar{N}(A)$. With respect to orbital based populations, the QTAIM approach generally yields larger absolute values of the net charges than the Mulliken, Löwdin, Natural Population Analysis (NPA) and Hirshfeld population analyses. This has been often interpreted as a spurious overestimation of the ionic contribution to the bonding [117], possibly due to the fact that the location of the zero-flux surface "depends on atomic sizes, which ought otherwise irrelevant" [118]. The reason of this criticism was shown irrelevant and due to simplistic and erroneous assumptions in the models adopted to claim the spurious "size effect" on QTAIM populations [119]. This criticism also originates in the belief of chemists that the charge distribution in the atomic basin is spherical and isotropic, so that the atomic charge directly reproduce the dipole moment, which is not the case. The anisotropy of the charge distribution in atomic basins can be further described by nucleus centred multipole distributions [120]. Moreover, the calculation of orbital contributions to the basin population can be achieved in order to analyze charge transfers and substituent effects [120].

The bond order interpretation has been pioneered by Cioslowski and Mixon [121] for closed-shell Hartree-Fock (HF) wave functions. The bond order B_{AB} is expressed in terms of the diagonal elements of the molecular orbital, φ_i, overlap matrix over the atomic basins A and B:

$$B_{AB} = 2 \sum_i \langle i|i\rangle_A \langle i|i\rangle_B \tag{28}$$

where

$$\langle i|i\rangle_A = \int_A \varphi_i(\mathbf{r})\varphi_i(\mathbf{r}) d\mathbf{r}$$

This definition based on the decomposition of the total integrated density into atomic and diatomic contributions, is a generalization of the Wiberg bond indexes [122] W_{AB}, avoiding the assignment of basis functions to individual atoms.

The analysis of the pair function usually made in the QTAIM framework, relies on a decomposition of this function in two contributions, a non-interacting one and the exchange-correlation density $\Pi_{xc}(\mathbf{r}, \mathbf{r}')$:

$$\Pi(\mathbf{r}, \mathbf{r}') = \rho(\mathbf{r})\rho(\mathbf{r}') + \Pi_{xc}(\mathbf{r}, \mathbf{r}') \tag{29}$$

The integrals of the exchange-correlation density over the basins Ω_A and Ω_B:

$$F(\Omega_A, \Omega_B) = \int_{\Omega_A} d\mathbf{r}_1 \int_{\Omega_B} \Pi_{xc}(\mathbf{r}_1, \mathbf{r}_2) d\mathbf{r}_2 \tag{30}$$

satisfy the sum rule:

$$\sum_B F(\Omega_A, \Omega_B) = -\bar{N}[\Omega_A] \tag{31}$$

Different complementary interpretations have been given to these integrals. Bader and Stephens consider $F(\Omega_A, \Omega_A)$

and $F(\Omega_A, \Omega_B)$ respectively as the measure of the total correlation within Ω_A and of the inter-basin correlation. Ángyan *et al*. [123] working with Mayer's definition of bond orders [124, 125] identify $-F(\Omega_A, \Omega_A)$ as a free valence index and $F(\Omega_A, \Omega_B) + F(\Omega_B, \Omega_A)$ as a topological bond order. This interpretation has been criticized by Fradera *et al*. [126], because $F(\Omega_A, \Omega_B) + F(\Omega_B, \Omega_A)$ which is related to the number of electrons shared by Ω_A and Ω_B does not determine the number of electron pairs. For this reason, $\lambda(\Omega_A) = -F(\Omega_A, \Omega_A)$ and $\delta(\Omega_A, \Omega_B) = F(\Omega_A, \Omega_B) + F(\Omega_B, \Omega_A)$ are respectively called localization and delocalization indexes (DI). A connection with the Wiberg indexes and further with the effective pair populations [127] has been made for $F(\Omega_A, \Omega_B)$ by Ponec and Uhlik [128]:

$$W_{AB} = 2\Pi_{AB}^{\text{eff}} = -2F(\Omega_A, \Omega_B) \tag{32}$$

In fact, as discussed by Bochicchio *et al*. [129], there is not a strict equality between the effective pair populations and $-F(\Omega_A, \Omega_B)$. The definition of multicentre bond indexes can be achieved by a generalization of the covariance operator (Eq. 15), for example the three-centre bond index is the expectation value of the operator [130]:

$$\hat{I}_{ABC} = \Big(\hat{N}(\Omega_A) - \bar{N}(\Omega_A)\Big)\Big(\hat{N}(\Omega_B) - \bar{N}(\Omega_B)\Big)\Big(\hat{N}(\Omega_C) - \bar{N}(\Omega_C)\Big) \tag{33}$$

which implies that the actual calculation of the three centre bond indexes requires the third order density distribution function. As a general rule, the three-centre two-electron ($3c-2e$) bonds have positive indexes whereas the three-centre four-electron ($3c-4e$) ones have negative indexes.

2.2.4. Energy partitioning in the QTAIM framework

In actual calculations the virial theorem is not exactly fulfilled and for an equilibrium geometry the ratio $\gamma = \langle\hat{V}\rangle/\langle\hat{T}\rangle = -2$ is not satisfied. The error in the molecular virial is corrected by multiplying each atomic kinetic energy by $-\gamma - 1$ such as the corrected atomic energies $E_e(\Omega_A) = (\gamma + 1)T(\Omega_A)$ sum to the total energy [58, 131]. The transferability of atomic energies in organic molecules has been discussed by Mandado *et al*. [132] who conclude that the virial correction should be avoided in order to get transferable energies and by Cortés-Guzmán and Bader [133] who recommend a self consistent virial scaling procedure. The atomic electronic energy is the sum of the kinetic energy contribution $T(\Omega_A)$ and of the basin virial $\mathcal{V}(\Omega_A)$:

$$E_e(\Omega_A) = T(\Omega_A) + \mathcal{V}(\Omega_A) = T(\Omega_A) + \int_{\Omega_A} \text{Tr}\overleftrightarrow{\sigma}(\mathbf{r})d\mathbf{r} \tag{34}$$

which can be expressed as the sum of four components arising from the action of $-\mathbf{r}\cdot\nabla$ on the potential energy operator $\hat{V}$:

$$\mathcal{V}(\Omega_A) = V_{\text{en}}(\Omega_A) + \sum_B \mathbf{R}_B \cdot \mathbf{F}_B(\Omega_A) + V_{\text{ee}}(\Omega_A) + \sum_{B\neq A} V(\Omega_A, \Omega_B) \tag{35}$$

where

$$V_{\text{en}}(\Omega_A) = -\sum_B \int_{\Omega_A} \frac{Z_B}{|\mathbf{r} - \mathbf{R}_B|}\rho(\mathbf{r})d\mathbf{r} \tag{36}$$

is the interaction energy of the density in basin Ω_A with the nuclei,

$$\begin{aligned} V_{\text{ee}}(\Omega_A) &= V_{\text{ee}}(\Omega_A, \Omega_A) + \sum_{B\neq A} V_{\text{ee}}(\Omega_A, \Omega_B) \\ &= \frac{1}{2}\left[\int_{\Omega_A}\int_{\Omega_A} \frac{\Pi(\mathbf{r}, \mathbf{r}')}{|\mathbf{r}' - \mathbf{r}|}d\mathbf{r}d\mathbf{r}' + \sum_{B\neq A}\int_{\Omega_A}\int_{\Omega_B} \frac{\Pi(\mathbf{r}, \mathbf{r}')}{|\mathbf{r}' - \mathbf{r}|}d\mathbf{r}d\mathbf{r}'\right] \end{aligned} \tag{37}$$

is the electron-electron repulsion which is equal to the sum of the electron-electron repulsion within Ω_A and half the electron-electron repulsion between Ω_A and the remaining basins,

$$\mathbf{F}_B(\Omega_A) = -Z_B \int_{\Omega_A} \frac{(\mathbf{r} - \mathbf{R}_B)}{|\mathbf{r} - \mathbf{R}_B|^3} \rho(\mathbf{r}) d\mathbf{r} \tag{38}$$

is the force exerted on the charge density of Ω_A by the nucleus of atom B, for equilibrium geometries

$$-\sum_A \sum_B \mathbf{R}_B \cdot \mathbf{F}_B(\Omega_A) = \sum_{A>B} \frac{Z_A Z_B}{|\mathbf{R}_B - \mathbf{R}_A|} = V_{\mathrm{nn}} \tag{39}$$

and

$$V(\Omega_A, \Omega_B) = \int_{\Omega_A} \int_{\Omega_B} (\mathbf{r}' \cdot \nabla_{\mathbf{r}'} - \mathbf{r} \cdot \nabla_{\mathbf{r}}) \frac{\Pi(\mathbf{r}, \mathbf{r}')}{|\mathbf{r}' - \mathbf{r}|} d\mathbf{r} d\mathbf{r}' \tag{40}$$

a remaining term arising of the action of the virial operator on the two-electron Coulomb operator which vanishes for the total system.

The Interacting Quantum Atoms (IQA) approach [134–137] is based on the QTAIM partitioning. It provides a decomposition of the energy of a molecule into atomic and diatomic contributions:

$$\begin{aligned} E &= \sum_A (T(\Omega_A) + V_{\mathrm{en}}(\Omega_A) + V_{\mathrm{ee}}(\Omega_A, \Omega_A)) + \sum_{B \neq A} V_{\mathrm{ee}}(\Omega_A, \Omega_B) + \sum_{A>B} \frac{Z_A Z_B}{|\mathbf{R}_B - \mathbf{R}_A|} \\ &= \sum_A (T^A + V_{\mathrm{en}}^{AA} + V_{\mathrm{ee}}^{AA}) + \sum_{A>B} (V_{\mathrm{nn}}^{AB} + V_{\mathrm{en}}^{AB} + V_{\mathrm{ne}}^{AB} + V_{\mathrm{ee}}^{AB}) \\ &= \sum_A E_{\mathrm{self}}^A + \sum_{A>B} E_{\mathrm{int}}^{AB} \end{aligned} \tag{41}$$

The atomic deformation energy E_{def}^A is defined as the difference of E_{self}^A and an energetic reference $E_{\mathrm{self}}^{A,0}$. This enables to compute the binding energy as: $E_{\mathrm{bind}} = \sum_A E_{\mathrm{def}}^A + \sum_{A>B} E_{\mathrm{int}}^{AB}$. The decomposition of the pair function into a classical Coulombic part and an exchange-correlation contribution (29) enables to divide V_{ee}^{AB} into a classical electrostatic term V_{C}^{AB} and a non-classical exchange-correlation term V_{xc}^{AB}.

The evaluation of the two-electron terms is hampered by numerical difficulties and therefore attempts have been made to compute V_{C}^{AB} and V_{xc}^{AB} with multipole expansions. The convergence of the atomic expansion of the electrostatic potential has been investigated by Kosov and Popelier [138, 139] and different schemes such as the continuous multipole method [140] and the introduction of inverse moments [141] enabled the potential to converge everywhere. The exchange energy can be also expressed in terms of an exchange multipole expansion where the exchange moments explicitly depend on the molecular orbitals [142].

2.2.5. QTAIM characterization of the bonding

In the QTAIM framework, two kinds of quantities can be used in order to characterize the bonding. On the one hand are the delocalization indexes which can be related to the degree of covalence and also to the bond multiplicity and on the other hand is a series of local indicators calculated at the BCP. These indicators rely on the local expression of the virial theorem: [58]

$$\frac{1}{4}\nabla^2\rho(\mathbf{r}) = 2G(\mathbf{r}) + \mathcal{V}(\mathbf{r}) \tag{42}$$

where $G(\mathbf{r}) \equiv T_s(\mathbf{r})$ is the definite positive kinetic energy and $\mathcal{V}(\mathbf{r}) = \mathrm{Tr}\overleftrightarrow{\sigma}(\mathbf{r})$ is the virial potential energy density. The sign of the Laplacian indicates which of the kinetic and potential energy densities locally dominates with respect to the average value $\langle\nabla^2\rho(\mathbf{r})\rangle = 0.0$. Negative and positive values of the Laplacian at the BCP, $\nabla^2\rho_b$, are therefore associated respectively to "shared" and "closed-shell" interactions [58, 143]. The other BCP indicators are the G_b/ρ_b ratio [143], the energy density at the BCP $H_b = G_b + \mathcal{V}_b$ introduced by Cremer and Kraka [144–146] the $|\mathcal{V}_b|/G_b$ dimensionless ratio [147] and H_b/ρ_b. These additional indicators enable to refine the classification of interactions and

to approach the current chemical terminology. Bianchi et al [148] proposed the classification of Table 3 based on the values of ρ_b, $\nabla^2\rho_b$, G_b, $\mathcal{V}_b$ and H_b. This classification says nothing on important bonding types such as hydrogen bonding or metallic bond. The $|\mathcal{V}_b|/G_b$ ratio distinguishes three bonding regimes limited by two values, 1 and 2,

Table 3: Trends of the BCP descriptors according to Bianchi *et al* [148]. ρ_b: density at the BCP, $\nabla^2\rho_b$: Laplacian of the density at the BCP, G_b: kinetic energy density at the BCP, $\mathcal{V}_b$: virial potential energy at BCP, H_b: energy density at BCP. G_b, $|\mathcal{V}_b|$ and $|H_b|$ increase from the top to the bottom of the table.

	ρ_b	$\nabla^2\rho_b$	G_b	$\mathcal{V}_b$	H_b
van der Waals	low	> 0	$G_b \cong \|\mathcal{V}_b\|$	< 0	> 0
ionic	low	> 0	$G_b \cong \|\mathcal{V}_b\|$	< 0	> 0
M-M	low	> 0	$G_b \cong \|\mathcal{V}_b$	< 0	< 0
dative	low	> 0	$G_b \cong \|\mathcal{V}_b\|$	< 0	< 0
polar-covalent	high	< 0	$G_b \ll \|\mathcal{V}_b\|$	$\ll 0$	$\ll 0$
covalent	high	< 0	$G_b \ll \|\mathcal{V}_b\|$	$\ll 0$	$\ll 0$

of this ratio [147]. When $|\mathcal{V}_b|/G_b > 2$, the importance of the potential energy in the local energy is larger than in the averaged virial regime, the bond degree H_b/ρ_b is large and negative and its absolute value provides a measure of the covalent character. This region is the shared-shell region. The intermediate or transit region corresponds to $1 < |\mathcal{V}_b|/G_b < 2$, the potential energy remains the dominant contribution to H_b. Therefore the bond degree is negative and smaller than in the shared-shell region. H_b/ρ_b tends to zero as $|\mathcal{V}_b|/G_b$ approaches 1 whereas $\nabla^2\rho_b$ is positive. In the closed-shell region, $|\mathcal{V}_b|/G_b < 1$, the kinetic energy is the leading contribution, the bond degree and $\nabla^2\rho_b$ are both positive; weak closed-shell interactions give rise to large bond degrees. Table 4 presents a third chart proposed by Macchi *et al.* [149, 150]. It takes into account both local BCP indicators and two integral properties, namely the delocalization index $\delta(\mathrm{A},\mathrm{B})$ and the electron density integrated over the whole interatomic surface $\oint_{AB}\rho(\mathbf{r}_s)d\mathbf{r}_s$. This latter quantity is expected large for shared interactions and small for closed-shell ones. In bulk metals $\nabla^2\rho_b$ is

Table 4: Macchi's classification based on local (BCP) and integral properties

bond type	ρ_b	$\nabla^2\rho_b$	G_b/ρ_b	H_b/ρ_b	$\delta(\mathrm{A},\mathrm{B})$	$\oint_{AB}\rho(\mathbf{r}_s)d\mathbf{r}_s$
bonds between light atoms						
covalent	large	$\ll 0$	< 1	$\ll 0$	~ formal bond order	large
intermediate	large	any value	≥ 1	$\ll 0$	<formal bond order	large
closed-shell	small	> 0	≥ 1	> 0	~ 0	small
bonds between heavy atoms ($Z > 18$)						
open-shell (e.g. Co-Co)	small	~ 0	< 1	< 0	formal bond order	medium/large
donor-acceptor (e.g. Co-As)	small	> 0	~ 1	< 0	<formal bond order	medium/large

generally positive [151, 152], but it may be negative as calculated for Al. The ratio $\xi_j = \rho_b/\nabla^2\rho_b$ has been introduced by Jenkins [153] as metallicity index, it had been further reformulated [154] as:

$$\xi_m = \frac{36(3\pi^2)^{2/3}}{5}\rho_b^{2/3}\xi_j \tag{43}$$

The classification due to Mori-Sánchez *et al.* [155] is dedicated to bonding in solids. It relies on three dimensionless indexes, all in the [0,1] interval: the valence electron density flatness, f, the global charge transfer index, c, and the

molecularity μ. The flatness is provided by the ratio

$$f = \frac{\rho_c^{\min}}{\rho_b^{\max}} \tag{44}$$

where $\rho_c^{\min}$ and $\rho_b^{\max}$ are the minimum and maximum values of the density found at respectively cage and bond critical points. The global charge transfer index is defined as:

$$c = \frac{1}{N} \sum_{\Omega=1}^{N} \frac{Q(\Omega)}{OS(\Omega)} \tag{45}$$

where $Q(\Omega)$ is the net charge of atom Ω, $OS(\Omega)$ is its nominal oxidation state. The sum runs over all atoms forming the unit cell of the crystal. In ionic compounds $Q(\Omega)$ approaches the nominal oxidation number $OS(\Omega)$ for each atom and the ratio of these two quantities measures the separation from the ideal ionic model for the Ω basin. Finally, the molecularity is given by:

$$\mu = \begin{cases} (\rho_b^{\max} - \rho_b^{\min})/\rho_b^{\max} & \text{if} \quad \nabla^2\rho_b^{\max} \times \nabla^2\rho_b^{\min} < 0 \\ 0 & \text{otherwise} \end{cases} \tag{46}$$

It is then possible to build a $f - c - \mu$ three-dimensional diagram in the spirit of the van Arkel-Katelaar triangle [156–159] to characterize a given compound. This classification nicely works for isotropically bonded crystals but both indexes are not well adapted to the case of layered crystals such as graphite or clay minerals.

The eigenvalues λ_1, λ_2 and λ_3 of the Hessian matrix of $\rho(\mathbf{r})$ at the BCP provide an additional piece of information for the characterization of the bonding. By convention $\lambda_1 \leq \lambda_2 < 0$ and $\lambda_3 > 0$. The ratio λ_1/λ_2 measures the anisotropy of the orthogonal curvatures and leads to the bond ellipticity $\epsilon = (\lambda_1/\lambda_2) - 1$ which ranges from 0 to infinity. The ellipticity is related to the π-character of the bond.

2.2.6. The Laplacian of the electron density

The topology of the charge density shows atoms in molecules, but nothing on the atomic shell structure or on the Lewis model of electron pairing. The Laplacian of the charge distribution, $\nabla^2\rho(\mathbf{r})$, reveals where the electron density is locally concentrated and where it is depleted [160]. This follows from a property of the second derivative of a scalar function expressed as a finite difference:

$$f''(x_0) = \frac{1}{h^2}\left(f(x_0 + h) + f(x_0 - h) - 2f(x_0)\right) \tag{47}$$

which shows that for $f''(x_0) < 0$, $f(x_0)$ is greater than the average $(f(x_0+h)+f(x_0-h))/2$ and therefore the function is said concentrated at x_0 whereas for $f''(x_0) > 0$ the function is depleted ($(f(x_0+h)+f(x_0-h))/2 > f(x_0)$). The regions where $\nabla^2\rho(\mathbf{r}) < 0$ are called charge concentrations whereas those for where it is positive are the charge depletions. The negative of the Laplacian, denoted $L(\mathbf{r})$ is often used instead of $\nabla^2\rho(\mathbf{r})$. $L(\mathbf{r})$ displays the shell structure of light atoms as a succession of pairs of charge concentrations and charge depletions whereas for transition elements with $Z > 20$, the pair corresponding to the valence shell is usually missing. The outermost region of charge concentration is the valence shell charge concentration (VSCC) which persists upon bond formation but happens to be very distorted. In a molecule, local maxima of $L(\mathbf{r})$ are found in both bonding and non-bonding regions of the VSCCs; their number and their size are found in general agreement with the pair domains of the VSEPR model providing a theoretical support to the model [160, 161]. The correlation with the topological properties of the conditional pair probability has been further discussed by Bader and Heard [162] who found a homeomorphism between the Laplacian of the charge density and that of the conditional pair probability. Moreover, the maxima of the charge concentration of the core outer shell explains why heavy alkaline-earth dihalides have bent geometries in contradiction with the VSEPR rules [163]. A similar behaviour of external core shell charge concentrations can be found in transition element carbonyls [164]. Figure 2 displays the 0.3 isocontour of the density Laplacian of ferrocene. The VSCCs correspond to the atomic cores, to the C−H and to the C−C bonds. The iron core presents bulges in the ring centre directions.

The full topology of the Laplacian has been studied by Popelier [165]. As $L(\mathbf{r})$ has both negative and positive values, Popelier was led to consider four types of regions: the valence shell charge concentrations, the valence shell

charge depletions (VSCDs), the core shell charge concentrations and the core shell charge depletions. The critical points are organized in three graphs corresponding the valence and core charge depletion regions. The valence shell charge concentration graph recovers the bonding and non-bonding maxima of the VSEPR picture, however bonds often give rise to two colinear maxima as it can be seen in Figure 2. The integration of the density over the $L(\mathbf{r})$ gradient field basins is very disappointing. For instance one gets 0.96 e^- for the core population of the ammonia nitrogen atom [166] because the partitioning does not assign the whole density.

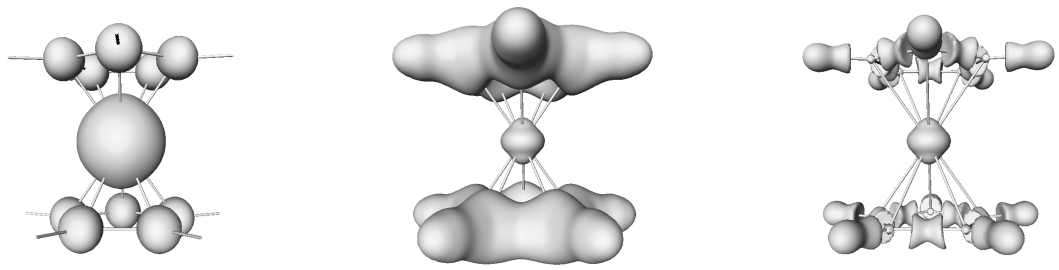

Figure 2: From left to right $L(\mathbf{r}) = -0.5$, 0.0 and 0.5 isosurfaces of $Fe(C_5H_5)_2$

2.2.7. The source function

The source function has been introduced by Bader and Gatti [86]. The density at a given point $\mathbf{r}$ can be expressed as the sum of contributions from all the other points of the space, *i.e.*:

$$\rho(\mathbf{r}) = \int LS(\mathbf{r}, \mathbf{r}')d\mathbf{r}' \tag{48}$$

The Local Source Function, $LS(\mathbf{r}, \mathbf{r}')$, is expressed as:

$$LS(\mathbf{r}, \mathbf{r}') = -\frac{\nabla^2\rho(\mathbf{r}')}{4\pi|\mathbf{r} - \mathbf{r}'|} \tag{49}$$

It measures how the Laplacian of the density at $\mathbf{r}'$ contribute to the density at the reference point. The magnitude of the contribution is proportional to the Laplacian absolute value and to the inverse distance to the reference point. The integral of the Local Source Function over a volume Ω called the Source Function contribution of Ω is denoted by $S(\mathbf{r}, \Omega)$. For space-filling non overlapping volumes, the electron density at $\mathbf{r}$ is the sum of the self-contribution ($\mathbf{r} \in \Omega$) and of the contributions of all the remaining volumes ($\mathbf{r} \notin \Omega$), *i.e.*:

$$\rho(\mathbf{r}) = S(\mathbf{r}, \Omega) + \sum_{\Omega' \neq \Omega} S(\mathbf{r}, \Omega') \tag{50}$$

Therefore, the Source Function provides a measure of the importance of the contribution of an atom or group of atoms to the density at a given point. In practice, the Source Function is evaluated at the bond critical points, the integration being carried out over atomic basins. The Source Function percentage contribution of Ω [90, 167] is given by:

$$S\%(\mathbf{r}, \Omega) = \left[\frac{S(\mathbf{r}, \Omega)}{\rho(\mathbf{r})}\right] \cdot 100 \tag{51}$$

The population of any atomic basin $\bar{N}(\Omega)$ can be expressed as the sum of a self-contribution $\bar{N}_i(\Omega)$ and of an outer contribution $\bar{N}_o(\Omega)$, since

$$\bar{N}(\Omega) = \int_{\Omega} S(\mathbf{r}, \Omega) d\mathbf{r} + \sum_{\Omega' \neq \Omega} \int_{\Omega} S(\mathbf{r}, \Omega') d\mathbf{r} \tag{52}$$

As mentioned by Gatti *et al*. [87] this partition of the atomic population presents some analogy with the Mulliken's decomposition of the gross population into net and overlap components [168]. Such a partitioning is reminiscent of the decomposition of the Mulliken's gross population of an atom in two parallel contributions, the net population, and one half of the overlap population.

2.3. The ELF and ELI-D approaches

Are partitions other than atomic significant? In chemistry we are used to think the matter not only in terms of atoms, but also in terms of bond and lone pairs, so it would be highly desirable to develop techniques enabling the partition of the molecular space into regions corresponding to such concepts.

2.3.1. How subatomic regions can be defined

The concepts of bond, lone pairs and associated domains do not emerge from quantum mechanics. They belong to a successful explanatory representation of the matter designed by the chemistry community in which groups of electrons account for the structural and chemical properties. Electron count is therefore essential in chemical explanation of the structure and reactivity.

The proof of the pudding being in the eating, such groups of electrons should leave their footprints in an organization of the electron density. In other words, it should be possible to find regions of space in which it is possible to find a given number of electrons, typically two, with a high probability. The concept of loge has been introduced by Raymond Daudel in 1953 [47]. The loges are space filling non-overlapping volumes "in which there is a high probability of finding a given number n of electrons (but not always the same) with a certain organization of their spins." [46] The determination of the best loge partition is a difficult problem which can be handled with the help of the missing information function [46]. However, the implementation of the procedure yields a huge numerical complexity which restrict its applicability to systems containing very few electrons. The Maximum Probability Domains (MPDs) are defined as regions of space which maximize the probability of finding a given number of electrons, n, inside them [71, 72, 169]. The MPDs are neither unique nor constrained non-overlapping.

The assumption that groups of electrons can be localized within space filling non-overlapping domains implies that eigenvalues of the domain population operators (Eq. 13), i.e. of the electron count, are peaked around characteristic values, say $N(\Omega)$. Therefore the population $\bar{N}(\Omega)$ should be close to $N(\Omega)$ and its variance which expresses the spread of the measurements of the number of electrons within Ω, should be minimal with respect to a variation of the domain boundaries. This proposition is illustrated in Figure 3 which displays the variance σ^2 of the integrated density $\bar{N}(r_m) = 4\pi \int_0^{r_m} \rho(r) r^2 dr$ as a function of $\bar{N}(r_m)$ for the calcium atom. The shell structure is fairly reproduced as the local minima of $\sigma^2(\bar{N}(r_m))$ occur at the expected values. The partition into non-overlapping variance region can be achieved by minimizing either the Froebenius norm of the covariance matrix [170]:

$$\|\boldsymbol{\sigma}^2\|_F = \left(\sum_{\Omega_A, \Omega_B} \langle \widehat{\sigma^2}(\Omega_A, \Omega_A) \rangle \right)^{1/2} \tag{53}$$

or its trace:

$$\mathrm{tr}\boldsymbol{\sigma}^2 = \sum_{\Omega_A} \langle \widehat{\sigma^2}(\Omega_A, \Omega_A) \rangle \tag{54}$$

The minimization of the variance with respect to the shell volumes implies that the variational equation

$$\frac{\delta \|\boldsymbol{\sigma}^2\|_F}{\delta V} = 0 \tag{55}$$

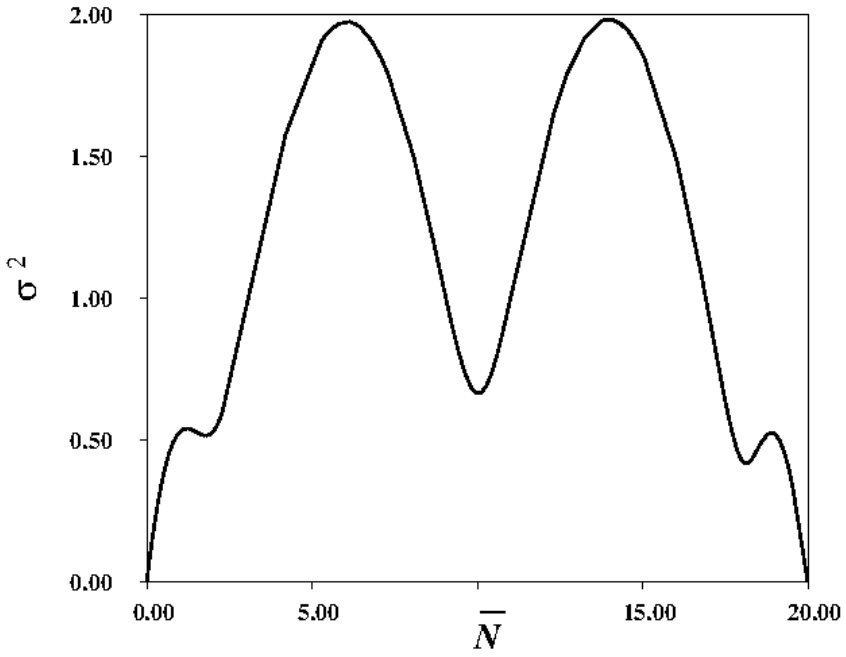

Figure 3: $\sigma^(\bar{N}(r_m))$ *vs.* $\bar{N}(r_m)$ for Ca

can be rewritten in terms of a surface integral thanks to the Stokes-Ostrogradskii theorem:

$$\frac{\delta||\boldsymbol{\sigma^2}||_F}{\delta V} = \oint_S \mathbf{n} \cdot \nabla\eta(\mathbf{r}) ds = 0 \tag{56}$$

in which $\eta(\mathbf{r})$ is a scalar function for which the bounding surface S is a zero flux surface. The determination of $\eta(\mathbf{r})$ from the expression of $||\boldsymbol{\sigma^2}||_F$ is hampered by the fact that $\sigma^2(\bar{N})$ involves a six dimensional integral and therefore good candidates have to be found among the function which account for the atomic shell structure already available. Ayers has introduced the covariance measure [170]

$$\xi^h_\sigma(\rho;\mathbf{r}) = \rho^\sigma \int h^{\sigma\sigma}(\mathbf{r},\mathbf{r}')d\mathbf{r}' \tag{57}$$

where $h^{\sigma\sigma}(\mathbf{r},\mathbf{r}')$ is the Fermi hole around the position $\mathbf{r}$.

2.3.2. The Electron Localization Function of Becke and Edgecombe

The Electron Localization Function (*ELF*) has been designed by Becke and Edgecombe to identify "localized electronic groups in atomic and molecular systems" [85]. It relies, through its kernel, $\chi(\mathbf{r})$ on the Laplacian of the HF conditional same spin pair probability scaled by the homogeneous electron gas kinetic energy density:

$$\chi(\mathbf{r}) = \frac{D_\sigma(\mathbf{r})}{D^0_\sigma(\mathbf{r})} \tag{58}$$

in which

$$D_\sigma(\mathbf{r}) = \tau_\sigma(\mathbf{r}) - \frac{1}{4}\frac{|\nabla\rho_\sigma(\mathbf{r})|^2}{\rho_\sigma(\mathbf{r})} \tag{59}$$

where $\tau_\sigma(\mathbf{r})$ is the σ spin contribution to the positive definite kinetic energy density. For a closed-shell singlet $D_\sigma(\mathbf{r})$ is the difference between the total positive definite kinetic energy density $T_s(\mathbf{r})$ and the von Weizsäcker kinetic energy density functional $T_{vW}(\mathbf{r})$ [171]:

$$D_\sigma(\mathbf{r}) = T_s(\mathbf{r}) - T_{vW}(\mathbf{r}) \tag{60}$$

whereas

$$D^0_\sigma(\mathbf{r}) = \frac{3}{5}(6\pi^2)^{2/3}\rho^{5/3}_\sigma(\mathbf{r}) \tag{61}$$

is the kinetic energy density of the homogeneous electron gas of density $\rho_\sigma(\mathbf{r})$. $\chi(\mathbf{r})$ provides a good approximation to Ayers's local covariance measure. In order to confined the function in the [0, 1] interval, a Lorentzian form has been adopted for the ELF:

$$ELF(\mathbf{r}) = \frac{1}{1+\chi(\mathbf{r})^2} \tag{62}$$

ELF fairly reproduces the shell structure of atoms even for heavy atoms for which other method fails.

Many other interpretations of ELF have been given so far in order to get expressions beyond the HF approximation or to provide relationships with other theoretical tools. Savin *et al.* have extended the ELF formula validity to DFT and Kohn-Sham orbitals. In this case the ELF kernel has the physical meaning of the ratio of the local excess kinetic energy density for the actual system and for the same density jellium. Orbital-based interpretations of ELF have been proposed by Burdett [172] and by Nalewajski *et al.* [173], who considered the non-additive interorbital Fisher information. Another route pioneered by Dobson [174] explicitly considers the pair functions. It has been independently developed by Kohout *et al.* with the Electron Localization Indicator (ELI) [68, 70] and by one of us [175], with the spin pair composition $c_\pi(\mathbf{r})$ enabling to generalize ELF to correlated wave functions [176, 177].

The Electron Localization Indicator is based on the restricted population approach which considers two local properties. On the one hand is the control property, ω, used to partition the space into mutually exclusive micro-cells Ω_i centred around the position $\mathbf{r}_i$, such as the integrated value of property ω has a fixed value. On the other hand, for ELI Kohout and coworkers have considered the electron density $\rho(\mathbf{r})$ and one of the spin components of the pair distribution $\Pi(\mathbf{r}, \mathbf{r}')$, the control quantity can be either a charge q or a number of pairs D. The ELI distributions are denoted by $\Upsilon^\sigma_\omega(\mathbf{r}_i)$ for same spin pairs and $\Upsilon^{\alpha\beta}_\omega(\mathbf{r}_i)$ for antiparallel spin pairs with $\omega = q$ or D. Connection with the ELF kernel can be achieved in the limit of infinitesimal volumes.

The spin pair composition is defined from the dimensionless ratio:

$$D_\mathrm{s}(\mathbf{r}) = 2\frac{\bar{N}_\parallel(\mathbf{r})}{\bar{N}(\mathbf{r})^2} \tag{63}$$

where

$$\bar{N}_\parallel(\mathbf{r}) = \int_V\int_V \Pi_{\alpha\alpha}(\mathbf{r}_1, \mathbf{r}_2)d\mathbf{r}_1 d\mathbf{r}_2 + \int_V\int_V \Pi_{\beta\beta}(\mathbf{r}_1, \mathbf{r}_2)d\mathbf{r}_1 d\mathbf{r}_2 \tag{64}$$

and $V(\mathbf{r})$ is a finite volume centred at the reference point $\mathbf{r}$ such as

$$\bar{N}(\mathbf{r}) = \int_V \rho(\mathbf{r}_1)d\mathbf{r}_1 \tag{65}$$

It had been numerically shown that

$$c_\pi(\mathbf{r}) = \bar{N}(\mathbf{r})^{-2/3}D_\mathrm{s}(\mathbf{r}) \tag{66}$$

is independent of the size of the volume. Moreover, $c_\pi(\mathbf{r})$ can be approximated by the ELF. That is:

$$ELF((\mathbf{r}) \approx \frac{1}{1+c^2_\pi(\mathbf{r})} \tag{67}$$

2.3.3. ELF gradient field analysis

Applying the gradient dynamical system partitioning technique to the ELF yields basins of attractors which correspond to cores, lone pairs and bond regions [63, 64]. As noted by Gillespie and Robinson: "This function (ELF) exhibits maxima at the most probable positions of localized electron pairs and each maximum is surrounded by a basin in which there is an increased probability of finding an electron pair. These basins correspond to the qualitative electron pair domains of the VSEPR model and have the same geometry as the VSEPR domains." [178]

The basins of the gradient field of ELF faithfully match the density partition of the Lewis's model. On the one hand are the core basins which gather the electron density of the inner atomic shells and on the other hand the valence basins accounting for the bond, lone pair and single electron domain. The core basins, labeled C(A) where A is the atomic symbol of the element, surround nuclei with atomic charge $Z > 2$. The number of core basins varies with the number of core shell of the element and also with the local symmetry in the molecule. For isolated atoms the spherical symmetry implies that the attractors corresponding to the electron pairs of the L, M, ... inner shells are degenerated on a sphere. There is therefore one basin for each shell. In molecules, the symmetry being lower than in isolated atoms, the number of core basins of atoms heavier than neon is larger than 1 and it is convenient to gather them in a single superbasin. It is sometimes interesting to consider the basins of the external core shell, the subvalence basins, to explain geometrical features [179, 180].

In the spirit of Lewis's model, the valence basins are characterized by the atomic valence shells to which they participate, or in other words by the core basins with which they share a boundary. The number of such atomic valence shells is called the synaptic order. Thus, there are monosynaptic, disynaptic, trisynaptic basins and so on. Monosynaptic basins, labeled V(A), correspond to the lone pairs of the Lewis model, and polysynaptic basins to the shared pairs of the Lewis model. In particular, disynaptic basins, labeled V(A, B) correspond to two-centre bonds, trisynaptic basins, labeled V(A, B, C) to three-centre bonds and so on. The valence shell of a molecule is the union of its valence basins. As hydrogen nuclei are located within the valence shell, they are counted as a formal core in the synaptic order because hydrogen atoms have a valence shell. For example, the valence basin of C-H bond is labeled V(C, H) and called protonated disynaptic. The valence shell of an atom, say A, in a molecule is the union of the valence basins whose label lists contain the element symbol A.

The concept of localization domain has been introduced [181] in order to discuss ELF isosurface graphical representations and also to define a hierarchy of the localization basins which can be related to chemical properties. A localization domain is defined as a volume limited by one or more closed isosurfaces $ELF(\mathbf{r}) = f$. It surrounds at least one attractor, in this case it is called irreducible, whereas if it contains more than one attractor, it is said reducible. Except for atoms and linear molecules, the irreducible domains are filled volumes, whereas the reducible ones can be either filled, hollowed or donuts. The increase of the bounding isosurface value splits the reducible domain into domains containing less attractors than the parent domain. The reduction of localization occurs at turning points which are index 1 critical points, located on the separatrix of the two basins involved in the parent domain. These critical points are called basin interconnection points often abbreviated by *bips* [182]. Ordering these turning points (localization nodes) by increasing $\eta(\mathbf{r})$ enables to build tree-diagrams reflecting the hierarchy of the basins [183].

2.3.4. The ELF population analysis

The ELF population analysis mostly relies on the calculation of the basin populations and of their covariance. The ELF populations are in general close to the intuitive values expected from the Lewis's pair model. This is consistent with the minimum variance interpretation of the ELF partition: the decomposition of Eq. 17 into spin contributions indicates that in the perfect localization limit σ^2 is zero only for a single electron or an opposite spin pair. The differences with the ideal population values are interpreted as consequences of local symmetry, electronegativity or mesomery. The basis set and correlation effects are consistent with chemical intuition [184]. The core populations are almost independent from the basis set quality, except for the STO-3G minimal basis set which systematically yields smaller values and some post Hartree-Fock methods (MP2, MP3, MP4 and QCISD) which often overestimate them by c.a. 0.1 e^- with respect to other methods. The populations of the monosynaptic basins decrease when polarization functions are added, whereas those of the disynaptic basins increase. The introduction of polarization functions does not change the separated atom energies but lowers the energy of the equilibrium geometry. In other words it increases the binding energy and thus the integrated density participating to the bond, *i.e.* the disynaptic basin population, is therefore expected. This implies a transfer of density from the monosynaptic basin (or lone pair) to the bond.

The ELF population analysis enables to define the valence shell population of an atom as the sum of the populations of the valence basins which encompass its core basin, *i.e.*:

$$\bar{N}_v(\mathrm{A}) = \sum_i \bar{N}[\mathrm{V_i(A)}] + \sum_{\mathrm{B}\neq\mathrm{A}} \sum_i \bar{N}[\mathrm{V_i(A,B,\dots)}] \tag{68}$$

This definition is consistent with the Lewis picture and it can be used to check the validity of electron count rules. The orbital contributions to the valence basins is another piece of information which, for example, enables to quantitatively estimate the σ-donation and π-back-donation in transition element complexes [185]. Combining the QTAIM and ELF/ELI-D approaches enables to define the contribution of the X atomic basin to the valence basin V(X,...) denoted by $\bar{N}[\mathrm{V(X,\dots)|X}]$. Raub and Jansen [186] have introduced a bond polarity index defined as:

$$p_{\mathrm{XY}} = \frac{\bar{N}[\mathrm{V(X,Y)|X}] - \bar{N}[\mathrm{V(X,Y)|Y}]}{\bar{N}[\mathrm{V(X,Y)|X}] + \bar{N}[\mathrm{V(X,Y)|Y}]} \tag{69}$$

A more general index is the bond fraction of the QTAIM atom X for the valence basin V(X,...), i.e.:

$$p(\mathrm{V(X,\dots)^X}) = \frac{\bar{N}[\mathrm{V(X,\dots)|X}]}{\bar{N}[\mathrm{V(X,\dots)}]} \tag{70}$$

The bond fraction ranges from 0.0, when the ELF/ELI-D basin does not overlap with the atomic basin of X, to 1.0 for a monosynaptic basin V(X) and is equal to 0.5 for a non polar bond [187]. In the ELI-D/QTAIM (or ELF/QTAIM) intersection technique, it is possible to recover the concept of oxidation numbers. The ELI-D based oxidation numbers (*ELIBON*) are calculated with the following formula:

$$ELIBON(\mathrm{X}) = Z(\mathrm{X}) - \bar{N}[\mathrm{C(X)}] - \sum \bar{N}[\mathrm{V(X,\dots)}] \cdot \Theta(N[\mathrm{V(X,\dots)}]) \tag{71}$$

where the sum runs over the valence basins defining the valence shell of centre X with

$$\Theta(N[\mathrm{V(X,\dots)}]) = \begin{cases} 0, \text{if there exists an atom Y with } p(\mathrm{V(X,\dots)^Y}) > p(\mathrm{V(X,\dots)^X}) \\ \frac{1}{m}, \text{if there exists } (m-1)\mathrm{X'} \text{with } p(\mathrm{V(X,\dots)^{X'}}) = p(\mathrm{V(X,\dots)^X}) = max \\ 1, \text{if all } p(\mathrm{V(X,\dots)^Y}) < p(\mathrm{V(X,\dots)^X}) \end{cases}$$

The population analysis is completed by considering the variance and covariance of the basin populations which help to understand the delocalization. A chemical explanation in terms of superposition of mesomeric structures can be derived from the population analysis data [100, 188] with the following assessments:

1. The electrons of the valence shell of an atom are distributed among the valence basins of this atom,
2. Non-bonding electrons are assigned to monosynaptic basins.
3. Bonding electrons are assigned to the polysynaptic basin whose label corresponds to the interpenetrating atomic shells,
4. several pairs may be assigned to one basin.

The calculation of ELF basin distributed multipoles moments [189] provides gives local moments related to bonds and lone pairs. A local multipole moment is expressed as the sum of the origin dependent charge transfer contribution, arising from lower order multipoles and the polarization contribution. The local dipolar polarization of the lone pairs is related to chemical reactivity, whereas bond quadrupole polarization moments which are related to the π character of the bonds, enable to discuss bond multiplicities, and to sort families of molecules according to their bond order.

The generalization to ELF basins of the interacting quantum atoms energy decomposition [134–137] can be achieved for the only potential energy because the ELF basin separatrix are not zero flux surfaces of the electron

density gradient field. However, the decomposition of the electron-electron repulsion into two-basin contributions:

$$V_{ee}(\Omega,\Omega') = \int_{\Omega}\int_{\Omega'} \frac{\Pi(\mathbf{r},\mathbf{r}')}{|\mathbf{r}'-\mathbf{r}|} d\mathbf{r} d\mathbf{r}' \tag{72}$$

which decompose in a purely Coulombic energy

$$V_{C}(\Omega,\Omega') = \int_{\Omega}\int_{\Omega'} \frac{\rho(\mathbf{r})\rho(\mathbf{r}')}{|\mathbf{r}'-\mathbf{r}|} d\mathbf{r} d\mathbf{r}' \tag{73}$$

and an exchange-correlation contribution

$$V_{xc}(\Omega,\Omega') = \int_{\Omega}\int_{\Omega'} \frac{\Pi_{xc}(\mathbf{r},\mathbf{r}')}{|\mathbf{r}'-\mathbf{r}|} d\mathbf{r} d\mathbf{r}' \tag{74}$$

is directly related to the VSEPR model as shown by Martín Pendás *et al.* [190].

2.3.5. The ELF classification of chemical interactions

The ELF analysis considers a dichotomous classification into shared-electron and unshared-electron interactions, proposed initially by Bader and Essén [143] in the QTAIM framework. In a shared-interaction the considered interacting atoms have at least one common polysynaptic basin in their valence shell. Covalent, dative and metallic bonds are subclasses of the shared-electron interaction whereas ionic, hydrogen and electrostatic bonds belong to the other class. The subclasses of each interaction are determined with the help of secondary criteria.

1. The core-valence bifurcation index, defined as the difference of $ELF_{(}$cv, the lowest value of the ELF for which the AH core basin is separated from the valence, and $ELF_{\mathrm{vv'}}$, the value at the saddle point linking the proton donor to the acceptor domains, called hydrogen bond interaction point. It indicates if an interaction is chemical or not. This index is useful to classify hydrogen bonds [191–193] and to characterize the adsorption on a catalyst [194]. It has been recently found that it provides a measure of the delocalization between the proton donor and proton acceptor moieties [195].

2. The topological behaviour of the ELF gradient field along the dissociative pathway is characterized by the variation of the number of basins, $\Delta\mu$, and if $\Delta\mu = 0$ by the variation of the synaptic order of the valence basin involved in the interaction ($\Delta\sigma$) [196].

3. The multiplicity of the disynaptic basin V(A,B) is not automatically correlated to an equal multiplicity of the A−B bond. On the one hand, the location of the attractors should be consistent with the symmetry of the system and therefore the disynaptic basins multiplicity can be explained by symmetry considerations rather than by chemical arguments. On the other hand, conventional multiple bonds are not always the dominant mesomeric structure of in realistic descripton of the system.

4. Multicentre bonds imply the presence of polysysnaptic basins.

5. When the bonding can be represented by a dominant mesomeric structure, the V(A,B) basin population should be approximately twice the expected bond order.

6. The covariance matrix elements (*i*) $\langle\widehat{cov}(\bar{N}[\mathrm{V_t(A)}], \bar{N}[\mathrm{V_t(B)}])\rangle$ where $\mathrm{V_t}$ is the union of the basins of the valence shell of A except V(A,B) or the V(A) and V(B) components of a protocovalent bond and (*ii*) $\langle\widehat{cov}(\bar{N}[\mathrm{C(A)}], \bar{N}[\mathrm{C(B)}])\rangle$ quantify respectively the delocalization in three-electron and charge-shift bonds and on the other hand in M-M bonds in polynuclear transition element complexes.

7. The bond polarity (p_{AB}) index enables to discuss polar bonds.

The properties of the different subclasses of bonds with respect to the above criteria are summarized in Table 5. Charge-shift and M-M bonds are on the borderline of the electron-shared and electron unshared interactions, because the disynaptic basin may be absent or replaced by a protocovalent pair of monosynaptic basins. The main difference with QTAIM based classification is that donor-acceptor bonds belong to the electron shared interaction.

Table 5: Classification of bonding interaction, according to *ELF* criteria. In the case of the charge-shift bonding V(A,B) may be replaced by a protocovalent pair of basin or absent, in M-M bond it may be absent.

bond type	ϑ	$\Delta\mu$	$\Delta\sigma$	$\bar{N}$[V(A, B)]	p_{AB}	covariance $\langle\widehat{cov}(\bar{N}[\mathrm{V_t(A)}], \bar{N}[\mathrm{V_t(B)}])\rangle$	$\langle\widehat{cov}(\bar{N}[\mathrm{C(A)}], \bar{N}[\mathrm{C(B)}])\rangle$
electron-unshared interactions							
van der Waals	>0	0	0			~ 0.0	0.0
weak H-bond	>0	0	0			~ 0.0	0.0
medium-strong H-bond	<0	0	0			~ 0.0	0.0
3*e*-bonds	<0					~ −0.3	0.0
intermediate bonds							
charge-shift bond	<0	≠ 0		<1.0		~ −0.2	0.0
M-M	<0			≪ 2× BO		~ −0.5× BO	
electron-shared interactions							
donor-acceptor	<0	0	≠ 0	~ 2× BO		~ 0.0	0.0
covalent	<0	≠ 0	0	~ 2× BO	~ 0.0	~ 0.0	0.0
polar covalent	<0	≠ 0	0	< 2× BO	≠ 0.0	~ 0.0	0.0

2.4. Treatment of heavy elements

In systems involving heavy elements, typically of period 6 and beyond, relativistic effects cannot be ignored. They can be taken into account by relativistic approximate calculations carried out in terms of one-electron 4-component Dirac orbitals within Dirac-Hartree-Fock, Dirac DFT and Dirac HF-CI. However, cruder approximations such as the Zero Order Regular Approximation (ZORA) hamiltonian, lead leading 2-component equations including spin-orbit and scalar interactions are also available. Spin-free core pseudo-potentials including corrections for the scalar interactions provide satisfactory results for a large number of cases.

Core pseudo-potentials must be used very carefully in topological analysis. In the QTAIM analysis the local maxima of the density which define the atomic basins are located at the nuclear position. In contrast, with core pseudo-potentials, there is a density hole and it is then necessary to search the interatomic bounding surfaces outside exclusion spheres surrounding the nuclear centres. In the case of the *ELF* analysis, the situation is even more critical because the valence basins *must* share a boundary with core basins. Consequently, only small core pseudopotentials can be used.

The two-component formalism is able to take the spin orbit coupling into account. A first indication of the importance of the spin coupling in ELF calculations has been presented by Schott *et al.* [197] in the framework of DFT calculations carried out with the ZORA hamiltonian incorporating scalar and spin-orbit (SO) relativistic corrections. The ELF and QTAIM analyses have been recently implemented in the spin-orbit DFT method [198] by Pilmé *et al.* [199, 200].

2.5. Computer programs

Richard Bader and coworkers have developed the first computational tools for the analysis of the electron density [201, 202]. The AIMPAC suite of program is available in open access at the URL: http://www.chemistry.mcmaster.ca/aimpac/-imagemap/imagemap.htm. The EXTREME 94 (EXT94b) locates the critical points (CPs) of the gradient fields of the

electron density as well as those of several other scalar fields such as the Laplacian of the electron density, the definite positive kinetic energy, the nuclear potential and the virial field. The properties used to classify the bonds are computed at these points. PROAIM [201, 202] and PROMEGA calculate integrated atomic basin properties: volume populations, multipoles, atomic kinetic, potential and total energies. These programs require a molecular wave function read in a `wfn` file provided by molecular program like Gaussian [203–206] or GAMESS [207]. AIM2000 [208–210] is an interactive program derived from AIMPAC which benefits from powerful graphical functionalities. AIMAll [211] works with `wfn, wfx` or Gaussian formatted checkpoint as input file. It handles correlated wave functions such as CCSD, CASSCF, CIS and support high angular momentum, up to h, basis functions. MORPHY98 is a program developed by Paul Popelier and his group [212–217] enabling the full topological analysis of the Laplacian. Cioslowski and coworkers have implemented vectorial algorithms and have contributed to introduce the QTAIM analysis in Gaussian94 and Gaussian98 [218, 219].

The electron density of periodic systems calculated with either CRYSTAL-98 [220] or EMBED-96 [221] programs can be analyzed with TOPOND98 [222]. This program carries out the topological analysis of $\rho(\mathbf{r})$ and $\nabla^2\rho(\mathbf{r})$, calculates the atomic basin properties (atomic volumes, spin components and total atomic populations, atomic kinetic and virial energies, atomic forces, "radial" atomic expectation values, atomic multipoles). TOPOND is now interfaced also with CRYSTAL-06 [223] and CRYSTAL-09 [224, 225]. These new versions of the code do not deal with properties depending on the non diagonal parts of the first-order density matrix. CRITIC [226, 227] is a program performing the topological analysis of the electron densities of crystalline solids. It works with LAPW (Linear Augmented Plane Wave) densities calculated by the WIEN2k package [228] or with *ab initio* Perturbed Ion (*ai*PI) densities [229]. It has the same functionality as TOPOND98.

An alternative procedure calculates the density on a grid further read in input by the QTAIM program. This technique pioneered by Iversen et al [230] uses the maximum entropy experimental density or a sampling of the density calculated by a muffin-tin plane wave method [231]. The analysis is restricted to the localization and characterization of the CPs and to the calculation of the Hessian matrix eigenvalues. Various algorithms provide accurate separatrices from numerical densities [232–235], enabling tthe calculation of basin properties. The InteGriTy program developed by C. Katan and coworker [233] is available in open access at the URL: http://www.gmcm.univ-rennes1.fr/moleculaire/integrity/index.htm whereas the program of Arnaldsson, Tang and Henkelman [234, 235] can be downloaded from http://theory.cm.utexas.edu/bader/

The TOPXD program [236] performs the complete topological analysis of experimental charge densities based on the Hansen-Coppens multipole formalism [237]. It is an adaptation of TOPOND98 to densities calculated within the aspherical atom refinement by the XD program [238]. The latest version of XD, XD2006 [239], includes the full topological analysis of electron densities and its derivatives and the Source Function analysis. PAMoC [240] carries out the analysis of experimental densities obtained by the Stewart multipole refinement formalism [241] and stored by the ValRay [242] program in a dedicated binary file.

The TopMod program [176, 177, 243] carries out the topological analysis of the ELF and electron densities gradient fields. The derivatives and the integrated basin properties are calculated analytically. TopChem [244] performs the analysis of different scalar functions ($\rho(\mathbf{r})$, $-\nabla^2\rho(\mathbf{r})$, ELF, Molecular Electrostatic Potential (MEP)) with a fully numerical grid-based algorithm. It enables the study of both molecular and periodic systems. An ELF version of CRITIC has been developed by Contreras-Garcia *et al*. [245] DGrid [246] is a very complete and general topological analysis program. It treats many local functions as ρ, ELF, ELI-D, ELI-A [68, 69], LOL [247], the Local Source function [86], the domain averaged Fermi-hole [248], etc... It performs the conversion of wave functions generated by many quantum chemical programs to an internal format. It locates the CPs, calculates their properties, determines the basins and carries out integrations over their volumes and calculates the delocalization indexes. It can be downloaded at http://www.cpfs.mpg.de/ kohout/dgrid.html. Multiwfn [249] is a multi-purpose wave function analysis program. It enables to carry out almost all the population analyses as well as the topological analysis of large sample of local functions such as $\rho(\mathbf{r}), \nabla^2\rho(\mathbf{r}), ELF, LOL, \ldots$. In input it accepts many types of files such as wfn, wfx, and fch. It includes a visualization module. The souce code iand the executables for several platforms (Windows, Linux and Mac OS X) can be downloaded at https://multiwfn.codeplex.com.

Finally we notice the EDF program [250] which computes the probability distribution functions over QTAIM and ELF basins determined in a previous calculation.

3. Bulk metals alloys and intermetallic phases

There is no clear chemical explanation of the diversity of the crystalline structures of bulk metallic elements. Usually the number of nearest neighbours is larger than the formal valence of the elements. In this case, neither partial two-centre nor multicentre bonding pictures are able to predict the local environment of each atom of the cell. The applications of the topological methods are expected to help the understanding of bonding in bulk metals. On the QTAIM side several questions have to be answered: are there bond paths between nearest neighbour atoms? are there non-nuclear attractors (NNAs)? how large is the population of these latter? how large is the variance of the atomic basin populations? The ELF/ELI analyses would provide the location of the valence attractors, the synapticity of the valence basins, the populations of these latter as well as insights on the delocalization. For both approaches very few papers have been published on this topic and unfortunately there are many missing entries. The reliability of the results often depends on the method used to determine the electron density and the localization function which are expected very flat in the valence regions. For example, the occurrence of NNAs in hexagonal close packed (hcp) Be has been a debated problem. Experimentally, their absence or their occurrence depends on the model used to extract the electron density. The maximum entropy method (MEM) with a procrystal density as a non-uniform prior does not yield NNAs [251] while they are recovered by a MEM analysis with uniform prior or a more conventional multipole model refinement approach [230]. Jayatilaka used the same set of experimental data to invert the Kohn-Sham equations in order to reconstruct Kohn-Sham crystalline orbitals which in the present case do not yield NNAs [252].

A systematic study of the ELI attractors has been carried out by Baranov and Kohout [253] for the hexagonal crystalline structure of 21 elements belonging to the main groups 1 and 2 as well as transition series. Except for Os, the positions of the attractors are near the centre of interstitial polyhedra or on the face of two similar polyhedra. The proposed nomenclature is Td and Oh for positions near the centre of a tetrahedron and of an octahedron, Td|Td and Oh|Oh for positions on shared faces. Table 6 summarizes the results of Baranov and Kohout obtained with vawe functions calculated with the FLPO code [254] with minimal localized basis functions. Calculations carried out with

Table 6: Attractor positions,synaptic order, basin populations of hexagonal crystalline structure of metals. For osmium OsOs positions are located near the middle of nearest neighbour lines, *ab* in a plane parallel to (001), *c* in a direction parallel to [00]

Attractors	synaptic order	population	Metals
Td|Td	5	1.94	Be, Mg
Td|Td	5	1.06-1.47	Sc, Ti, Y, Zr
Oh	6	1.04-1.13	
Td	4	0.22-0.43	Ca, Sr, Ba
Oh	6	0.83-1.03	
Oh|Oh	3 or 9 (Li)	0.19-1.17	Li, Na, Zn, Cd, Re
Td	4	0.18-1.21	
Oh|Oh	3	0.07-0.52	Cr, Fe, Co, Ni, Tc, Ru
Td	4	0.65-0.92	
Oh	6	0.39-0.85	
OsOs-*ab*	2	0.47	Os
OsOs-*c*	2	0.34	

the Exciting program [255], which uses both augmented plane waves and localized orbitals, yield different attractor

patterns for 13 of the 21 the investigated metals due to migration, splitting or annihilation of attractors. Such effects are also observed upon isotropic cell rescaling. Non nuclear attractors are found for Li, Be and Sc at the positions of the ELI-D attractors. These results support the picture provided by the jellium model in which the density as well as the ELI-D function are strictly constant outside the core basins. Therefore both the gradient and the Hessian matrix elements of these two functions are identically zero in these regions and all the points are non hyperbolic critical points. In real and calculated systems the fulfilment of the hyperbolicity requirement ensures the structural stability of the gradient dynamic systems. However, it is conceivable that a rather small variation of the control space parameters (*i.e.*, the nuclear coordinates, the method of calculation, ...) should be strong enough to make some of them non hyperbolic and therefore to yield a changes of topology through bifurcation catastrophes.

Alkali and alkaline-earth elements. At zero pressure and room temperature, the stable modification of alkali metal is body centred cubic (bcc). However, at low temperature, Li and Na lattices are of the α-Sm (9R) type [256] which can be viewed as a distorted hcp structure. Under compression both bcc and 9R evolve towards a face-centred cubic (fcc) structure and later exhibit the same pressure-induced symmetry lowering [257]. The electron density of the bcc structure of Li and Na have been first investigated by Mei *et al.* who found a network of NNAs located at position (8*c*). In another periodic calculation, carried out with a split-valence basis set the NNAs are found at positions (12*d*) for Li and K and (24*h*) for Na [109]. In all investigated systems, the density function is almost constant in the interstitial regions. Baranov and Kohout [258] have calculated and analyzed the covariance of the atomic populations of bcc sodium. The value of the diagonal element $\langle\sigma^2(\mathrm{Na},\mathrm{Na})\rangle = 0.80$, is almost twice that calculated for Na_2 (0.50), whereas the covariance elements amount -0.05 which each first neighbour atom and -0.03 with each second neighbour. This implies that the sum of the covariance matrix elements involving the remaining atoms is $8\times0.05 + 6\times0.03 - 0.6 = -0.22$ showing that the delocalization extends to atoms which do not share any boundary.

The ELF and ELI-D attractors are found in interstitial tetrahedral or octahedral positions which varies with the method used to determine the wave function. For example, the valence attractors are found in position (6*b*) by periodic Hartree-Fock [109] and TB-LMTO-ASA [259] or in (12*d*) by FPLO calculations [259]. The localization window defined as the interval $[ELF(\mathbf{r}_a), ELF\mathbf{r}_s)]$ where $ELF(\mathbf{r}_a)$ and $ELF(\mathbf{r}_s)$ are the value of ELF at the valence attractors and at the index 1 saddle points between valence basins. For all systems, the localization window is very narrow: 0.003 for Li and Na, 0.016 for K.

Under very high pressure, the valence density of bulk alkali metals tends to be more localized than in the low pressure phases. This is evidenced by the value of ELF at the valence attractors which takes values of the order of 0.9 and higher [260, 261]. In the potassium crystal above 25 Gpa, ELF displays valence maxima ($ELF \approx 0.95$) at interstitial positions the basins of which containing roughly 2 e^- each [260]. In the $C2cb-40$ phase of Li at 85 Gpa, the ELF analysis reveals three sets of attractors, denoted $M1, M2, M3$, each located on a 8*b* site with rather high values of ELF of 0.961 ($M1$), 0.947 ($M2$), and 0.896 ($M3$). The basins of these attractors form pseudo anions holding 2, 2, and 1 e^-, for $M1, M2$ and $M3$ respectively which can merge in superbasins containing up to six electrons and separated by regions where $ELF < 0.4$ [261].

The structures of alkaline-earth metals are closed packed except for Ba and Ra which crystallize in the bcc system. Non nuclear attractors are found in tetrahedral sites for hcp Be [253] and cubic closed packed (ccp) Ca [109]. The ELI-D attractors are found on the shared face of two tetrahedral interstices for hcp Be and Mg, in both tedrahedral and octahedral sites for hcp Ca-Ba. The valence population decreases as Z increases: 1.98 e^- for Be and Mg, 1.75 e^- for Ca and Sr and 1.27 e^- for Ba. The populations of the basins located in octahedral sites are always larger than those of the tetrahedral ones. In the ccp structure of Ca the ELF attractors are located at positions (8*c*) at the centre of tetrahedra.

Transition elements. The shell populations of the first transition atoms are close to the occupancies of the corresponding atomic ground state atomic configurations [262]. It can be therefore expected that the bonding in bulk transition elements would present similarities with alkaline and alkaline-earth elements. Most of transition series elements crystallize in closed packed structures (hcp and ccp), however group 5 and 6 metals have a bcc structure whereas Mn is cubic and Hg rhombohedral. In all systems studied either by ELF [109] or by ELI-D [253, 258] the attractors are found either in interstitial positions or on shared faces of polyhedra. The calculated valence populations are generally slightly larger than those found for alkali and alkaline-earth metals, for example it attains 1.75 e^- for the hcp modification of Sc which has formally one electron in its valence shell [253]. The excess with respect with the formal

occupancy increases with the atomic number.

Group 13-15 elements. Only few topological studies have been published so far on the bonding in metallic main group elements crystals and all concern Aluminium. Aluminium crystallizes in the fcc system and therefore each atom is surrounded by twelve nearest neighbours. The one-electron density analysis based on a periodic Hartre-Fock wave function [109] revealed the presence of NNAs at special positions 24*d* and 96*k*. The attractors of the ELF are found at positions 24*d*, *i.e.* at the bond midpoints for calculations carried out either in the LMTO-ASA [259, 263] or Hartree-Fock [109] frameworks whereas FLPO yields attractors at positions 32*f*, that is shifted towards the tetrahedral voids. The ELF value at the saddle points linking the valence basins are slightly lower than those at the attractors, *i.e.* 0.58 *vs.* 0.62.

In order to have a flavour on the bonding in bulk main group metals we have carried out periodic Hartree-Fock calculations on the crystalline phases of gallium, indium and tin at their experimental lattice parameter values [264]. Gallium has a *Bmab* structure in which each atom is surrounded by seven neighbours: one at 2.44 Å and the six remaining ones in three groups of two at distances between 2.7 and 2.8 Å. The left side of Figure 4 displays the $ELF = 0.6$ localization domains of Ga. The valence attractors are distributed in two sets. In the first group, 8 attractors with $ELF = 0.77$ are located at position 8*f* whereas the 16 attractors of the second group found in 16*g* correspond to a lower ELF value (0.70). Each pair of Ga atoms at 2.44 Å is connected by two disynaptic valence basins whose attractors belong to the first set. The basins on the attractors of the second group are also disynaptic and involve the Ga pairs at 2.70 Å. The basins of the $ELF = 0.70$ attractors are connected by $ELF = 0.46$ saddle points. They determine successive strata of localization domains extending in the directions perpendicular to the *c* axis. The connections along the *c* direction happen for $ELF = 0.29$. This is consistent with the anisotropy of the electrical resistivity [265]

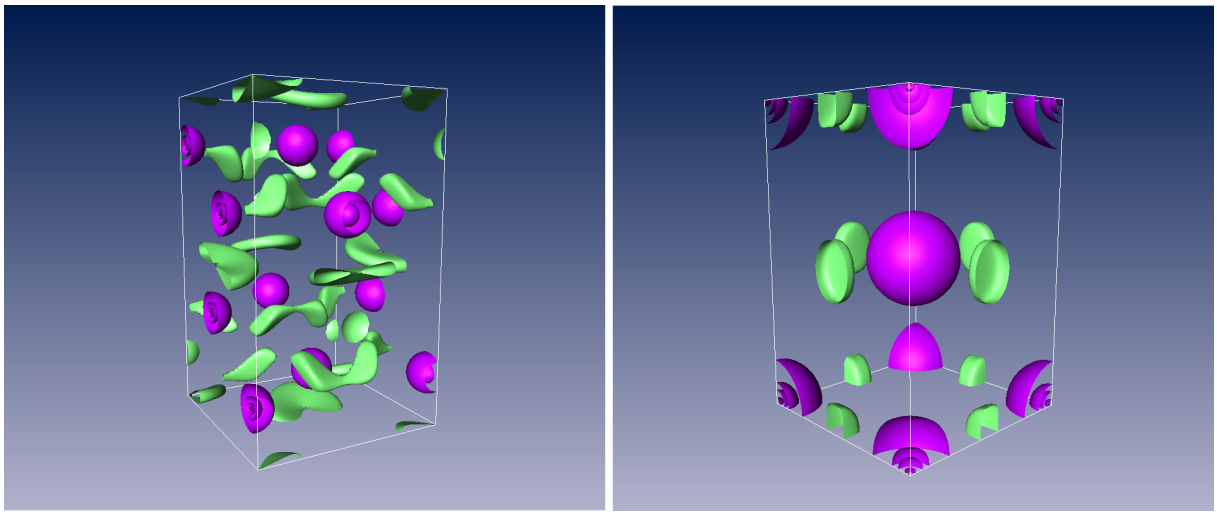

Figure 4: Left: Ga $ELF = 0.6$ localization domains, right: In $ELF = 0.45$ domains. Color code: magenta = core, green = disynaptic valence.

The valence attractors of indium are located at the nearest neighbour bond midpoints (position 4*c* of the I_4/mmm group) as shown in the right side of figure Figure 4. The ELF function value at these attractors is 0.535. In order to merge the irreducible valence domains into a single reducible one it is necessary to lower the ELF value of the bounding isosurface to 0.353, the linking saddle points being in position 8*f*, in other words at the midpoints of the second neighbour distance.

The crystalline structure of the conducting phase of tin (white tin) is I_{4_1}/amd. Each atom is surrounded by a first shell of four neighbours at 3.02 Å forming a distorted tetrahedron and by a second shell of six atoms slightly farther. Figure 5 displays the localization domains of white (left side) and grey (right side) tin. The ELF attractors are located at the midpoints of the first neighbour bonds. The value of ELF at this point is rather high, 0.74 whereas the saddle

points between the basins have an ELF value of 0.46. Grey tin is an insulator, it has a diamond structure and the attractors of the ELF, also located at the Sn-Sn bond midpoints, have a larger value (0.85) than those of white tin. This value is consistent with the picture of a covalent bonding expected in an insulating material.

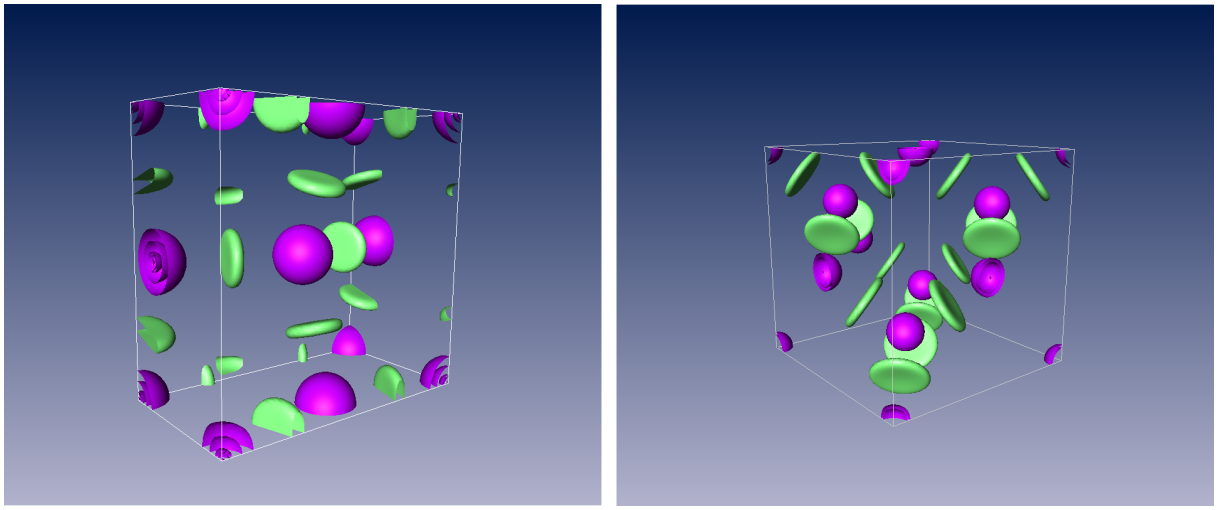

Figure 5: Left: white tin $ELF = 0.65$ localization domains, right: grey tin $ELF = 0.76$ domains. Color code: magenta = core, green = disynaptic valence.

The bonding in bulk metals appears to result of a competition between the jellium and the covalent limit pictures. Although the number of valence electrons and the core size of the element are certainly the dominant factors which determine the bonding, the lack of data on main group metals prevent from drawing conclusions. As a general rule, when the number of valence electrons is less than 3 (*i.e.* alkali, alkaline-earth and transition elements) the jellium picture prevails and therefore the maxima of the ELF or ELI-D are found within the interstitial voids yielding polysynaptic localization basins. Such non directional bonding favours closed packed (hcp and ccp) or semi closed packed (bcc) structures. However, the phase diagrams of many metals present several modifications. Our preliminary results on Ga, In and Sn, and to a lesser extend those on Al, indicate that the two centre character of the bonding becomes predominant for group 13-16 metals. The closed packed structures of thallium and lead are not consistent with this statement.

3.1. Alloys and intermetallic phases

Alloys and intermetallic phases display a great diversity of M-M interactions including ionic bonding as well as covalence. With this respect, the topological analysis of ELF (or ELI-D) is particularly suitable to characterize the bonding as exemplified in the classical review article of Savin *et al.* [65] on the ELF and in several more recent reviews dedicated to particular classes of alloys and intermetallic phases [187, 266, 267]. The QTAIM partition provide additional pieces of information since it enables to quantify the charge transfers occurring between different atoms. Among the studied systems we can mention systems containing aluminium atoms [63, 263, 268–270], gallium [182, 271, 272], Laves phases [273], Heusler and half-Heusler alloys [187, 274] and Zintl Klemm phases [275–278].

3.1.1. Al-containing alloys and intermetallic phases

Historically, the study of the intermetallic phases containing aluminium has been one of the motivations for carrying out the ELF partitioning [63, 263] who studied the series Al $\longrightarrow$ CaAl $\longrightarrow$ SrAl $\longrightarrow$ BaAl $\longrightarrow$ CaAlSi $\longrightarrow$ Si with the help of the LMTO method in order to observe the qualitative as well as quantitative changes occuring when going from an expected purely metallic bonding to a purely covalent one. $CaAl_2$ belongs to the particular category of intermetallic compounds called Laves phase, in this system, each calcium transfers one electron to the Al network as indicated by the QTAIM analysis. Each Al atom has 6 Al nearest neighbours which are involved in disynaptic

V(Al,Al) basins populated by 1.30 e^-. In $SrAl_2$ the alkaline-earth centres are formally Sr^+. Each Al has 5 nearest neighbours which form a covalent network of hexagonal and square rings; there are three types of Al-Al bonds corresponding to internuclear distances of 2.786 Å, 2.799 Å and 2.930 Å which give rise to V(Al,Al) disynaptic basins with populations of 2.01, 2.13 and 1.60 e^-, respectively. The bonding situation is quite different in $BaAl_4$: on the one hand the net charge of Ba is +0.65 e^- and there are two kinds of Al atoms, the basal atoms with a positive charge of 0.63 e^- and the apical ones with a negative charge of -0.75 e^-. Disynaptic basins connect both apical atoms one another ($\bar{N}[V(Al_{ap}, Al_{ap})] = 2.05e^-$ and apical atoms to basal ones ($\bar{N}[V(Al_{ap}, Al_{bas})] = 1.45e^-$). In the last compound, $CaAl_2Si_2$, there are only V(Al,Si) and V(Si) valence basins.

The $CuAl_2$ structure is usually described in terms of a common building element, a square antiprism $[CuAl_{8/4}]$. Closely related arrangements are found in other intermetallic phases such as Pt_3Ga_7, $PdSn_4$, $PtSn_4$, $PtPb_4$, $RhBi_4$ and $PdGa_5$. The atomic net charges evaluated in the QTAIM framework are respectively -1.6 for Cu and +0.8 for Al in agreement with the electronegativity difference [268]. The ELF analysis reveals three kinds of valence basins (see Figure 6) which account for the bonding in polyhedra and between polyhedra. The V(Al,Al) basin, denoted Ω_A in Figure 6, has its attractor located at the midpoint of the shortest Al-Al contact which connects a building block to another. The *ELF* value at the attractor, 0.80, and the calculated population close to 2 e^- are consistent with a covalent bond. The V(Al,Al,Cu,Cu) basin (Ω_B) is shared by two polyhedra. Its population which is very sensitive to the quantum chemical method of calculation ranges from 1.4 e^-(LMTO-ASA) to 2.7 e^- (FLPO). The third kind of basin, V(Al,Cu,Cu) which has a population ranging from 0.8 e^-(LMTO-ASA) to 0.3 e^- (FLPO) belongs to a single polyhedron. The *ELF* is very flat in the regions close to the V(Al,Al,Cu,Cu) and V(Al,Cu,Cu) basin boundary and the values at the attractors are respectively 0.60 which can be interpreted as a consequence of the delocalization between these basins.

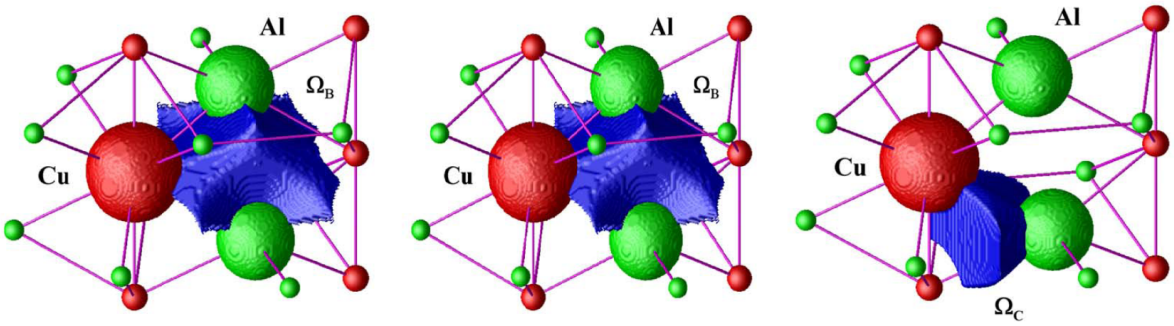

Figure 6: *ELF* basins of $CuAl_2$. Color code: green= C(Al), red=C(Cu), magenta=V(Al,Al) (Ω_A), blue=V(Al,Al,Cu,Cu) (Ω_B) and V(Al,Cu,Cu) (Ω_C). Adapted with permission from Journal of Solid Sate Chemistry, 179, 177O. Copyright (2006) Elsevier Inc.

The QTAIM partition of the Al_5Co_2 crystal shows three types of aluminium centres, Al(1), Al(2), Al(3) with atomic populations all close to 12 e^- and two types of cobalt atoms Co(1) and Co(2). The Co(1) centres which are surrounded by 3 Al(2) and 6 Al(3) have an atomic population of 29.5 e^- while the Co(2)s have larger population of 30.5 e^- and have 2 Al(1), 2 Al(2) and 6 Al(3) neighbours [270]. The ELI-D displays disynaptic basins V(Co(1),Al(3)) and V(Co(2),Al(2)) as well as small basins located in tetrahedron formed by one Co and 3 Al. The basin population of V(Co(1),Al(3)), 0.92 $^-$ is the sum of contributions from Co(1), Al(3) and to a lesser extend Al(2) atomic basins amounting to 0.49, 0.31 and 0.11 e^-, respectively. The population of V(Co(2),Al(2)) is small, *i.e.* 0.39 e^-, and equally distributed between the two atomic basins. Finally, the sum of the population of the interstitial basins amounts to 1.07 e^- distributed between the Co(1), Co(2), Al(1) and Al(3) type atoms. This bonding picture suggests an organization in terms of interacting $Co(1)Al(3)_6$ and $Co(2)_3Al(2)_3$ atomic clusters [270].

3.1.2. Laves phases, half-Heusler compounds and Zintl-Klemm phases

Laves phases are constituted by a group of intermetallic systems of stoichiometry AB_2 in which A is generally an alkaline or alkaline-earth element and B another metal element. The B atoms form tetrahedra around the A centres

and the atomic site ratio ranges from 1.06 to 167. The bonding is mostly governed by the electronegativity difference between A and B which is expected to rule the charge transfers between A and B atoms as well as the valence electron concentration. The QTAIM and ELI-D partitions carried out on a large representative sample of systems by Ormeci *et al*. [273] confirm this hypothesis as illustrated in Figure 7. All the ELI-D attractors are usually located inside

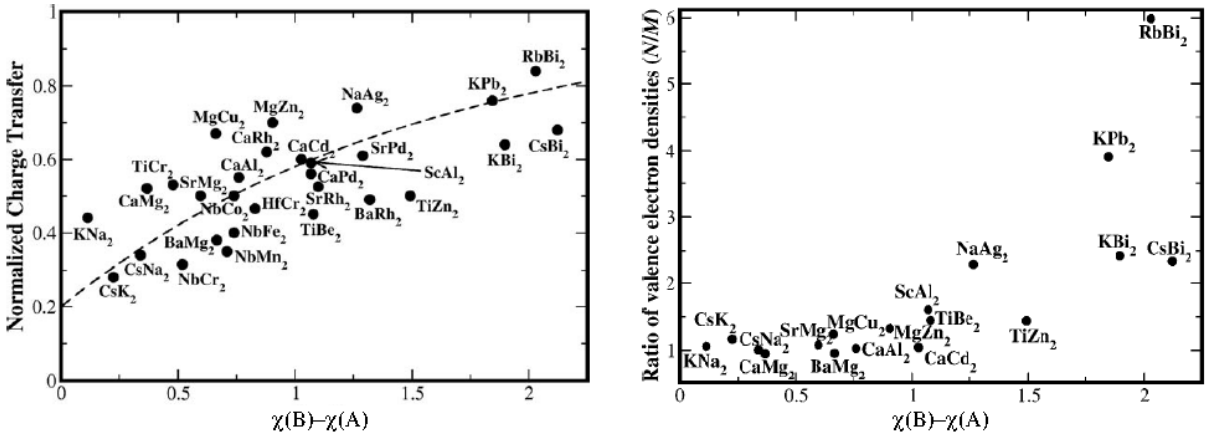

Figure 7: QTAIM charge transfer (left] and ratio of the valence electron density (right) *vs.* Sanderson's electronegativity difference. Adapted with permission from Angew. Chem. Int. Ed. 49, 8997. Copyright (2010) Wiley-VCH Verlag GmbH & Co. KGaA, Weinheim

polyhedra formed by A and B atoms, for example in the A_4 and AB_3 tetrahedra in systems containing only alkali metals. In KPb_2 six attractors are found in the external shell of each Pb atom which implies a local closed-shell like configuration and therefore a rather covalent bonding within the Pb_4 tetrahedra.

Non metal or semi-metal atoms enter in the composition of many half-Heusler phases of the MgAgAs-type and Zintl Klemm compounds. In this case, most of the *ELF* or ELI-D studies do not report the presence of basins involving two metal atoms [187, 274, 279] whereas the QTAIM delocalization indexes between atomic centres are often close to zero. Exceptions have been found for compounds whose composition involves two transition elements like TMTM′Sb or TMTM′Sn for which δ(TM,TM′) is calculated greater than 0.25 [279]. In Zintl-Klemm phases M-M interactions other than ionic are observed in polyanions of post-transition elements. In the K_8In_{11} and Rb_8In_{11} systems, the *ELF* attractors are located at the top of the In_{11} deltahedra [275]. The configuration of the valence attractors does not correspond to any well known representation of the chemical bond and corresponds to a shell of valence electrons experiencing a central potential, a picture consistent with the shell structure model of clusters [280, 281].

4. Two centre M-M bonds in molecular systems

4.1. M-M bonds of groups 1 and 2 elements

All the combinations of alkali metal diatomic molecules have been observed either in the gas phase or at very low temperature in solids. Although no stable complex involving two bonded group 1 elements have been reported so far [15], neutral and charged clusters, M_n or M_n^{a+} have been studied by quantum chemical techniques. QTAIM studies have been reported for Li_2 [105–107], Na_2 and Na_4 [105], Li_n planar clusters ($n = 4, 5, 6$) [106]. In all systems there is no bonding critical point between pairs of atoms, instead the alkali centres are linked through non-nuclear attractors located either at the M-M midpoint for bimetallic clusters or close to the centres of triangles formed by the alkali atoms for the planar systems. The populations reported for the basins of the non-nuclear attractors are of the order of 1 e^-. The *ELF* and ELI-D of the gradient fields of Li_2 [282, 283] are characterized by a circular attractor in the bond mid-plane perpendicular to the Li-Li line which defines a unique V(Li,Li) disynaptic valence basin with a population very close to 2 e^-. In higher stoichiometry clusters Li_n, $n = 3, 6$ in their ground state, only Li_3 has clearly disynaptic basins one with a population of 1.15 e^- and a negligible spin density and two with a population of 0.98 e^- in which the

unpaired electron is delocalized implying a large covariance of their populations [282]. In the high spin complexes, it is again Li_3 which has disynaptic basins, with a population of 0.98 e^- each, the single electron being equally shared [282]. In the complexes of stoichiometry larger than 3, the bonding is ensured by multisynaptic attractors as described in section 5.

Alkaline-earth metals do not form chemically bounded dimers but instead van der Waals complexes. The stabilization of the dimer at room temperature requires the presence of ligands like in guanidinato and β-diketiminato magnesium(I) dimers [15] whereas computational studies predict a reasonable stability for PhMMPh. The study of Berski and Durlak addresses the stability and the nature of the bonding in the $[C_{10}H_{18}Mg_2N_4]$ and $[C_{10}H_{18}Ca_2N_4]$ model compounds. The $\rho(\mathbf{r})$ gradient field of $[C_{10}H_{18}Mg_2N_4]$ presents a non-nuclear attractor whatever is the functional used to calculate the electron density, whereas there is no NNA whatever the DFT calculation level for $[C_{10}H_{18}Ca_2N_4]$. In Mg_2^{2+} which has a $D_{\infty h}$ symmetry, the *ELF* analysis shows a circular attractor in the σ_h plane, the presence of ligands lowers the symmetry giving rise to three valence point attractors. The populations of the three V(Mg,Mg) basins sums up to c.a. 1.96 e^-. For the $[C_{10}H_{18}Ca_2N_4]$ complex, there are only two V(Ca,Ca) attractors and the sum of their basin populations is also close to 2 e^- [284].

4.2. Transition elements homometallic bonds

4.2.1. Multiple M-M bonds

The concept of a multiple bond between two metal atoms was introduced by Cotton *et al.* in 1965, upon crystallization of the dipotassium dirhenium octahalide compound, exhibiting a very short Re-Re distance of 2.24 Å[9]. The latter was assigned to a quadruple $\sigma^2\pi^4\delta^2$ bonding between two $[ReCl_4]^-$ units. Since then, many transition element complexes, featuring double up to quintuple M-M bonds were reported and reviewed [3, 36, 285]. Figure 8 displays some early representatives, the chromium complexes excepted. In the latter, the quintuple Cr-Cr bonds are very short and confined in a much narrow bond distance range than the quadruple Cr-Cr bonds, suggesting that they are approaching the lower limit of the M-M bond distance [286].

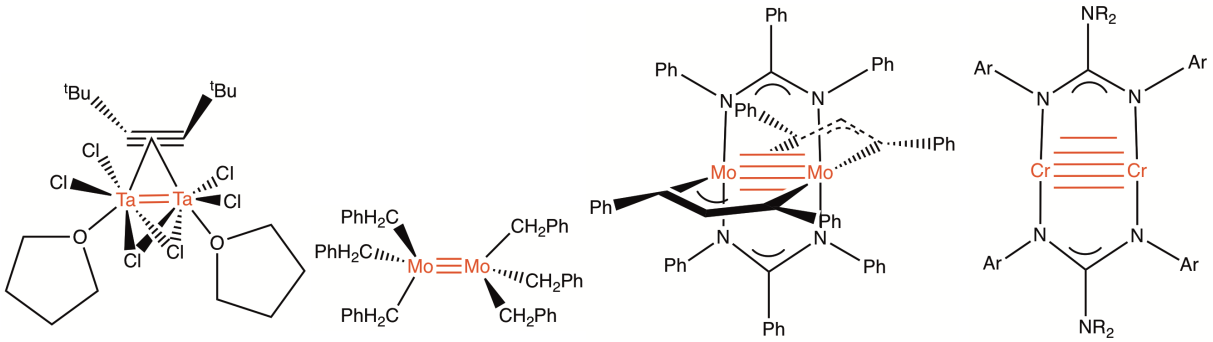

Ta-Ta: 2.68Å[287] Mo-Mo: 2.18Å[288] Mo-Mo: 2.092Å[289] Cr-Cr: 1.71Å[11]

Figure 8: Examples of multiple M-M bonds

Numerous theoretical studies, based on molecular orbital (MO) analysis, Energy Decomposition Analysis (EDA) or QTAIM and ELF topological analyses, have been devoted to the nature and the strength of multiple M-M bonds. They generally rely on single-determinant descriptions of the electronic structure, although multireference methods such as CASPT2 may be sometimes required for the determination of the relative stability of the various electronic states of the polymetallic compounds and the accurate description of the included M-M bonds [290].

J. Andres *et al.* performed QTAIM and ELF topological analyses of a series of so-called "paddlewheel" bimetallic complexes [291], involving second row transition elements, bridged by four chelating formamidinate ligands (Figure 9). Within this series, the M-M bond fluctuates widely from a very strong quadruple Mo-Mo bond to a weak Pd-Pd interaction (Table 7). Although a large QTAIM Mo-Mo delocalization index of about 3.0 is consistent with the anticipated quadruple Mo-Mo bond, the low value of the electron density at the related bond critical point made

the classification of the Mo-Mo bond ambiguous from QTAIM only. The four equivalent disynaptic V(Mo,Mo) valence basins of low population (0.15 e) and the huge electron delocalization between the metallic cores (cov(C(Mo), C(Mo)) = -1.255) are the ELF signatures of the Mo-Mo quadruple bond. This ELF picture of the M-M bond may be related to charge-shift bonding, introduced recently for the description of the C-C bonds of the propellane ring and for hydrogen-halide bonding [292]. Charge-shift or M-M bonds are at the borderline of electron-shared and closed-shell interactions because their disynaptic basin may be absent or replaced by a protocovalent pair of monosynaptic basins [40]. From this topological picture, the Mo-Mo multiple bond may be described by a resonance between several electron configurations due to the fluctuation of the metal d electrons within the cores. The bond orders ranging from zero (Pd) up to four (Mo) linearly correlate with the M-M distances and the covariances between the metal cores (Table 7) [291]. .

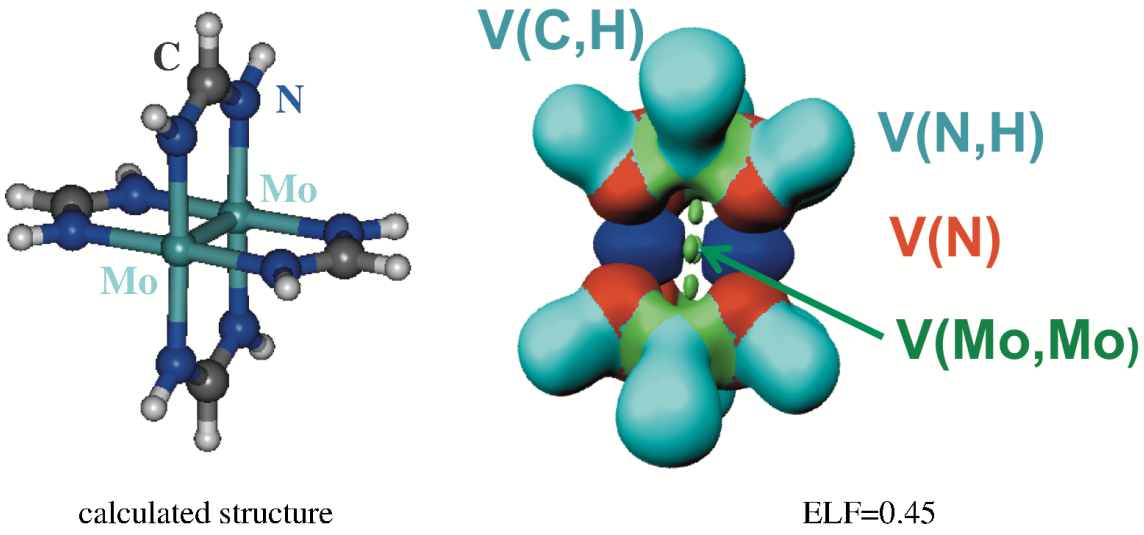

Figure 9: Calculated structure and ELF topological analysis of the paddlewheel bimetallic Mo complex featuring a quadruple Mo-Mo bond. B3LYP/Def2TZVP level of calculation.

Table 7: Bond length R(M-M), formal bond order B.O., QTAIM delocalization index δ(M,M), basin population $\bar{N}$[V(M, M)] and core population covariance matrix element $\langle\widehat{\sigma^2}(\mathrm{C(M)}, \mathrm{C(M)})\rangle$ for a series of "paddlewheel" bimetallic complexes

	M = Mo	M = Ru	M = Rh	M = Pd
R(M-M) (Å)	2·092	2·493	2·459	2·691
B.O.	4	2	1	0
δ (M,M)	2·93	1·316	1·035	0·294
$\bar{N}$[V(M, M)]	0·15×4	0·25	0·32	
$\langle\widehat{\sigma^2}(\mathrm{C(M)}, \mathrm{C(M)})\rangle$	−1·255	−0·551	−0·373	−0·124

With a current record of 1.71 Å, the ultrashort Cr-Cr bonds in aminopyridinate, amidinates or guanidinates chromium complexes [285, 293] have been assigned to quintuple Cr-Cr bonds enforced by chelating ligands steric constraints [293]. The corresponding Cr-Cr bond order of 4.2, calculated from the QTAIM delocalization index between the Cr atoms [294], is consistent with a formal quintuple Cr-Cr bond. ELI-D studies show that the electrons for the Cr-Cr bonding are not only localized in the valence region, but can also be found in the spatial region of the third shell of chromium atoms. The majority of the QTAIM bond order contribution (57%) are indeed found to

originate from the two chromium third atomic shell similarly to earlier reports and description of the quadruple bond of Mo_2(formamidinate)$_4$ [288]. A significantly lower value of the QTAIM delocalization index of 3.6 was obtained for a Cr_2 dimer bonded to two diazadiene ligands, indicating a substantial difference from the Cr-Cr bonding in the above amidinates complexes [295]. Bond orders weaker than 5 are also consistent with the MO analysis in which the quintuple bond implies five metal-based orbitals for M-M bonding. Besides to the major electronic configuration with all the bonding σ, π and δ occupied orbitals, a sizeable configuration corresponds to a double excitation $(\delta)^2(\delta^*)^2$. The effective bond order is therefore smaller than five as a result of a sizeable occupation of the δ^* antibonding orbitals [296].

The above and today reported topological analyses show that in contrast to the ELF and QTAIM picture of covalent bonding between main group elements, the two-centre multiple M-M bond is characterized by a large fluctuation between the two metal cores and a low population of the disynaptic V(M, M) ELF basin and may be related to charge-shift bonding.

4.2.2. Single M-M bonds

In addition to the binuclear rhodium complexes of the above "paddlewheel" metal complexes, single M-M bonds have been characterized using topological analyses (mainly QTAIM) for transition elements of group 4 and group 12 at both ends of the transition series.

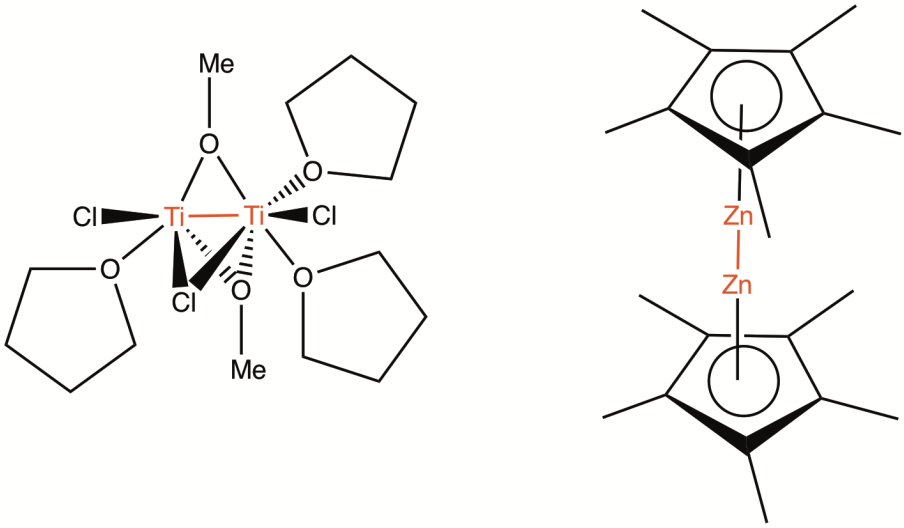

Figure 10: Representative complexes of single Ti-Ti and Zn-Zn bonds

The short intermetallic distance (2.543 Å) and the diamagnetism of alkoxo-bridged dinuclear complexes of Ti(III) indicated the presence of a Ti-Ti bond, as revealed by an attractor of weak ELF value located between the Ti(III) centres [297]. A short intermetallic contact (2.942 Å) in a dinuclear Ti(III) formamidinate complex was also assigned to the presence of a single Ti-Ti bond on the basis of the analysis of the calculated electron density (bond order 0.96) [298]. Carmona's discovery of the first structurally characterized example of a stable Zn-Zn bond in decamethyldizincocene ($Cp^*Zn{-}ZnCp^*$), with a intermetallic distance of 2.305 Å and two parallel Cp^* rings [23] prompted a number of theoretical investigations [23]. In contrast to other M-M bonds of the transition element series, the Zn-Zn bond in dizincocene and other Zn-Zn bonded species, is mediated primarily by overlap of the 4s orbitals with low s/p_z or s/d_{z2} mixing depending on the ligands [23]. QTAIM topological analysis of homodinuclear metallocenes $Cp{-}M{-}M{-}Cp$ (M = Ni, Cu, Zn) display the typical signature of metallic bonding at the M-M bond critical point: a low electron density, a positive Laplacian $\Delta\rho$ (closed-shell interaction) and a small negative energy density H (associated with an electron-shared or covalent character of the bond) [299]. The covalent character is increasing according to the following Zn < Cu < Ni order. The large QTAIM delocalization indexes between the metal atomic basins ranging from

0.94 (Zn), 1.44 (Cu) up to 2.29 (Ni) are consistent with a single Zn-Zn and multiple Cu-Cu and Ni-Ni bonds, that are further supported by the presence of ELF disynaptic V(M, M) basins with populations of about 3 e. In contrast, the M-M bonds in binuclear main-group-metal metallocenes (M = Be, Mg, Ca) exhibit topological signatures of covalent M-M bonds [300].

ELF contour maps were calculated using periodic DFT and plane wave basis sets for various dimetallocenes of group 12 metals (M = Zn, Cd, Hg). Zinc retains central η^5−C_5H_5 coordination in the dimer while Cd shifts to an off-centre position and mercury to the edge displaced η^1−C_5H_5 coordination [301]. A point attractor and a torus attractor of close ELF value (ELF ≈ 0.6) are found in the middle of the Zn-Zn bond [301]. The latter is not just a simple σ-bond arising from overlap of Zn 4s orbitals and small contributions of s/p_z and s/d_{z^2} mixing. There is also a weak π-bond contribution arising from zinc d_{xz} and d_{yz} overlap [301]. The heavier Cd-Cd and Hg-Hg molecular analogs of the above Zn-Zn bonded systems are scarce because coordination of ligands tends to induce disproportionation to M° and M^{II} . The Cd-Cd bond appears rather similar to the Zn-Zn analog, with dominant 5s character mixed with some 5p_z. In the mercury congener, however, relativistic stabilization of the 6s orbital reduces the $5d_{z^2}/6s$ separation, and ∼ 5% d_{z^2} character is present in the Hg-Hg bonding HOMO. In conjunction with the lanthanide contraction, the result is that the Hg-Hg bond (2.5738(3) Å) is slightly shorter than its Cd-Cd analog (2.6257(5) Å) [4, 23].

Group 12 Di-uranium fullerene $U_2@C_{80}$ was detected recently using mass spectrometry. A cage-driven single U-U bond was characterized in the latter $U_2@C_{80}$ fullerene using QTAIM analysis [302]. U-U bonds fall in the negative energy density regions, denoting an electron-shared U-U interaction. The delocalization index between the U atoms is close to one thus consistent with a single U-U bond. Lower delocalization indexes within the 0.25-0.65 range, were reported for other similar dimetallofullerenes [303] in which the signature of the M-M bond is an ELF V(M, M) valence basin with populations ranging from 1.40 in $Sc_2@C_{82}$ and 1.62 in $Y_2@C_{82}$ up to 1.8–1.9 in $Lu_2@C_{76,82}$. Disynaptic V(M, M) attractors with an ELF value lower than 0.5 were also reported for group 12 metals (M = Zn, Cd, Hg) encapsulated in $C_{50}X_{10}$ (X = CH, N, B) fullerenes and were assigned to a M-M bond analogous to the one in M_2Cp_2 complexes described above [304]

The Laplacian of alpha-electron density highlights a spin density concentration between the U atoms. This is consistent with the MO analysis showing that the one-electron two-centre U-U bond at 3.9 Å with a strength of about 18 kcal/mol is realized mainly via U(5f) orbitals. A concept of unwilling metal bonding is suggested: the encapsulated U atoms are strongly bound to the cage and carry a positive charge. Pushing the U(5f) electron density into the U-U bonding region reduces electrostatic repulsion between enclosed atoms, thus forcing U-U bonds of increasing strength as the cage size decreases within the present $U_2@C_N$ ($N = 60, 70, 80, 84, 90$) series.

The Th-Th bond could be tuned from quadruple ($H_3AsThThAsH_3$) to single (ONThThNO) by changing the ligand L in the LThThL complexes series. QTAIM metrics (low ρ_i , positive $\Delta\rho$ and negative H) are typical of M-M bonds and are linearly correlated with the Th-Th distance [305].

4.2.3. Weak covalent M-M interactions

Weak covalent Pd(II)-Pd(II) or Ag(I)-Ag(I) interactions were recently characterized by QTAIM analysis by Ofredi *et al*. [306, 307]. The covalent character and the strength of the M-M bond were estimated from the QTAIM energy densities at the bond critical point and were shown to increase upon oxidation of one or both metallic centres. Such cation-cation interactions between $d^8 - d^{10}$ systems are referred to as metallophilic interactions [16, 308]. They are weaker than most covalent or ionic bonds but stronger than other van der Waals interactions, and roughly comparable in strength with typical hydrogen bonds. They are expected stronger in systems with larger relativistic effects and are very sensitive to the electronic effects of the ligands. The metallophilic interactions weaken along the series of metals of group 11 [309]. Cuprophilic interactions have been the subject of debates [309–313]. At the MP2 level, their strength has been calculated three times weaker than aurophilic interactions [314]. However, the oxidation of one Cu(I) centre involved in the cuprophilic interaction, results in the formation of a stronger single Cu(II)-Cu(I) bond in the corresponding mixed-valence complex [315, 316].

Topological analyses are expected unique tools for characterizing such weak M-M interactions. QTAIM analyses of unsupported or bridged Cu(I) dimers have been recently reported [317]. The range value of the ratio of the local electron potential energy density (V_{bcp}) to the kinetic energy density (G_{bcp}) at the bond critical point located between the copper atoms, namely $1 < |V_{bcp}|/G_{bcp} < 2$, suggests that the Cu-Cu interactions are not perfectly ionic but have some electron-shared (covalent) character [317].

The interest of combining QTAIM and ELF analyses is illustrated below for the characterization of the binuclear copper-amidinate complex (**1**). The latter is used as a precursor in the synthesis of copper nanoparticles [318]. It is anticipated that the knowledge and control of the M-M bonding in the precursor complex may help in tuning the final shape and size of the nanoparticles and the understanding of the mechanism of the formation of copper nanoparticles.

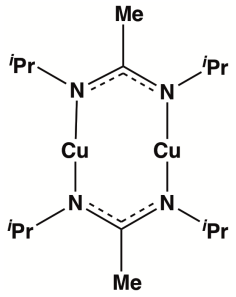

Scheme 1: Structure of binuclear copper complex **1**

ELF topological analysis of the amidinate anion and of the bimetallic amidinate precursor. The weight of the most representative mesomeric forms of the amidinate anion, estimated from the ELF populations and covariances of the valence basins (Scheme 2) are shown below. The major mesomeric form exhibits a zwitterionic description of the imine C-N bond.

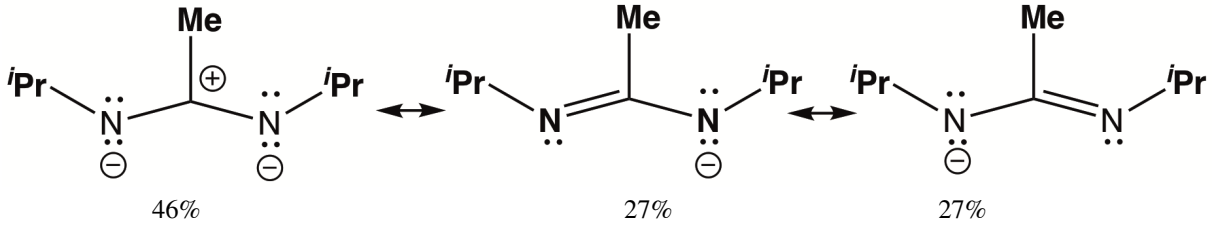

Scheme 2: mesomeric structures of the amidinate anion

In the experimental structure of copper-bisamidinate complex 1 of quasi-C_i symmetry [319], the intermetallic distance (2.414 Å) is a little larger than twice the covalent radius of Cu (2.34 Å) and considerably shorter than twice its van der Waals radius (5.76 Å), suggesting a cuprophilic interaction. The C_i or C_{2v}-symmetric structures, calculated at the B3PW91/Def2TZVP level are quasi-degenerated and in good agreement with the experimental structure. In both the C_{2v}-symmetric or centrosymmetric binuclear complex **1**, the ELF description of both amidinate ligands is very similar to the one of the free amidinate anion (almost same populations and covariances as shown in Figure 11). The disynaptic ELF valence basin V(Cu,N) exhibits a population slightly larger than the one of V(N) in the free amidinate anion (3.6 *vs* 3.4 e^-) and the corresponding attractor is located closer to the nitrogen atom than the V(N) attractor in the free amidinate anion (0.613 *vs* 0.725 Å), suggesting that the weight of the zwitterionic mesomeric form increased slightly in the copper complex **1**. The covariance between V(Cu,N) and the core basin of copper, namely Cov(V(Cu,N), C(Cu)) = -0.27 is indicative of a dative Cu-N bond although the QTAIM atomic contribution of Cu to the V(Cu, N) basin is weak (0.22 e^-, *i.e.* lower than 10% of the basin population). As expected, the formal oxidation state of copper is calculated equal to I from the ELF populations substracting to the atomic number of copper the populations of the core and sub-valence basins of copper (29 - C(Cu) -V(Cu) = 29 -27.5 - 0.38 = 1.1).

The dative Cu-N bond exhibits therefore a strong ionic character that may be described by two Cu^+ ions in electrostatic interaction with the major mesomeric form of the amidinate anion. The disynaptic V(Cu,Cu) basin is

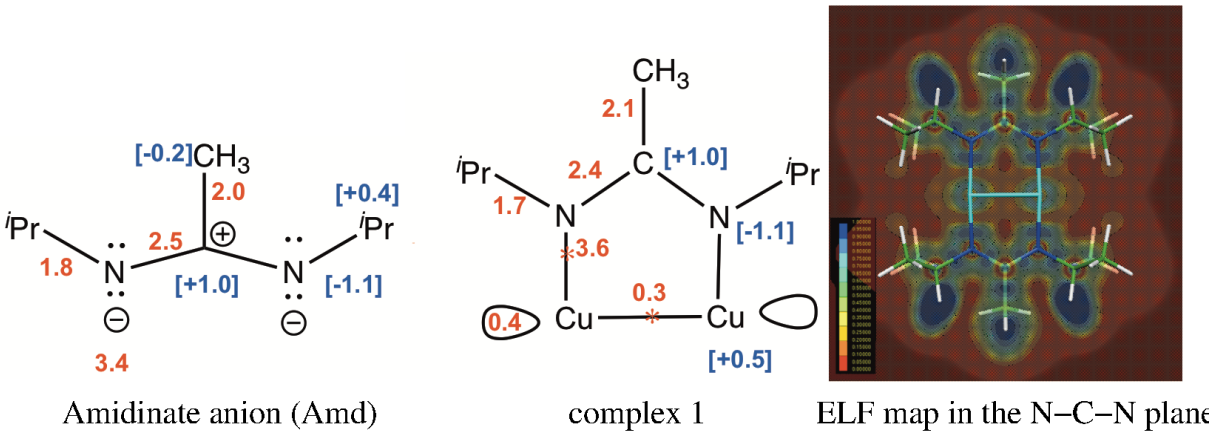

Figure 11: Average populations of ELF basins (*in red*) and QTAIM atomic charges (*in blue*) for the amidinate anion (*left*) and for the C_i -symmetric bis-amidinate copper complex **1** (*middle*), one amidinate anion has been omitted for clarity. B3PW91/Def2TZVP// PBE-D3/Def2TZVP level of calculation.

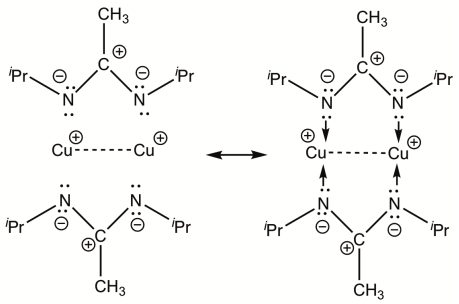

Scheme 3: Most representative mesomeric forms of binuclear copper complex **1.**

indicative of an electron-shared Cu-Cu bond, that is further supported by the large QTAIM covariance between Cu atomic basins (-0.16). The low population of V(Cu, Cu) (0.3 e^-) is however indicative of a weak covalent character that is also supported by the existence of two sub-valence monosynaptic V(Cu) basins. Such sub-valence V(M) basins have been already reported for transition element cations interacting with large biological molecules by Benoit de Courcy *et al.*, the volume and population of which increasing with the covalent character of the bond [180, 320].

Table 8: QTAIM topological parameters of complex **1** at the bond critical points (bcp). E_{int} (kcal/mol) = -313.754 V_{bcp} (au) [321][32]. B3PW91/Def2TZVP// PBE-D3/Def2TZVP level of calculation.

	ρ_{bcp} (au)	$\Delta\rho_{bcp}$ (au)	δ	H_{bcp} (au)	H_{bcp}/ρ_{bcp} (au)	V_{bcp} (au)	E_{int} (kcal/mol)
Cu-N	0·112301	+0·441717	0·658	−0·041532	−0·369	−0·193493	60·7
	0·112139	+0·441364	0·658	−0·041412	−0·369	−0·193164	60·6
	0·112139	+0·441364	0·658	−0·041412	−0·369	−0·193164	60·6
	0·112301	+0·441717	0·658	−0·041532	−0·369	−0·193493	60·7
Cu-Cu	0·039746	+0·115848	0·328	−0·005215	−0·044	−0·039391	12·4

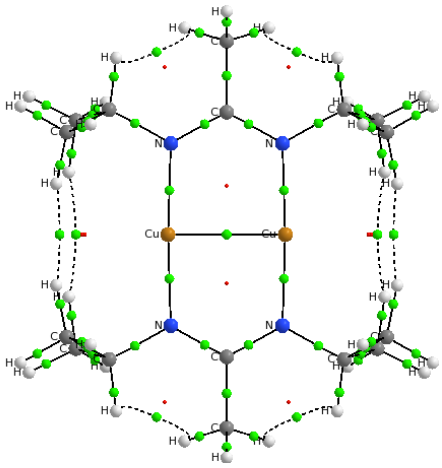

Figure 12: QTAIM molecular graph B3PW91/Def2TZVP// PBE-D3/Def2TZVP level of calculation. Bond critical points in green.

QTAIM analysis of the binuclear Cu_2Amd_2 complex **1**. According to the Macchi's classification [149], the QTAIM topological parameters at the Cu-N bond critical points are indicative of a donor-acceptor (dative) Cu-N bond ($\Delta\rho_{bcp} > 0$ and $H_{bcp} < 0$). The degree of covalency as measured by the H_{bcp}/ρ_{bcp} ratio is the same for the four Cu-N bonds (0.37) as well as the Cu-N interaction energies (60.7 kcal/mol) estimated from the Espinosa correlation [321] (Table 8). Similar Cu-N dative bonds with a strong ionic character were recently characterized in copper-histidine complexes [322].

The QTAIM topological parameters at the Cu-Cu bond critical points are indicative of a closed-shell Cu-Cu interaction with a weak covalent character ($\Delta\rho_{bcp} > 0$ and $H_{bcp} < 0$). The degree of covalency as measured by the H_{bcp}/ρ_{bcp} ratio is the same for the four Cu-N bonds (0.044) and is consistent with the above *ELF* analysis, as the Cu-Cu interaction energies (12.4 kcal/mol).

The topological signature of the cuprophilic interaction in complex **1**, namely a two-centre M-M bond with a weak covalent character, is a disynaptic V(M, M) ELF basin of low population and sub-valence basins, that are consistent with the low covalent character of the closed-shell interaction characterized from the QTAIM energy densities values.

Non-covalent interactions. As already mentioned in the introduction, d^8 metal centre should not be involved in M-M bonding due to the filling of all the M-M antibonding orbitals, expected to cancel out the M-M bonding orbitals. However, the net overall bonding interaction in square-planar Rh(I), Ir(I) or Pt(II) oligomeric stacks, is well-documented and was explained by the symmetry-allowed mixing of d_{z^2} orbitals with the (n+1) metal *s* and p_z orbitals [323]. The Pd(II)-Pd(II) bond was considered only recently in a series of Pd(II)-pyridine dimers supported by bridging acetate or triflate anions. A weak closed-shell interaction is characterized by QTAIM analysis (low electron density and positive Laplacian at the bond critical point, that are linearly correlated to the Pd-Pd distance) [323]. The Pd-Pd interaction is weaker than the one in related Rh, Ir and Pt systems.

Similar weak noncovalent Pd···Pd interactions have been reported recently in heterobimetallic (Pd-Pd) or heterotrimetallic (Pd-Ir) complexes involving the 2-indenylidene pincer ligand [324]. The low value of the Wiberg bond index (0.11) and stabilizing energies of $Pd(_1)\rightarrow Pd(_2)$ (42 kcal/mol) and $Pd(_2)\rightarrow Pd(_1)$ (30 kcal/mol) of the same range (2^{nd} order perturbation Natural Bond Orbital analysis (NBO)), suggest weak noncovalent Pd···Pd interactions, further supported by QTAIM analysis.

Grimme *et al.* pointed out that the M-M attractive $d^8 - d^8$ interactions accounts only for 10-15% of the total dispersion contribution to the binding energy, suggesting a strong effect of the ligands [325]

4.3. Heterometallic bonds

In a complementary approach to the previous section dedicated to homometallic MM bonds, the scope of this section is restricted to the description of the specificities of a M-M bond resulting from the interaction of two different metal centres.

One specificity is the degree of polarity of the heterometallic M-M′ bonds, expected large by combining metal from both ends of the transition metal series, for example an electron-rich "early-late" transition element with another electron-poor metal centre. This will be illustrated below through the characterization of a polar Ti-Co covalent bond by combining QTAIM and *ELF* topological analyses [326].

Alternatively to covalent bonds, unsymmetrically bonded mononuclear fragments may result in the formation of a dative M-M′ bond, one metal centre acting as a ligand for the other unsaturated metal centre (M→M′). The great variety of dative bonds involving a Lewis basic transition element and a Lewis acidic metal was illustrated in a recent review [41]. ELF and QTAIM topological analysis of a dative nickel-iron interaction in model complexes of [NiFe] hydrogenase will be presented in the next section.

4.3.1. Dative M-M bonds

When a transition element centre M is adjacent to another unsaturated or electron-poor metal centre M′, the more electron-rich metal centre can act as a ligand L (Green classification [327]) to form a dative M→M′ bond. This is illustrated hereafter for a bimetallic nickel complex exhibiting a short intermetallic distance of 2.41 Å in the crystal structure [328].

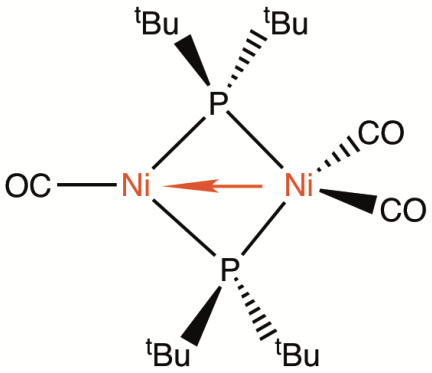

Scheme 4: Bimetallic nickel complex **2** exhibiting a dative Ni-Ni bond.

The Ni-Ni bond in the above diamagnetic complex **2** may be understood either as (i) covalent or (ii) dative:

(i) covalent Ni(I)-Ni(I) and antiferromagnetic coupling between two Ni(I) centres with 16 and 18 e^- respectively (symmetrically dividing the +2 charge on the nickel needed to balance the two anionic phosphide ligands).

(ii) dative Ni(0)→Ni(II). The tetrahedral symmetry may be related to a d^{10} Ni(0) centre, while the planar geometry may be related to a d^8 Ni(II) centre, bonded to two anionic phosphide ligands thus giving a "neutral" three-coordinate 14 e^- Ni(II) moiety. The dative bond with the electron-rich Ni(0)-carbonyl moiety (18 e^-) is bringing up the Ni(II) moiety to 16e^-, i.e. the electron-count expected for a square-planar d^8 Ni(II) atom.

The geometry and chemical reactivity of the binuclear Ni complex is consistent with the dative bond assignement.

A dative Ni→Fe bond was characterized in model complexes of [NiFe] hydrogenase, catalyzing the reversible oxidation of molecular hydrogen thus playing a vital role for anaerobic bacteria [329]. Thiolate-bridged heterobimetallic Ni-Fe complexes such as complexes **3** and **4** (Scheme 5) have been used to mimic the protonation of the active site of [NiFe] hydrogenases,

Consistently with previous theoretical studies of complex **3**, *ELF*, ELI-D and QTAIM studies are in favor of a covalent Ni(I)-Fe(I) bond [330]. However, the Ni-Fe bonding is released in the quasi-degenerated Fe(0): Ni(II) isomer or in the oxidized Ni(II) Fe(I) complex [**3**]$^+$ [331] Although complex **4** has the same electron count than [**3**]$^+$, it exhibits a dative Ni(I)→Fe(II) bond and the related geometric distinction, namely a planar Ni(I) in [**3**]$^+$ versus a SF_4-like Ni(I) in **4** [[330, 332]

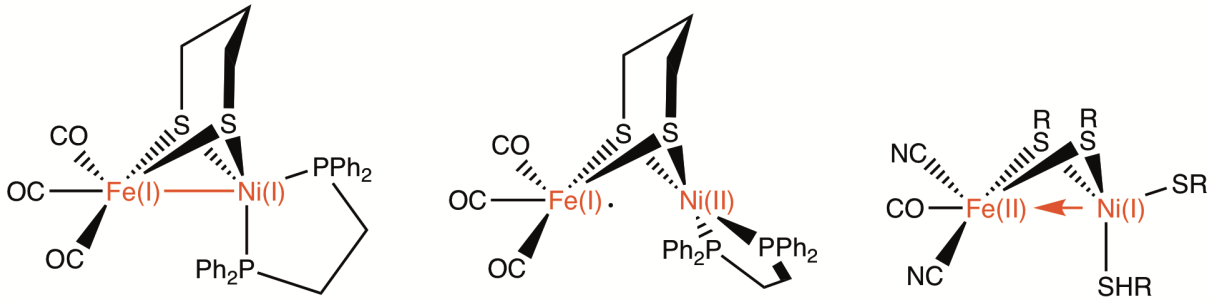

Scheme 5: Thiolate-bridged heterobimetallic Ni−Fe complexes **3** (left) [**3**]$^+$ (middle) and **4** (right), studied as mimics of [Ni−Fe] hydrogenase.

Os→Cr and Os→W adducts featuring a donor-acceptor M-M interaction with a weak degree of covalency, according to NBO (Wiberg bond index about 0.2) and EDA analyses were recently reported [325].

4.3.2. Polar covalent M-M bonds

The concept of bond polarity used in main group chemistry, based on electronegativities, is not straightforward for M-M bonds, because it is expected strongly influenced by the ligands involved in the coordination sphere rather than by the intrinsic properties of the metal only. The polarity of Ti−Co bonds in dinuclear complexes, was investigated on model complexes (Scheme 6), using joint QTAIM and ELF topological analyses. While the covalent M-M bond order was found less than 0.5, the bonding analysis suggests that the titanium atom carries a large positive charge, while the cobalt atom is nearly neutral. Partial charges greater than 0.5 e^- were calculated for the complex fragments. The latter results are consistent with the highly polar character of the Ti-Co bonds [326].

A Ti-Co donor-acceptor bond was ruled out from energy decomposition analyses (EDA). The covalent and electrostatic contributions to the Ti-Co attraction have similar strength. The Ti-Co bond can therefore be classified as a polar single bond, which has only little π contribution [333].

Recently, Ca-Fe and Yb-Fe bonds in heterobimetallic Fe complexes were shown to exhibit similar QTAIM signatures to the ones of the above polar Ti-Co bond and were shown predominantly electrostatic in nature from EDA analysis [334].

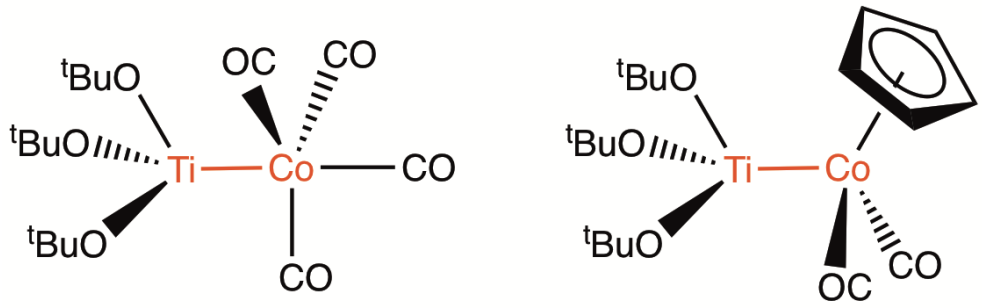

Scheme 6: Model complexes used for the investigation of the nature and polarity of the Ti-Co bond.

4.3.3. Non-covalent M-M bonds

The term hemichelation was coined for supported bimetallic complexes exhibiting a noncovalent M-M′ interaction [335]. For $(CO)_3$Cr−MLX hemichelates (M = Pd, Pt), there is no BCP although the M-M interaction is revealed by ETS-NOCV [335].

A 14-electron Rh(I) centre could be isolated in the L_2Rh(I)···Cr$(CO)_3$ (arene) hemichelate (L = norbornadiene or CO). The Cr···Rh attractive non-covalent interactions was characterized using non-covalent interactions (NCI) analysis. The positive value of the Laplacian $\Delta\rho$ and the low electron density value at the Cr-Rh bond critical point are indicative of a non-covalent interaction [336]. Interaction energies calculated from ETS-NOCV analyses are ranging from 6.0 up to 38.0 kcal/mol depending on the ligands. The Cr→Rh donor-acceptor character is slightly larger than that of the Rh→Cr back-donation.

A dominant attractive electrostatic contribution to the stabilization of Pd(II) hemichelates, involving noncovalent interactions between a $Cr(CO)_3$ moiety and a Pd(II) centre, was evidenced using QTAIM, ETS-NOCV, EDA and NBO analyses [337]. ELF and QTAIM topological analyses of indenyl-palladium complexes stabilized by fluxional non-covalent interactions, show that the fluxionality is the direct consequence of the weakness of the polar intermetallic interaction [335].

A weak noncovalent supported Fe-Pd interaction was characterized using NBO and QTAIM analyses, in a cationic bimetallic complex involving the coordination of PdX (X = Cl, Br) to 1,1′-bis(diphenylphosphino)ferrocene [338]

Most of the topological studies of this section rely on QTAIM analysis; The discrimination between a dative and a covalent M-M bond on the one hand and between weakly covalent or noncovalent M-M interaction at the other hand is therefore not straightforward. In the absence of bond critical point, NCI analysis would be required for a clearcut distinction between weakly covalent or noncovalent bonds. ELF topological analyses should help for the discrimination between dative and (polar)-covalent MM bonds.

5. Multicentre bonding in polynuclear cluster complexes

In the previous sections, M-M bonds generally involving metal centres in high oxidation state were considered. The present section will be rather devoted to M-M bonds formed in low-valent complexes such as the first row carbonyls $Mn_2(CO)_{10}$ and $Fe_2(CO)_9$ and related polynuclear cluster complexes. The 17 e^- count of each monometallic carbonyl moiety requires the formation of a single M-M bond to satisfy the 18 e^- rule. However, the existence of this M-M bond is difficult to establish [3]. Theoretical analyses, especially topological analyses are expected helpful. Indeed, many QTAIM analyses have been reported and reviewed [150, 299, 339–341].The ELF topological description of polynuclear metal cluster complexes was also reviewed [342, 343]. From these reports, in contrast to the multiple M-M bond in binuclear complexes, multicentric bonding, involving eventually the bridging ligands, and low electron delocalization between the cores of the metal atoms are evidenced in polynuclear cluster complexes. The scope of the present section will be therefore restricted to recent QTAIM studies and/or ELF topological analyses reported subsequently to the above reviews. The topological analysis of *ELF* or ELI-D is the choice technique enabling the unambiguous characterization of multicentre bonding thanks to the synaptic order concept.

As it had been shown in section 3, multicentre bonding is frequently encountered in bulk alkali, alkaline-earth bulk metals as well as in intermetallic phases. In this section, the discussion is focussed on small aggregates in which the metallic centres are or not linked to ligands.

5.1. Homometallic bonds

EHMO calculations performed on octahedral metal clusters, namely $[Sn_6H_6]^{4+}$, $[Sn_6]^{2-}$, $[Zr_5Cl_{12}(PMe_3)_5]^{2-}$, $[Zr_5Cl_{12}(PMe_3)_5H_4]$ and Zr_5 indicate the presence of polysynaptic basins and of bridging hydrogens [65].

As mentioned in the previous section, the Li_n, $n = 4, 5, 6$ complexes in their ground state are bonded by partial multicentre two-electron bonds and by multicentre one-electron bonds in the high spin state. The ground state of Li_4 is calculated to have a planar rhomboidal D_{2h} structure with edges of 3.05 Å, whereas the distance between the nearest opposite vertices is shorter, *i.e.* 2.62 Å. Four valence attractors are located, outside of the rhombus, on the bisection of each edge. There are in principle four disynaptic basins V(Li,Li), each with a population $\bar{N}[\mathrm{V(Li,Li)}] = 0.98e^-$. The value of the covariance matrix elements with the two neighbouring V(Li,Li) basins are -0.39 when the two basins belong to the valence shell of a Li at an acute angle vertex and -0.5 when they are in an obtuse angle vertex. This large absolute value suggests that disynaptic basins should be collected two by two in trisynaptic basins, all the more so that the ELF value at the saddle point between two such disypnatic basins is 0.994 to be compared to 0.996, the value at the attractors. It is interesting to note, that a calculation carried out with the same basis set and the B3LYP hybrid functional [344, 345] instead of B3PW91 [344, 346] used by Alikhani and Shaik [282] yields two attractors at positions close to the B3PW91 saddle point. The bonding picture is therefore that of two bonding electron pairs each centred in an acute isosceles triangle as illustrated in Figure 13. The high spin state has a T_d structure and the

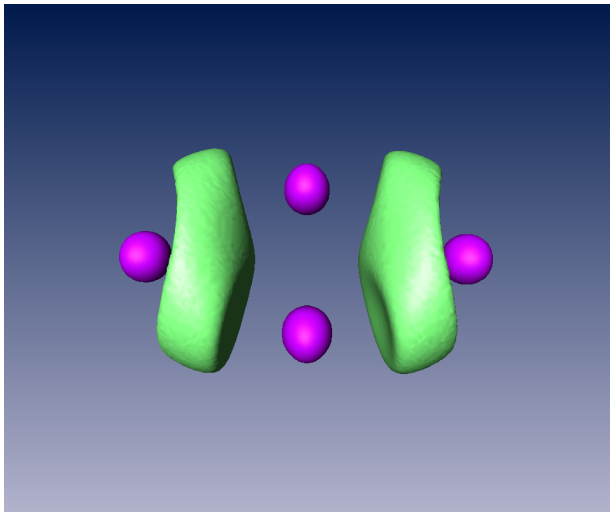

Figure 13: $ELF = 0.975$ isosurface of the Li_4 ground state. Color code: magenta=core, green=trisynaptic

four attractors are located in front of the faces of the tetrahedron. In both ground state and high spin state of Li_5 the 5 electrons are distributed among four basins we temptatively assign as trisynaptic. The Li_6 cluster has valence basins clearly of synaptic order 4 whereas the $^7B_2$ state of this system displays four trisynaptic basins, each with a population of 1.10 e^-, the remaining valence density being in two small basins of synatic order 4.

The iron tetramer Fe_4 ground state is calculated to have fourteen unpaired electrons, it has a D_{2h} structure which determines a tetrahedron with two different edge lengths $R_{1,2} = R_{3,4} = 2.55$ Å and all other $R_{i,j} = 2.26$ Å. The electron density has one non-nuclear attractor at the centre of the tetrahedron and bond critical points at the mid-points of the edges. The ELF analysis reveals 21 valence attractors: one at the centre of the tetrahedron is tetrasynaptic, 4 at the top of faces are trisynaptic, for each edge there is a pair of attractors which can be merged since $ELF = 0.437$, the value at the saddle point between them is very close to that of one the attractors of the pair ($ELF = 0.438$) and therefore theirs basins can be safely merged, the four last are monosynatic and far apart the nuclei. The population of the core

basins, $\bar{N}$[C(Fe)] = 23.78e^-, has a contribution of 2.94 e^- due to unpaired density and a large variance σ^2 = 1.92 which corresponds to one unpaired electron less than in the free atom. Each summed disynaptic basin as well as each trisynaptic basin contains almost 1 e^- whereas the population of the tetrasynaptic and monosynaptic basins are respectively 0.14 e^- and 0.26 e^- [347].

The main fragment resulting from mass spectral analysis of three anionic Mo(IV) dithiolene complexes is $Mo_2S_4O_2^-$. The non-symmetrical experimental fragmentation into this dinuclear core is consistent with the least *ELF* topological change principle [348]. The stability of the dinuclear $Mo_2S_4O_2^-$ fragment is assigned: (i) a strong Mo−Mo bond characterized by a disynaptic V(Mo,Mo) of low population (0.42) and a large covariance between the Mo cores and (ii) a delocalization of core electrons of Mo on the bridge sulfido groups and terminal oxygen atoms.

QTAIM studies have been performed to investigate the M-M bond in three types of disulfido carbonyl clusters: $Fe_2(\mu{-}S_2)(CO)_6$ (**5**), a model complex of [FeFe] hydrogenases, a co-crystallized trinuclear complex $Fe_3(\mu_3{-}S)_2(CO)_9$ (**6**) and the related triphenyphosphine complex $Fe_2(\mu{-}S_2)(CO)_5(PPh_3)$ (**7**) [349]. As already emphasized in previous QTAIM and ELI-D studies of $Fe_3(\mu{-}H)(\mu{-}COMe)(CO)_{10}$ [350], it is not possible to rely on the sign of the Laplacian only to assign the nature of bonds involving heavy element such as transition elements. The presence of a BCP is sensitive to the DFT calculation level and to the basis set, because the structure of **5** is close to a catastrophe point. On the basis of the delocalization indexes, resp. 0.496 and 0.502 calculated at the B3LYP/def2-TZVP level, a Fe−Fe bond with partial covalent character is assigned to complexes **5** and **7**. A lower covalent character is found for the parent disulfido carbonyl complex $Mn_2(\mu{-}S_2)(CO)_6$ ($\delta(\Omega_{Mn(1)}, \Omega_{Mn(2)})$ = 0.186). For complex **6**, a delocalized $Fe(_1){-}Fe(_3){-}Fe(_2)$ interaction ($\delta(\Omega_{Fe(1)}, \Omega_{Fe(3)})$ = 0.329), whereas no interaction is found between Fe(1) and Fe(2) ($\delta(\Omega_{Fe(1)}, \Omega_{Fe(2)})$ = 0.074).

5.2. Multicentre bonds involving non-metal elements from the bridging ligands

A first example of bridging non-metal atom is provided by Al_2H_6 which has been observed by photo-detachment spectroscopy [351]. The structure of Al_2H_6 is the analog of diborane with two bridging hydrogen atoms. We have carried out the *ELF* analysis of Al_2H_6 and of the AlH_6^- anion and found trisynaptic protonated basins as displayed in Figure 14. The populations of the V(Al,H,Al) basins are calculated 2.02 and 2.04 e^- in Al_2H_6 and AlH_6^-, respectively.

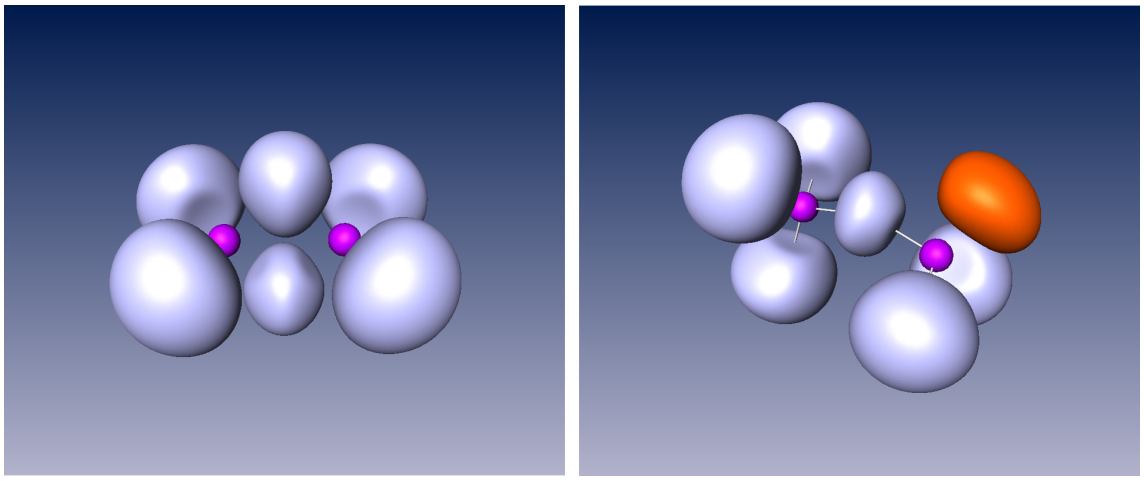

Figure 14: *ELF* = 0.85 isosurface of Al_2H_6 (left) and $Al_2H_6^-$. Color code: magenta=core, redbrick= monosynaptic, light blue= protonated disynaptic V(Al,H) or trisynaptic V(Al,H,Al)

The trimethyl aluminium dimer is another example of multicentre M-M bond involving a non metal atom, here a carbon. The bonding in Al_2Me_6 (Figure 15 is very similar to that of Al_2H_6, the V(Al,H) and V(Al,H,Al) being replaced by V(Al,C) and V(Al,C,Al) basins whose populations are 2.05 and 2.13 e^-. In both Al_2H_5 and Al_2Me_6 the bridging bond have to be considered as dative because they result of the dimerization in which the monomeric species play simultaneously the roles of Lewis acid and Lewis base.

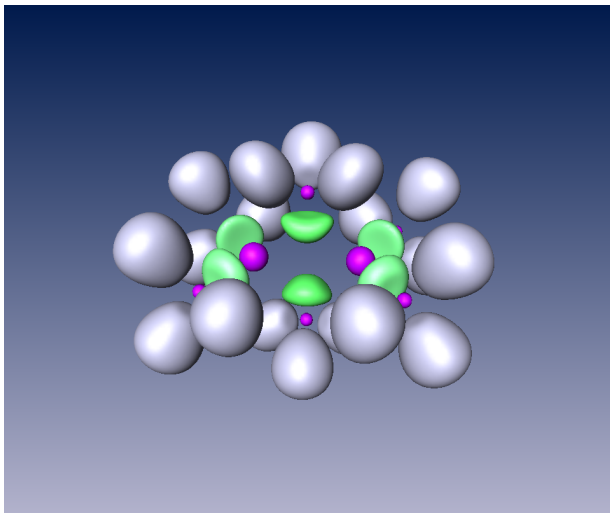

Figure 15: $ELF = 0.85$ isosurface of Al_2Me_6. Color code: magenta=core, light blue= protonated disynaptic V(C,H), green= disynaptic V(Al,C) or trisynaptic V(Al,C,Al)

The M−M, bonding interactions in the group 7 transition element carbonyl complexes $[M_2(CO)_{10}]$ and $[M_3(\mu{-}H)_3(CO)_{12}]$ (M = Mn, Tc, Re) have been studied using ELF and QTAIM topological analyses as well as the source function (SF). The results confirm that the metal atoms in the homobinuclear $[M_2(CO)_{10}]$ complexes are connected through a localized M−M bond that implicates little electron density (it increases from M = Mn to Tc and Re). On the other hand, such a bonding has not been found in the trinuclear $[M_3(\mu{-}H)_3(CO)_{12}]$ complexes, which, instead, contain a $6c - 6e$ bonding interaction delocalized over their six-membered $M_3(\mu{-}H)_3$ ring, as revealed by the non-negligible non-bonding delocalization indexes. The existence of significant CO to M π-back-donation, slightly higher in the trinuclear clusters than in the binuclear complexes, is indicated by the $M\cdots O_{CO}$ delocalization indexes and SF calculations [352].

In contrast to the ELF and QTAIM picture of dicentric multiple M-M bonds, characterized by a large electron delocalization between metal cores, the one of M-M bonding in polymetallic clusters, is characterized by multicentre bonding.

6. Conclusion

This review presents a rather large panorama of chemical situations illustrating the capability of topological approaches for the description and the characterization of the M-M bonding. The aim of such studies is, in our opinion, to inspire and support *chemical explanations* of the structure and of the properties of molecules and materials. By *chemical explanations*, we mean explanations in terms of the group and period of the elemental atom constituting the system of interest and assuming the hypothesis that the electrons tend to form stable groups more or less localized the organization of which can be anticipated. In contrast, the molecular orbital and valence-bond approaches belong to *Quantum Chemical explanations* because they rely upon the calculus of the approximate solutions of the Schrödinger equation. Keeping this goal in mind we realize that a lot of work remain to be done.

From the literature it appears clearly that most published works concern group 1-13 elements although group 14-15 atoms are involved in M-M bonds [14, 353]. The metals of these groups offer a large variety of M-M bonding situations since they can form rings and cages with bonds of the various multiplicities allowed by the number of their valence electrons.

In the M-M bond the core-valence separation is preserved including for transition-metals for which the effective number of valence electrons hardly exceeds two. Therefore, the density outside of the core basins contributes to essentially covalent or dative bonds including the metallic bond. Therefore, the valence shells of transition element

atoms in molecules and bulk metals present many analogies with those of alkali and alkaline-earth elements. The main distinctive feature of transition elements, together with lanthanides and actinides, is the delocalization of the density of the subvalence shell which is testified by the variance of the core population which reaches values as large as 2.5 in the case of Mo. This large variance not only implies delocalization of the valence density but also the subvalence shells of the nearest neighbour transition elements contributing to a charge shift type contribution to the bonding explained in terms of δ bond by the Quantum Chemical explanations. The delocalization of the subvalence shell density has its origin in the local spin multiplicity which is often different of that in the ground state free atom. The evaluation of the variance of the core populations has to be extended to bulk metals, as it has been already done for Cu by Baranov and Kohout [258]. The core charge-shift hypothesis may explain the differences and the similarities of the properties of metals of different groups, for example the boiling point of most transition elements of period 4 is of the order of 3000 K, except Zn which has a complete d^{10} subshell, for which it is 1180 K a value close to that of K (1032 K).

For an accurate description of heavy metals, relativistic corrections are required and therfore use of programs designed for two component wave functions [199, 200] are called to increase in the next years.

Appendix A: Mathematical glossary

Dynamical system:. a *dynamical system* is a vector field of class C^1 bound on a manifold M. Such a vector field has no discontinuities. To any point m belonging to the M manifold corresponds one vector $X(m)$ and only one which is at least one-time differentiable. The solutions of the system of equations $dm/dt = \mathbf{X}(m)$ are locally unique and therefore there is only one trajectory passing through m. The trajectories are determined by integrating $dm/dt = \mathbf{X}(m)$ with respect to the fictitious time variable t. The limit sets of M of $m(t)$ for$t \leftrightarrow \pm\infty$ are called the α and ω limit set.

Gradient dynamical system:. the vector field of a *gradient dynamical system* is the gradient of a function called *potential function*, *i.e.*: $\mathbf{X}(m) = \nabla V(m)$.

Critical points:. the *critical points* (or *limit points* of a *dynamical system* are the points of M for which $\mathbf{X}(m_c) = 0$. A *critical point* is either a α or an ω limit of a trajectory. The set of points of M by which are built trajectories having m_c as ω limit is called the *stable manifold* of m_c, the *unstable manifold* of m_c is the set for which m_c is an α limit. The dimension of the *unstable manifold* is given by the *index* of the critical point which is the number of direction in which M increases in the neighbourhood of m_c. The set of the *critical points* of a *dynamical system* satisfies the Poincaré-Hopf formula:

$$\sum_P (-1)^{I_P} = \chi(M)$$

where I_P is the index of the *critical point* P and $\chi(M)$ the Euler characteristic of the manifold. A *critical point* of *index* zero is an *attractor* of the *dynamical system*. The *stable manifold* of an *attractor* is called the *basin of the attractor*. The *stable manifold* of a *critical point* of *index* greater than zero is a *separatrix*, it is the border of two or more basins. The *index* of a *critical point* m_c of a *gradient dynamical system* is the number of positive eigenvalues of the matrix of the second derivatives of the *potential function* at m_c. In this case, a *critical point* is said *hyperbolic* if none of the eigenvalues is zero.

Domain:. if any two points a and b of a set M_A can be connected by a path belonging to M_A, the set M_A is a *domain*.

Acknowledgements

Computational studies were performed using HPC resources from CALMIP (Grant 2016 [0851]) and from GENCI-[$CINES/IDRIS$] (Grant 2016 [085008]).

References

[1] G. Parkin (Ed.), Metal-Metal Bonding, Springer Berlin Heidelberg, Berlin, Heidelberg, 2010. .

[2] M. N. Sokolov, P. A. Abramov, Chalcogenide clusters of groups 8-10 noble metals, Coord. Chem. Rev. 256 (2012) 1972 – 1991. .

[3] J. McGrady, 9.11 - metal-metal bonding, in: J. Reedijk, K. Poeppelmeier (Eds.), Comprehensive Inorganic Chemistry II (Second Edition), Elsevier, Amsterdam, second edition edition, 2013, pp. 321 – 340. .
[4] S. T. Liddle (Ed.), Molecular Metal-Metal Bonds, Wiley-VCH Verlag GmbH & Co. KGaA, 2015. .
[5] V. G. Kuznetsov, P. A. Koz'min, A study of the structure of (PyH)HReCl$_4$, Zh. Strukt. Khim. 4 (1963) 55–62. .
[6] J. F. Berry, Metal–metal bonds in chains of three or more metal atoms: From homometallic to heterometallic chains, in: G. Parkin (Ed.), Metal-Metal Bonding, Springer Berlin Heidelberg, Berlin, Heidelberg, 2010, pp. 1–28. .
[7] J. F. Berry, F. A. Cotton, L. M. Daniels, C. A. Murillo, X. Wang, Oxidation of Ni$_3$(dpa)$_4$Cl$_2$ and Cu$_3$(dpa)$_4$Cl$_2$: Nickel-nickel bonding interaction, but no copper-copper bonds, Inorg. Chem. 42 (2003) 2418–2427. ; B. E. Villarroya, C. Tejel, M.-M. Rohmer, L. A. Oro, M. A. Ciriano, M. Bénard, Discrete iridium pyridonate chains with variable metal valence: Nature and energetics of the Ir-Ir bonding from DFT calculations, Inorg. Chem. 44 (2005) 6536–6544. ; V. P. Georgiev, P. Mohan, D. DeBrincat, J. E. McGrady, Low-symmetry distortions in extended metal atom chains (emacs): Origins and consequences for electron transport, Coord. Chem. Rev. 257 (2013) 290 – 298. .
[8] F. A. Cotton, N. F. Curtis, B. F. G. Johnson, W. R. Robinson, Compounds containing dirhenium(iii) octahalide anions, Inorg. Chem. 4 (1965) 326–330. .
[9] F. A. Cotton, C. B. Harris, Molecular structure of dipotassium octachlorodirhenate(ii) di- hydrate, K$_2$[Re$_2$X$_8$]2 H$_2$O, Inorg. Chem. 4 (1965) 330–333. .
[10] F. A. Cotton, Metal-metal bonding in [Re$_2$X$_8$]$^{2-}$ ions and other metal atom clusters, Inorg. Chem. 4 (1965) 334–336. .
[11] A. Noor, T. Bauer, T. K. Todorova, B. Weber, L. Gagliardi, R. Kempe, The ligand-based quintuple bond-shortening concept and some of its limitations, Chem. Eur. J. 19 (2013) 9825–9832. .
[12] F. A. Cotton, Chromium compounds, in: F. A. Cotton, C. A. Murillo, R. A. Walton (Eds.), Multiple Bonds Between Metal Atoms, Springer US, Boston, MA, 2005, pp. 35–68. .
[13] S. Nagase, Multiple bonds between lead atoms and short bonds between transition metals, Pure Appl. Chem. 85 (2013) 649–659. .
[14] R. J. Less, D. S. Wright, Group 14 metal-metal bonds, in: S. T. Liddle (Ed.), Molecular Metal-Metal Bonds, Wiley-VCH Verlag GmbH & Co. KGaA, 2015, pp. 485–517. .
[15] C. Jones, P. Mountford, A. Stasch, M. P. Blake, s-block metal-metal bonds, in: S. T. Liddle (Ed.), Molecular Metal-Metal Bonds, Wiley-VCH Verlag GmbH & Co. KGaA, 2015, pp. 23–45. .
[16] H. Schmidbaur, A. Schier, Argentophilic interactions, Angew. Chem. Int. Ed. Engl. 54 (2015) 746–784. .
[17] L. R. Falvello, B. M. Foxman, C. A. Murillo, Fitting the pieces of the puzzle: The δ bond, Inorg. Chem. 53 (2014) 9441–9456. .
[18] W. Bateer, S. Yoichi, I. Shinji, K. Keisaku, I. Tasuku, Charge shift along the metal-metal bond in molybdenum-tungsten mixed-metal complexes, [M$_3$(μ3- O)$_2$(μ–CH$_3$COO)$_6$(H$_2$O)$_3$]$^{2+}$ (M$_3$ = Mo$_2$W and MoW$_2$) and [MoW(O)$_2$(μ–O)$_2$(μ–NN′–EDTA)]$^{2-}$, Chem. Lett. 16 (1987) 1955–1958. .
[19] J. Andrés, M. Feliz, J. Fraxedas, V. Hernandez, J. T. Lopez-Navarrete, R. Llusar, G. Sauthier, F. R. Sensato, B. Silvi, C. Bo, J. M. Campanera, Combined theoretical and experimental analysis of the bonding in the heterobimetallic cubane-type Mo$_3$NiS$_4$ and Mo$_3$CuS$_4$ core clusters, Inorg. Chem. 46 (2007) 2159–2166. .
[20] B. Doistau, C. Rossi-Gendron, A. Tron, N. D. McClenaghan, L.-M. Chamoreau, B. Hasenknopf, G. Vives, Switchable platinum-based tweezers with Pt–Pt bonding and selective luminescence quenching, Dalton Trans. 44 (2015) 8543–8551. .
[21] R. J. Eisenhart, L. J. Clouston, C. C. Lu, Configuring bonds between first-row transition metals, Acc. Chem. Res. 48 (2015) 2885–2894. .
[22] D. Bravo-Zhivotovskii, M. Yuzefovich, M. Bendikov, K. Klinkhammer, Y. Apeloig, The synthesis and molecular structure of the first two-coordinate, dinuclear σ-bonded mercury(I) RHgHgR compound, Angew. Chem. Int. Ed. Engl. 38 (1999) 1100–1102. .
[23] E. Carmona, A. Galindo, Direct bonds between metal atoms: Zn, Cd, and Hg compounds with metal–metal bonds, Angew. Chem. Int. Ed. Engl. 47 (2008) 6526–6536. .
[24] V. J. Catalano, M. A. Malwitz, Short metal-metal separations in a highly luminescent trimetallic Ag(I) complex stabilized by bridging NHC ligands, Inorg. Chem. 42 (2003) 5483–5485. .
[25] B. Doistau, J.-L. Cantin, L.-M. Chamoreau, V. Marvaud, B. Hasenknopf, G. Vives, Mechanical switching of magnetic interaction by tweezers-type complex, Chem. Commun. 51 (2015) 12916–12919. .
[26] M. H. Chisholm, Electronically coupled mm quadruple bonded complexes of molybdenum and tungsten, in: G. Parkin (Ed.), Metal-Metal Bonding, Springer Berlin Heidelberg, Berlin, Heidelberg, 2010, pp. 29–57. .
[27] N. Xamonaki, A. Asimakopoulos, A. Balafas, M. Dasenaki, I. Choinopoulos, S. Coco, E. Simandiras, S. Koinis, Tetrathiomolybdate complexes of rhodium(I) with molybdenum-rhodium interactions, Inorg. Chem. 55 (2016) 4771–4781. .
[28] M. D. Hopkins, H. B. Gray, V. M. Miskowski, $\delta \rightarrow \delta^*$ revisited: What the energies and intensities mean, Polyhedron 6 (1987) 705 – 714. .
[29] C. Kittel, Quantum Theory of Solids, John Wiley and sons, New York, 1963. .
[30] N. W. Ashcroft, N. D. Mermin, Solid State Physics, Saunders College Publishing, 1976. .
[31] G. N. Lewis, Valence and the Structure of Atoms and Molecules, Dover, New York, 1966. .
[32] L. Pauling, The Nature of the Chemical Bond, Cornell University Press, Ithaca, 1948. .
[33] W. P. Anderson, J. K. Burdett, P. T. Czech, What is the metallic bond?, J. Am. Chem. Soc. 116 (1994) 8808–8809. .
[34] L. C. Allen, J. F. Capitani, What is the metallic bond?, J. Am. Chem. Soc. 116 (1994) 8810–8810. .
[35] M. Li, W. A. Goddard III, Interstitial-electron model for lattice in fcc metals, Phys. Rev. B 40 (1989) 12155–12163. .
[36] J. E. McGrady, Introduction and general survey of metal–metal bonds, in: S. T. Liddle (Ed.), Molecular Metal-Metal Bonds, Wiley-VCH Verlag GmbH & Co. KGaA, 2015, pp. 1–22. .
[37] F. A. Cotton, D. G. Nocera, The whole story of the two-electron bond, with the δ bond as a paradigm, Acc. Chem. Res. 39 (2000) 483–490. .
[38] B. O. Roos, A. C. Borin, L. Gagliardi, Reaching the maximum multiplicity of the covalent chemical bond, Angew. Chem. Int. Ed. 46 (2007) 1469–1472. .
[39] J. Hicks, E. J. Underhill, C. E. Kefalidis, L. Maron, C. Jones, A mixed-valence tri-zinc complex, [LZnZnZnL] (L=bulky amide), bearing a linear chain of two-coordinate zinc atoms, Angew. Chem. Int. Ed. Engl. 54 (2015) 10000–10004. .
[40] B. Silvi, The Relevance of the *ELF* Topological Approach to the Lewis, Kossel, and Langmuir Bond Model, in: P. D. M. Mingos (Ed.),

The Chemical Bond - 100 years old and getting stronger., Springer Berlin Heidelberg, Berlin, Heidelberg, 2016, pp. 213–247. .
[41] J. Bauer, H. Braunschweig, R. D. Dewhurst, Metal-only Lewis pairs with transition metal Lewis bases, Chem. Rev. 112 (2012) 4329–4346. .
[42] R. S. Osborn, D. Rogers, Crystal structure of the red form of 2,2'-bipyridyldichloroplatinum(II), J. Chem. Soc., Dalton Trans. (1974) 1002–1004. .
[43] K. R. Mann, J. G. Gordon, H. B. Gray, Characterization of oligomers of tetrakis(phenyl isocyanide)rhodium(I) in acetonitrile solution, J. Am. Chem. Soc. 97 (1975) 3553–3555. .
[44] S. Sculfort, P. Braunstein, Intramolecular d^{10}-d^{10} interactions in heterometallic clusters of the transition metals, Chem. Soc. Rev. 40 (2011) 2741–2760. .
[45] C. A. Coulson, Valence, Clarendon, Oxford, 1952. .
[46] C. Aslangul, R. Constanciel, R. Daudel, P. Kottis, Aspects of the localizability of electrons and molecules: Loge theory and related methods, in: P.-O. Löwdin (Ed.), Advances in Quantum Chemistry, volume 6, Academic Press, New York, 1972, pp. 93–141. .
[47] R. Daudel, Sur la localisabilité des corpuscules dans les noyaux et les cortèges électroniques des atomes et des molécules, Compt. Rend. Acad. Sci. 237 (1953) 601–603. .
[48] R. Daudel, S. Odiot, H. Brion, Théorie de la localisabilité des corpuscules .1. la notion de loge et la signification géometrique de la notion de couche dans le cortège électronique des atomes, J. Chim. Phys. 51 (1954) 74–77. .
[49] R. Daudel, H. Brion, S. Odiot, Localizability of electrons in atoms and molecules—application to the study of the notion of shell and of the nature of chemical bonds, J. Chem. Phys. 23 (1955) 2080–2083. .
[50] C. Aslangul, R. Constanciel, R. Daudel, L. Esnault, E. V. Ludeña, The loge theory as a starting point for variational calculations. i. general formalism, Int. J. Quant. Chem. 8 (1974) 499–522. .
[51] R. F. W. Bader, Binding regions in polyatomic molecules and electron density distributions, J. Am. Chem. Soc. 86 (1964) 5070–5075. .
[52] R. F. W. Bader, W. H. Henneker, P. E. Cade, Molecular charge distributions and chemical binding, J. Chem. Phys. 46 (1966) 3341–3363. .
[53] R. F. W. Bader, P. M. Beddall, P. E. Cade, Partitioning and characterization of molecular charge distributions, J. Am. Chem. Soc. 93 (1971) 3095–3107. .
[54] R. F. W. Bader, Molecular fragments or chemical bonds?, Acc. Chem. Res. 8 (1975) 34–40. .
[55] R. F. W. Bader, T. T. Nguyen-Dang, Y. Tal, Quantum topology of molecular charge distributions. ii. molecular structure and its change, J. Chem. Phys. 70 (1979) 4316–4329. .
[56] R. F. W. Bader, T. T. Nguyen-Dang, Quantum theory of atoms in molecules –dalton revisited, in: Advances in Quantum Chemistry, volume 14, Academic Press, New York, 1981, pp. 63–124. .
[57] R. F. W. Bader, Atoms in molecules, Acc. Chem. Res. 18 (1985) 9–15. .
[58] R. F. W. Bader, Atoms in Molecules: A Quantum Theory, Oxford Univ. Press, Oxford, 1990. .
[59] R. F. W. Bader, A quantum theory of molecular structure and its applications, Chem. Rev. 91 (1991) 893–928. .
[60] R. F. W. Bader, S. Johnson, T.-H. Tang, P. L. A. Popelier, The electron pair, J. Phys. Chem. 100 (1996) 15398–15415. .
[61] R. F. W. Bader, The quantum mechanical basis of conceptual chemistry, Monatshefte für Chemie 136 (2005) 819–854. .
[62] R. F. W. Bader, Everyman's derivation of the theory of atoms in molecules, J. Phys. Chem. A 111 (2007) 7966–7972. .
[63] U. Häussermann, S. Wengert, R. Nesper, Unequivocal partitioning of crystal structures. exemplified by intermetallic phases containing aluminium., Angew. Chem. Int. Ed. Engl. 33 (1994) 2073–2076. .
[64] B. Silvi, A. Savin, Classification of chemical bonds based on topological analysis of electron localization function, Nature 371 (1994) 683–686. .
[65] A. Savin, R. Nesper, S. Wengert, T. F. Fässler, ELF: The electron localization function, Angew. Chem. Int. Ed. Engl. 36 (1997) 1809–1832. .
[66] A. Savin, On the significance of ELF basins, J. Chem. Sci. 117 (2005) 473–475. .
[67] B. Silvi, I. Fourré, E. Alikhani, The topological analysis of the electron localization function : a key for a position space representation of chemical bonds, Monatshefte für Chemie 136 (2005) 855–879. .
[68] M. Kohout, K. Pernal, F. R. Wagner, Y. Grin, Electron localizability indicator for correlared wavefunctions. i. parallel spin pairs, Theor. Chem. Acc. 112 (2004) 453–459. .
[69] M. Kohout, K. Pernal, F. R. Wagner, Y. Grin, Electron localizability indicator for correlared wavefunctions. i. antiparallel spin pairs, Theor. Chem. Acc. 113 (2005) 287–293. .
[70] F. R. Wagner, V. Bezugly, M. Kohout, Y. Grin, Charge decomposition analysis of the electron localizability indicator: A bridge between the orbital and direct space representation of the chemical bond, Chem. Eur. J. 13 (2007) 5724–5741. .
[71] E. Cancès, R. Keriven, F. Lodier, A. Savin, How electrons guard the space: shape optimization with probability distribution criteria, Theor. Chem. Acc. 111 (2004) 373–380. .
[72] A. Gallegos, R. Carbó-Dorca, F. Lodier, E. Cancès, A. Savin, Maximal probability domains in linear molecules, J. Comput. Chem. 26 (2005) 455–460. .
[73] O. M. Lopes, Jr., B. Braida, M. Causa, A. Savin, Understanding Maximum Probability Domains with Simple Models, in: Hoggan, PEE and Brandas, EJJ and Maruani, J and Piecuch, P and Delgado Barrio, G (Ed.), Advances in the theory of quantum systems in chemistry and physics, volume 22 of *Progress in Theoretical Chemistry and Physics*, Springer, Dordrecht, 2012, pp. 173–184. .
[74] E. Francisco, A. Martín Pendás, M. A. Blanco, Electron number probability distributions for correlated wave functions, J. Chem. Phys. 126 (2007) 094102. .
[75] A. Martín Pendás, E. Francisco, M. A. Blanco, Spin resolved electron number distribution functions: How spins couple in real space, J. Chem. Phys. 127 (2007) 144103. .
[76] A. Martín Pendás, E. Francisco, M. A. Blanco, Pauling resonant structures in real space through electron number probability distributions, J. Phys. Chem. A 111 (2007) 1084–1090. .
[77] A. Martin Pendas, E. Francisco, M. A. Blanco, An electron number distribution view of chemical bonds in real space, Phys. Chem. Chem.Phys. 9 (2007) 1087–1092. .

[78] P. L. A. Popelier, F. Aicken, Atomic properties of amino acids: Computed atom types as a guide for future force-field design, ChemPhysChem 4 (2003) 824–829. .
[79] P. L. A. Popelier, Atoms In Molecules: an Introduction, Pearson Education Group, Harlow, 2000. .
[80] P. L. A. Popelier, Quantum chemical topology: on bonds and potentials. in structure and bonding, in: D. J. Wales (Ed.), Structure and Bonding. Intermolecular Forces and Clusters, volume 115, Springer, Heidelberg, 2005, pp. 1–56. .
[81] R. F. W. Bader, The lagrangian approach to chemistry, in: C. F. Matta, R. J. Boyd (Eds.), The Quantum Theory of Atoms in Molecules: From Solid State to DNA and Drug Design, John Wiley & Sons Inc, New York, 2007, pp. 37–59. .
[82] R. F. W. Bader, On the non-existence of parallel universes in chemistry, Found. Chem. 13 (2011) 11–37. .
[83] P. L. A. Popelier, On quantum chemical topology, in: R. Chauvin, C. Lepetit, B. Silvi, E. Alikhani (Eds.), Applications of Topological Methods in Molecular Chemistry, Springer International Publishing, Cham, 2016, pp. 23–52. .
[84] N. O. J. Malcolm, P. L. A. Popelier, On the full topology of the laplacian of the electron density ii: Umbrella inversion of the ammonia molecule, J. Phys. Chem. A 105 (2001) 7638–7645. .
[85] A. D. Becke, K. E. Edgecombe, A simple mesure of electron localization in atomic and molecular systems, J. Chem. Phys. 92 (1990) 5397–5403. .
[86] R. F. W. Bader, C. Gatti, A Green's function for the density, Chem. Phys. Lett. 287 (1998) 233 – 238. .
[87] C. Gatti, F. Cargnoni, L. Bertini, Chemical information from the source function, J. Comput. Chem. 24 (2003) 422–436. .
[88] C. Gatti, D. Lasi, Source function description of metal-metal bonding in d-block organometallic compounds, Faraday Discuss. 135 (2007) 55–78. .
[89] E. Monza, C. Gatti, L. Lo Presti, E. Ortoleva, Revealing electron delocalization through the source function, J. Phys. Chem. A 115 (2011) 12864–12878. .
[90] C. Gatti, O. A. M., E. Monza, L. Lo Presti, Exploring chemistry through the source function for the electron and the electron spin densities, in: R. Chauvin, C. Lepetit, B. Silvi, E. Alikhani (Eds.), Applications of Topological Methods in Molecular Chemistry, Springer International Publishing, Cham, 2016, pp. 101–129. .
[91] P. Fuentealba, C. Cardenas, R. Pino-Rios, W. Tiznado, Topological analysis of the fukui function, in: R. Chauvin, C. Lepetit, B. Silvi, E. Alikhani (Eds.), Applications of Topological Methods in Molecular Chemistry, Springer International Publishing, Cham, 2016, pp. 227–241. .
[92] A. Martín Pendás, E. Francisco, A. Gallo Bueno, J. M. Guevara Vela, A. Costales, Emergent scalar and vector fields in quantum chemical topology, in: R. Chauvin, C. Lepetit, B. Silvi, E. Alikhani (Eds.), Applications of Topological Methods in Molecular Chemistry, Springer International Publishing, Cham, 2016, pp. 131–150. .
[93] R. H. Abraham, C. D. Shaw, Dynamics: The Geometry of Behavior, Addison Wesley, Redwood City, CA, 1992. .
[94] R. H. Abraham, J. E. Marsden, Foundations of Mechanics, Addison Wesley, Redwood City, CA, 1994. .
[95] J. Palis, S. Smale, Structural Stability Theorems, American Mathematical Society, Providence, 1970. .
[96] R. Thom, Stabilité Structurelle et Morphogénèse, Intereditions, Paris, 1972. .
[97] E. Wigner, On the quantum correction for thermodynamic equilibrium, Phys. Rev. 40 (1932) 749–759. .
[98] J. R. Shewell, On the formation of quantum-mechanical operators, Am. J. Phys. 27 (1959) 16–21. .
[99] S. Diner, P. Claverie, Statistical and stochastic aspects of the delocalization problem in quantum mechanics, in: O. Chalvet, R. Daudel, S. Diner, J. P. Malrieu (Eds.), Localization and Delocalization in Quantum Chemistry, volume II, Reidel, Dordrecht, 1976, pp. 395–448. .
[100] B. Silvi, How topological partitions of the electron distributions reveal delocalization, Phys. Chem. Chem. Phys. 6 (2004) 256–260. .
[101] R. F. W. Bader, P. M. Beddall, Virial field relationship for molecular charge distributions and the spatial partitioning of molecular properties, J. Chem. Phys. 56 (1972) 3320–3329. .
[102] R. F. W. Bader, P. M. Beddall, Virial partitioning of charge distributions and properties of diatomic hydrides, J. Am. Chem. Soc. 95 (1973) 305–315. .
[103] S. Srebrenik, R. F. W. Bader, Towards the development of the quantum mechanics of a subspace, J. Chem. Phys. 63 (1975) 3945–3961. .
[104] K. Collard, G. G. Hall, Orthogonal trajectories of the electron density, Int. J. Quant. Chem. 12 (1977) 623–637. .
[105] W. L. Cao, C. Gatti, P. J. MacDougall, R. F. W. Bader, On the presence of nonnuclear attractors in the charge distribution of Li and Na cluster, Chem. Phys. Lett. 141 (1987) 380–385. .
[106] C. Gatti, P. Fantucci, G. Pacchioni, Charge-density topological study of bonding in lithium clusters.1. planar Li_n clusters (n=4,5,6), Theor. Chim. Acta (Berlin) 72 (1987) 433–458. .
[107] J. Cioslowski, Nonnuclear attractors in the Li_2 molecule, J. Phys. Chem. 94 (1990) 5496–5498. .
[108] C. Mei, K. E. Edgecombe, V. H. Smith Jr., A. Heilingbrunner, Topological analysis of the charge density of solids: bcc sodium and lithium, Int. J. Quant. Chem. 48 (1993) 287–293. .
[109] B. Silvi, C. Gatti, Direct space representation of the metallic bond., J. Phys. Chem. A 104 (2000) 947–953. .
[110] A. Martín Pendás, M. A. Blanco, A. Costales, P. Mori Sánchez, V. Luaña, Non-nuclear maxima of the electron density, Phys. Rev. Lett. 83 (1999) 1930–1933. .
[111] R. F. W. Bader, Principle of stationary action and the definition of a proper open system, Phys. Rev. B 49 (1994) 13348–13356. .
[112] R. F. W. Bader, The zero-flux surface and the topological and quantum definition of an atom in a molecule, Theor. Chem. Acc. 105 (2001) 276–283. .
[113] T. A. Keith, R. F. W. Bader, Y. Aray, Structural homeomorphism between the electron density and the virial field, Int. J. Quant. Chem. 57 (1996) 183–198. .
[114] R. F. W. Bader, A bond path: A universal indicator of bonded interactions., J. Phys. Chem. A 102 (1998) 7314. .
[115] L. J. Farrugia, C. Evans, D. Lentz, i. M. Roemer, The QTAIM approach to chemical bonding between transition metals and carbocyclic rings: A combined experimental and theoretical study of $(\eta^5-C_5H_5)Mn(CO)_3$, $(\eta^6-C_6H_6)Cr(CO)_3$, and $(E)-(\eta^5-C_5H_4)CF{=}CF(\eta^5-C_5H_4)(\eta^5-C_5H_5)_2Fe_2$, J. Am. Chem. Soc. 131 (2009) 1251–1268. .
[116] R. F. W. Bader, T. T. Nguyen-Dang, Y. Tal, A topological theory of molecular structure, Rep. Prog. Phys. 44 (1981) 893. .
[117] S. M. Bachrach, Population analysis and electron densities from quantum mechanics, in: K. B. Lipkowwitz, D. B. Boyd (Eds.), Reviews in

Computational Chemistry, VCH, New York, 1994, pp. 171–227. .
[118] C. L. Perrin, Atomic size dependence of bader electron populations: significance for questions of resonance stabilization, J. Am. Chem. Soc. 113 (1991) 2865–2868. .
[119] C. Gatti, P. Fantucci, Are bader electron populations atomic size dependent?, J. Phys. Chem. 97 (1993) 11677–11680. .
[120] T. Slee, A. Larouche, R. F. W. Bader, Properties of atoms in molecules: dipole moments and substituent effects in ethyl and carbonyl compounds, J. Phys. Chem. 92 (1988) 6219–6227. .
[121] J. Cioslowski, S. T. Mixon, Covalent bond orders in the topological theory of atoms in molecules, J. Am. Chem. Soc. 113 (1991) 4142–4145. .
[122] K. B. Wiberg, Application of the Pople-Santry-Segal CNDO method to the cyclopropylcarbinyl and cyclobutyl cation and to bicyclobutane, Tetrahedron 24 (1968) 1083–1096. .
[123] J. G. Ángyán, M. Loos, I. Mayer, Covalent bond orders and atomic valence indices in the topological theory of atoms in molecules, J. Phys. Chem. 98 (1994) 5244–5248. .
[124] I. Mayer, Bond orders and valences in the SCF theory: a comment, Theor. Chim. Acta (Berlin) 67 (1985) 315–322. .
[125] I. Mayer, On bond orders and valences in the ab initio quantum chemical theory, Int. J. Quant. Chem. 29 (1986) 73–84. .
[126] X. Fradera, M. A. Austen, R. F. W. Bader, The Lewis model and beyond, J. Phys. Chem. A 103 (1998) 304–314. .
[127] R. Ponec, M. Strnad, Population analysis of pair densities: A link between quantum chemical and classical picture of chemical structure, Int. J. Quant. Chem. 50 (1994) 43–53. .
[128] R. Ponec, F. Uhlik, Electron pairing and chemical bonds. on the accuracy of the electron pair model of chemical bond, J. Mol. Struct. (Theochem) 391 (1997) 159–168. .
[129] R. C. Bochicchio, R. Ponec, L. Lain, A. Torre, Pair population analysis within AIM theory, J. Phys. Chem. A 104 (2000) 9130–9135. .
[130] R. C. Bochicchio, R. Ponec, L. Lain, A. Torre, Multicenter bonding within the AIM theory, Theor. Chem. Acc. 105 (2001) 292–298. .
[131] K. B. Wiberg, R. F. W. Bader, C. D. H. Lau, Theoretical analysis of hydrocarbon properties. 2. additivity of group properties and the origin of strain energy, J. Am. Chem. Soc. 109 (1987) 1001–1012. .
[132] M. Mandado, A. Vila, A. M. Graña, R. A. Mosquera, J. Cioslowski, Transferability of energies of atoms in organic molecules, Chem. Phys. Lett. 371 (2003) 739–743. .
[133] F. Cortés-Guzmán, R. F. W. Bader, Transferability of group energies and satisfaction of the virial theorem, Chem. Phys. Lett. 379 (2003) 183–192. .
[134] A. Martín Pendás, M. A. Blanco, E. Francisco, Two-electron integrations in the quantum theory of atoms in molecules, J. Chem. Phys. 120 (2004) 4581–4592. .
[135] A. Martín Pendás, E. Francisco, M. A. Blanco, Two-electron integrations in the quantum theory of atoms in molecules with correlated wave functions, J. Comput. Chem. 26 (2005). .
[136] M. A. Blanco, A. Martín Pendás, E. Francisco, Interacting quantum atoms: A correlated energy decomposition scheme based on the quantum theory of atoms in molecules, J. Chem. Theory Comput. 1 (2005) 1096–1109. .
[137] E. Francisco, A. Martín Pendás, M. A. Blanco, A molecular energy decomposition scheme for atoms in molecules, J. Chem. Theory Comput. 2 (2006) 90–102. .
[138] D. S. Kosov, P. L. A. Popelier, Atomic partitioning of molecular electrostatic potentials, J. Phys. Chem. A 104 (2000) 7339–7345. .
[139] D. S. Kosov, P. L. A. Popelier, Convergence of the multipole expansion for electrostatic potentials of finite topological atoms, J. Chem. Phys. 113 (2000) 3969–3974. .
[140] P. L. A. Popelier, M. Rafat, The electrostatic potential generated by topological atoms: a continuous multipole method leading to larger convergence regions, Chem. Phys. Lett. 376 (2003) 148–153. .
[141] M. Rafat, P. L. A. Popelier, The electrostatic potential generated by topological atoms. ii. inverse multipole moments, J. Chem. Phys. 123 (2005) 204103. .
[142] M. Rafat, P. L. A. Popelier, Topological atom-atom partitioning of molecular exchange energy and its multipolar convergence, in: C. F. Matta, R. J. Boyd (Eds.), The Quantum Theory of Atoms in Molecules: From Solid State to DNA and Drug Design, John Wiley & Sons Inc, New York, 2007, pp. 121–140. .
[143] R. F. W. Bader, H. Essén, The characterization of atomic interactions, J. Chem. Phys. 80 (1984) 1943–1960. .
[144] D. Cremer, E. Kraka, Chemical bonds without bonding electron density - does the difference electron-density analysis suffice for a description of the chemical bond?, Angew. Chem. Int. Ed. Engl. 23 (1984) 627–628. .
[145] D. Cremer, E. Kraka, A description of the chemical bond in terms of local properties of the electron density and energy, Croat. Chem. Acta 57 (1983) 1259–1281. .
[146] E. Kraka, D. Cremer, Description of chemical reactions in terms of the properties of the electron density, J. Mol. Struct. (Theochem) 255 (1992) 189–206. .
[147] E. Espinosa, I. Alkorta, J. Elguero, E. Molins, From weak to strong interactions: A comprehensive analysis of the topological and energetic properties of the electron density distribution involving X−H···F−Y systems, J. Chem. Phys. 117 (2002) 5529–5542. .
[148] R. Bianchi, G. Gervasio, D. Marabello, Experimental electron density analysis of $Mn(CO)_{10}$: Metal-metal and metal-ligand bond characterization, Inorg. Chem. 39 (2000) 2360–2366. .
[149] P. Macchi, D. M. Proserpio, A. Sironi, Experimental electron density in a transition metal dimer: Metal-metal and metal-ligand bonds, J. Am. Chem. Soc. 120 (1998) 13429–13435. .
[150] P. Macchi, A. Sironi, Chemical bonding in transition metal carbonyl clusters: complementary analysis of theoretical and experimental electron densities., Coord. Chem. Rev. 238-239 (2003) 383–412. .
[151] Y. Aray, J. Rodriguez, D. Vega, Topology of the electron density and cohesive energy of the face-centered cubic transition metals, J. Phys. Chem. B 104 (2000) 4608–4612. .
[152] G. Gervasio, R. Bianchi, D. Marabello, About the topological classification of the metal-metal bond, Chem. Phys. Lett. 387 (2004) 481–484. .
[153] S. Jenkins, Direct space representation of metallicity and structural stability in sio solids, J. Phys.: Condensed Matter 14 (2002) 10251–

10263. .
[154] S. Jenkins, P. Ayers, S. Kirk, P. Mori-Sánchez, A. Martín Pendás, Bond metallicity of materials from real space charge density distributions, Chem. Phys. Lett. 471 (2009) 174–177. .
[155] P. Mori-Sánchez, A. Martín Pendás, V. Luaña, A classification of covalent, ionic, and metallic solids based on the electron density, J. Am. Chem. Soc. 124 (2002) 14721–14723. .
[156] A. E. van Arkel, Molecules and Crystals in Inorganic Chemistry, Butterworths, London, 1949. .
[157] J. A. A. Ketelaar, Chemical Constitution: An Introduction to the Theory of Chemical Bond, Elsevier, New York, 2nd edition, 1958. .
[158] L. C. Allen, Extension and completion of the periodic table, J. Am. Chem. Soc. 114 (1992) 1510–1511. .
[159] W. B. Jensen, A quantitative van arkel diagram, J. Chem. Educ. 72 (1995) 395–398. .
[160] R. F. W. Bader, P. J. MacDougall, C. D. H. Lau, Bonded and nonbonded charge concentrations and their relation to molecular geometry and reactivity, J. Am. Chem. Soc. 106 (1984) 1594–1606. .
[161] R. F. W. Bader, R. J. Gillespie, P. J. MacDougall, A physical basis for the VSEPR model of molecular geometry, J. Am. Chem. Soc. 110 (1988) 7329–7336. .
[162] R. F. W. Bader, G. L. Heard, The mapping of the conditional pair density onto the electron density, J. Chem. Phys. 111 (1999) 8789–8798. .
[163] I. Bytheway, R. J. Gillespies, T.-H. Tang, R. F. W. Bader, Core distortions and geometries of the difluorides and dihydrides of Ca, Sr, and Ba, Inorg. Chem. 34 (1995) 2407–2414. .
[164] F. Cortés-Guzmán, R. F. W. Bader, Complementarity of QTAIM and mo theory in the study of bonding in donor-acceptor complexes, Coord. Chem. Rev. 249 (2005) 633–662. .
[165] P. L. A. Popelier, On the full topology of the laplacian of the electron density, Coord. Chem. Rev. 197 (2000) 169–189. .
[166] N. O. J. Malcolm, P. L. A. Popelier, The full topology of the laplacian of the electron density: scrutinising a physical basis for the VSEPR model, Faraday Discuss. 124 (2003) 353–363. .
[167] C. Gatti, The source function descriptor as a tool to extract chemical information from theoretical and experimental electron densities, in: D. Stalke (Ed.), Electron Density and Chemical Bonding II: Theoretical Charge Density Studies, Springer Berlin Heidelberg, Berlin, Heidelberg, 2012, pp. 193–285. .
[168] R. S. Mulliken, Electronic population analysis on LCAO-MO molecular wavefunctions. i., J. Chem. Phys. 23 (1955) 1833–1840. .
[169] M. Menéndez, A. Martín Pendás, B. Braïda, A. Savin, A view of covalent and ionic bonding from maximum probability domains, Comput. Theor. Chem. 1053 (2015) 142 – 149. .
[170] P. W. Ayers, Electron localization functions and local measures of the covariance, J. Chem. Sci. 117 (2005) 441–454. .
[171] C. F. von Weizsäcker, Zur theorie der kermassen, Z. Phys. 96 (1935) 431–458. .
[172] J. K. Burdett, T. A. McCormick, Electron localization in molecules and solids: The meaning of ELF, J. Phys. Chem. A 102 (1998) 6366–6372. .
[173] R. F. Nalewajski, A. M. Koster, S. Escalante, Electron localization function as information measure, J. Phys. Chem. A 109 (2005) 10038–10043. .
[174] J. F. Dobson, Interpretation of the Fermi hole curvature, J. Chem. Phys. 94 (1991) 4328–4333. .
[175] B. Silvi, The spin pair compositions as local indicators of the nature of the bonding, J. Phys. Chem. A 107 (2003) 3081–3085. .
[176] E. Matito, B. Silvi, M. Duran, M. Solà, Electron localization function at the correlated level, J. Chem. Phys. 125 (2006) 024301. .
[177] F. Feixas, E. Matito, M. Duran, M. Solá, B. Silvi, Electron localization function at the correlated level: A natural orbital formulation, J. Chem. Theory Comput. 6 (2010) 2736–2742. .
[178] R. J. Gillespie, E. A. Robinson, Models of molecular geometry, J. Comput. Chem. 28 (2007) 87–97. .
[179] R. J. Gillespie, S. Noury, J. Pilmé, B. Silvi, An electron localization function study of the geometry of d^0 molecules of the period 4 metals Ca to Mn, Inorg. Chem. 43 (2004) 3248–3256. .
[180] B. de Courcy, L. G. Pedersen, O. Parisel, N. Gresh, B. Silvi, J. Pilmé, J.-P. Piquemal, Understanding selectivity of hard and soft metal cations within biological systems using the subvalence concept. 1. application to blood coagulation: Direct cation-protein electronic effects versus indirect interactions through water networks, J. Chem. Theory Comput. 6 (2010) 1048–1063. .
[181] A. Savin, B. Silvi, F. Colonna, Topological analysis of the electron localization function applied to delocalized bonds, Can. J. Chem. 74 (1996) 1088–1096. .
[182] M. Kohout, F. R. Wagner, Y. Grin, Electron localization function for transition-metal compounds, Theor. Chem. Acc. 108 (2002) 150–156. .
[183] M. Calatayud, J. Andrés, A. Beltrán, B. Silvi, The hierarchy of localization basins: a tool for the understanding of chemical bonding exemplified by the analysis of the VO_x and VO_x^+ (x=1-4) systems., Theoret. Chem. Acc. 105 (2001) 299–308. .
[184] B. Silvi, R. J. Gillespie, C. Gatti, Electron density analysis, in: J. Reedijk, K. Poeppelmeier (Eds.), Comprehensive Inorganic Chemistry II, volume 9, Elsevier, Oxford, 2013, pp. 188–226. .
[185] J. Pilmé, B. Silvi, M. Alikhani, Structure and stability of M−CO, M = first-transition-row metal: An application of density functional theory and topological approaches, J. Phys. Chem. A 107 (2003) 4506–4514. .
[186] S. Raub, G. Jansen, A quantitative measure of bond polarity from the electron localization function and the theory of atoms in molecules, Theor. Chem. Acc. 106 (2001) 223–232. .
[187] D. Bende, Y. Grin, F. R. Wagner, Chemical bonding in mgagas-type compounds, in: C. Felser, A. Hirohata (Eds.), Heusler Alloys - Properties, Growth, Applications, Springer, Berlin, 2015, pp. 133–156. .
[188] C. Lepetit, B. Silvi, R. Chauvin, ELF analysis of out-of-plane aromaticity and in-plane homoaromaticity in carbo[n]annulenes and [n]pericyclines, J. Phys. Chem. A 107 (2003) 464–473. .
[189] J. Pilme, J.-P. Piquemal, Advancing beyond charge analysis using the electronic localization function: Chemically intuitive distribution of electrostatic moments, J. Comput. Chem. 29 (2008) 1440–1449. .
[190] A. Martín Pendás, E. Francisco, M. Blanco, Electron-electron interactions between ELF basins, Chem. Phys. Lett. 454 (2008) 396–403. .
[191] F. Fuster, B. Silvi, Does topological approach characterizes the hydrogen bond?, Theoret. Chem. Acc. 104 (2000) 13–21. .
[192] M. E. Alikhani, F. Fuster, B. Silvi, What can tell the topological analysis of ELF on hydrogen bonding?, Structural Chemistry 16 (2005)

203–210. .
[193] S. Gutierrez-Oliva, L. Joubert, C. Adamo, F. Bulat, J. Zagal, A. Toro-Labbe, Bridging the gap between the topological and orbital description of hydrogen bonding: The case of the formic acid dimer and its sulfur derivatives, J. Phys. Chem. A 110 (2006) 5102–5107. .
[194] E. Krebs, B. Silvi, P. Raybaud, Topological analysis of the interactions between organic molecules and co(ni)mos catalytic active phases, J. Chem. Theory Comput. 5 (2009) 580–593. .
[195] B. Silvi, H. Ratajczak, Hydrogen bonding and delocalization in the *ELF* analysis approach., Phys. Chem. Chem.Phys. 18 (2016) 27442–27449. .
[196] X. Krokidis, S. Noury, B. Silvi, Characterization of elementary chemical processes by catastrophe theory, J. Phys. Chem. A 101 (1997) 7277–7282. .
[197] E. Schott, X. Zárate, R. Arratia-Pérez, Relativistic scalar and spin–orbit density functional calculations of the electronic structure, nics index and ELF function of the $[Re_2(CO)_8(\mu-BiPh)_2]$ and $[Re_2(CO)_8(\mu-BiPh_2)_2]$ clusters, Polyhedron 30 (2011) 846 – 850. .
[198] M. Valiev, E. Bylaska, N. Govind, K. Kowalski, T. Straatsma, H. V. Dam, D. Wang, J. Nieplocha, E. Apra, T. Windus, W. de Jong, Nwchem: A comprehensive and scalable open-source solution for large scale molecular simulations, Comput. Phys. Comm. 181 (2010) 1477 – 1489. .
[199] J. Pilmé, E. Renault, T. Ayed, G. Montavon, N. Galland, Introducing the ELF topological analysis in the field of quasirelativistic quantum calculations, J. Chem. Theory Comput. 8 (2012) 2985–2990. .
[200] J. Pilmé, E. Renault, F. Bassal, M. Amaouch, G. Montavon, N. Galland, QTAIM analysis in the context of quasirelativistic quantum calculations, J. Chem. Theory Comput. 10 (2014) 4830–4841. .
[201] F. W. Biegler-Konig, T. T. Nguyen-Dang, Y. Tal, R. F. W. Bader, Calculation of the average properties of atoms in molecules, J. Phys. B: Atom. Mol. Phys. 14 (1981) 2739–2751. .
[202] F. W. Biegler-Konig, R. F. W. Bader, T.-H. Tang, Calculation of the average properties of atoms in molecules. ii, J. Comput. Chem. 3 (1982) 317–328. .
[203] M. J. Frisch, G. W. Trucks, H. B. Schlegel, P. M. W. Gill, B. G. Johnson, M. A. Robb, J. R. Cheeseman, T. Keith, G. A. Petersson, J. A. Montgomery, K. Raghavachari, M. A. Al-Laham, V. G. Zakrzewski, J. V. Ortiz, J. B. Foresman, J. Cioslowski, B. B. Stefanov, A. Nanayakkara, M. Challacombe, C. Y. Peng, P. Y. Ayala, W. Chen, M. W. Wong, J. L. Andres, E. S. Replogle, R. Gomperts, R. L. Martin, D. J. Fox, J. S. Binkley, D. J. Defrees, J. Baker, J. P. Stewart, M. Head-Gordon, C. Gonzalez, , J. A. Pople, Gaussian 94, Revision D.4, Gaussian Inc. Pittsburgh PA, 1995. .
[204] M. J. Frisch, G. W. Trucks, H. B. Schlegel, G. E. Scuseria, M. A. Robb, J. R. Cheeseman, V. G. Zakrzewski, J. A. Montgomery, Jr., R. E. Stratmann, J. C. Burant, S. Dapprich, J. M. Millam, A. D. Daniels, K. N. Kudin, M. C. Strain, O. Farkas, J. Tomasi, V. Barone, M. Cossi, R. Cammi, B. Mennucci, C. Pomelli, C. Adamo, S. Clifford, J. Ochterski, G. A. Petersson, P. Y. Ayala, Q. Cui, K. Morokuma, D. K. Malick, A. D. Rabuck, K. Raghavachari, J. B. Foresman, J. Cioslowski, J. V. Ortiz, A. G. Baboul, B. B. Stefanov, G. Liu, A. Liashenko, P. Piskorz, I. Komaromi, R. Gomperts, R. L. Martin, D. J. Fox, T. Keith, M. A. Al-Laham, C. Y. Peng, A. Nanayakkara, M. Challacombe, P. M. W. Gill, B. Johnson, W. Chen, M. W. Wong, J. L. Andres, C. Gonzalez, M. Head-Gordon, E. S. Replogle, J. A. Pople, Gaussian 98, Revision A.9, Gaussian Inc. Pittsburgh PA, 1998. .
[205] M. J. Frisch, G. W. Trucks, H. B. Schlegel, , G. E. Scuseria, M. A. Robb, J. R. Cheeseman, J. A. Montgomery, Jr., T. Vreven, K. N. Kudin, J. C. Burant, J. M. Millam, S. S. Iyengar, J. Tomasi, V. Barone, B. Mennucci, M. Cossi, G. Scalmani, N. Rega, G. A. Petersson, H. Nakatsuji, M. Hada, M. Ehara, K. Toyota, R. Fukuda, J. Hasegawa, M. Ishida, T. Nakajima, Y. Honda, O. Kitao, H. Nakai, M. Klene, X. Li, J. E. Knox, H. P. Hratchian, J. B. Cross, C. Adamo, J. Jaramillo, R. Gomperts, R. E. Stratmann, O. Yazyev, A. J. Austin, R. Cammi, C. Pomelli, J. W. Ochterski, P. Y. Ayala, K. Morokuma, G. A. Voth, P. Salvador, J. J. Dannenberg, V. G. Zakrzewski, S. Dapprich, A. D. Daniels, M. C. Strain, O. Farkas, D. K. Malick, A. D. Rabuck, K. Raghavachari, J. B. Foresman, J. V. Ortiz, Q. Cui, A. G. Baboul, S. Clifford, J. Cioslowski, B. B. Stefanov, A. L. G. Liu, P. Piskorz, I. Komaromi, R. L. Martin, D. J. Fox, T. Keith, M. A. Al-Laham, C. Y. Peng, A. Nanayakkara, M. Challacombe, P. M. W. Gill, B. Johnson, W. Chen, M. W. Wong, C. Gonzalez, , J. A. Pople, Gaussian 03, Revision A.1, Gaussian, Inc., Wallingford, CT, 2003. .
[206] M. J. Frisch, G. W. Trucks, H. B. Schlegel, G. E. Scuseria, M. A. Robb, J. R. Cheeseman, G. Scalmani, V. Barone, B. Mennucci, G. A. Petersson, H. Nakatsuji, M. Caricato, X. Li, H. P. Hratchian, A. F. Izmaylov, J. Bloino, G. Zheng, J. L. Sonnenberg, M. Hada, M. Ehara, K. Toyota, R. Fukuda, J. Hasegawa, M. Ishida, T. Nakajima, Y. Honda, O. Kitao, H. Nakai, T. Vreven, J. A. Montgomery, Jr., J. E. Peralta, F. Ogliaro, M. Bearpark, J. J. Heyd, E. Brothers, K. N. Kudin, V. N. Staroverov, R. Kobayashi, J. Normand, K. Raghavachari, A. Rendell, J. C. Burant, S. S. Iyengar, J. Tomasi, M. Cossi, N. Rega, J. M. Millam, M. Klene, J. E. Knox, J. B. Cross, V. Bakken, C. Adamo, J. Jaramillo, R. Gomperts, R. E. Stratmann, O. Yazyev, A. J. Austin, R. Cammi, C. Pomelli, J. W. Ochterski, R. L. Martin, K. Morokuma, V. G. Zakrzewski, G. A. Voth, P. Salvador, J. J. Dannenberg, S. Dapprich, A. D. Daniels, ÃČ. Farkas, J. B. Foresman, J. V. Ortiz, J. Cioslowski, D. J. Fox, Gaussian 09 Revision D.01, 2009. Gaussian Inc. Wallingford CT 2009. .
[207] M. W. Schmidt, K. K. Baldbridge, J. A. Boatz, S. T. Elbert, M. S. Gordon, J. J. Jensen, S. Koseki, N. Matsunaga, K. A. Nguyen, S. Su, T. L. Windus, M. Dupuis, J. A. Montgomery, Gamess, J. Comput. Chem. 14 (1993) 1347–1363. .
[208] F. Biegler-König, Calculation of atomic integration data, J. Comput. Chem. 21 (2000) 1040–1048. .
[209] F. Biegler-König, J. Schönbohm, D. Bayles, Aim2000, J. Comput. Chem. 22 (2001) 545–559. .
[210] F. Biegler-König, J. Schönbohm, Update of the aim2000-program for atoms in molecules, J. Comput. Chem. 23 (2002) 1489–1494. .
[211] T. A. Keith, AIMAll (Version 14.11.23), Overland Park KS, USA, 2014. .
[212] P. L. A. Popelier, Morphy, a program for an automated "atoms in molecules" analysis, Comput. Phys. Commun. 93 (1996) 212–240. .
[213] P. L. A. Popelier, Integration of atoms in molecules: a critical examination, Mol. Phys. 87 (1996) 1169–1187. .
[214] P. L. A. Popelier, A method to integrate an atom in a molecule without explicit representation of the interatomic surface, Comput. Phys. Comm. 108 (1998) 180–190. .
[215] P. L. A. Popelier, A fast algorithm to compute atomic charges based on the topology of the electron density, Theor. Chem. Acc. 105 (2001) 393–399. .
[216] O. Nathaniel, J. Malcom, P. L. A. Popelier, An improved algorithm to locate critical points in a 3d scalar field as implemented in the program morphy, J. Comput. Chem. 24 (2003) 437–442 . .

[217] O. Nathaniel, J. Malcom, P. L. A. Popelier, An algorithm to delineate and integrate topological basins in a three-dimensional quantum mechanical density function, J. Comput. Chem. 24 (2003) 1276–1282 . .
[218] J. Cioslowski, An efficient evaluation of atomic properties using a vectorized numerical integration with dynamic thresholding, Chem. Phys. Lett. 194 (1992) 73–78. .
[219] J. Cioslowski, A. Nanayakkara, M. Challacombe, Rapid evaluation of atomic properties with mixed analytical/numerical integration, Chem. Phys. Lett. 203 (1993) 137–142. .
[220] V. R. Saunders, R. Dovesi, C. Roetti, M. Causà, N. M. Harrison, R. Orlando, C. M. Zicovitch-Wilson, CRYSTAL98, User's manual, Torino, Italy, 1998. .
[221] C. Pisani, U. Birkenheuer, F. Corà, R. Nada, S. Casassa, EMBED96 User's manual, Università di Torino, Torino, Italy, 1996. .
[222] C. Gatti, Topond98 manual, CNR-CSRSRC, Milano, Italy, 1998. .
[223] R. Dovesi, V. R. Saunders, C. Roetti, R. Orlando, C. M. Zicovich-Wilson, F. Pascale, B. Civalleri, K. Doll, N. M. Harrison, I. J. Bush, P. D'Arco, M. Llunell, CRYSTAL06 User's Manual, Torino, Italy, 2006. .
[224] R. Dovesi, R. Orlando, B. Civalleri, C. Roetti, V. R. Saunders, , C. M. Zicovich-Wilson, Crystal: a computational tool for the ab initio study of the electronic properties of crystals, Zeit. Kristallogr. 220 (2005) 571–573. .
[225] R. Dovesi, V. R. Saunders, C. Roetti, R. Orlando, C. M. Zicovich-Wilson, F. Pascale, B. Civalleri, K. Doll, N. M. Harrison, I. J. Bush, P. D'Arco, M. Llunell, CRYSTAL09 User's Manual, Torino, Italy, 2009. .
[226] A. Martín Pendás, V. Luaña, The CRITIC program, Universidad de Oviedo, Oviedo, Spain, 1995. .
[227] A. Otero de la Roza, M. Blanco, A. Martín Pendás, V. Luaña, Critic: a new program for the topological analysis of solid-state electron densities, Comp. Phys. Comm. 180 (2009) 157–166. .
[228] K. Schwarz, P. Blaha, G. Madsen, Electronic structure calculations of solids using the wien2k package for material sciences, Comput. Phys. Comm. 147 (2002) 71–76. ; K. Schwarz, P. Blaha, Solid state calculations using wien2k, Computational Materials Science 28 (2003) 259–273. .
[229] M. Blanco, Métodos cuánticos locales para la simulación de materiales iónicos. Fundamentos, algoritmos y aplicaciones, Tesis doctoral, Ph.D. thesis, Universidad de Oviedo, 1997. .
[230] B. B. Iversen, F. K. Larsen, M. Souhassou, M. Takata, Experimental evidence for the existence of non-nuclear maxima in the electron-density distribution of metallic beryllium. a comparative study of the maximum entropy method and the multipole refinement method, Acta Cryst. B 51 (1995) 580–591. .
[231] Y. Aray, J. Rodriguez, J. Rivero, Numerical determination of the topological properties of the electronic charge density in molecules and solids using density functional theory, J. Phys. Chem. A 101 (1997) 6976–6982. .
[232] B. P. Uberuaga, E. R. Batista, H. Jónsson, Elastic sheet method for identifying atoms in molecules, J. Chem. Phys. 111 (1999) 10664–10669. .
[233] C. Katan, P. Rabiller, C. Lecomte, M. Guezo, V. Oison, M. Souhassou, Numerical computation of critical properties and atomic basins from three-dimensional grid electron densities, J. Appl. Cryst. 36 (2003) 65–73. .
[234] G. Henkelman, A. Arnaldsson, H. Jonsson, A fast and robust algorithm for bader decomposition of charge density, Comput. Mat. Science 36 (2006) 354–360. .
[235] W. Tang, E. Sanville, G. Henkelman, A grid-based bader analysis algorithm without lattice bias, J. Phys.: Condensed Matter 21 (2009) 084204. .
[236] A. Volkov, C. Gatti, Y. Abramov, P. Coppens, Evaluation of net atomic charges and atomic and molecular electrostatic moments through topological analysis of the experimental charge density, Acta Cryst. A 56 (2000) 252–258. .
[237] N. K. Hansen, P. Coppens, Testing aspherical atom refinements on small-molecule data sets, Acta Cryst. A34 (1978) 909–921. .
[238] T. Koritsanszky, S. Howard, T. Richter, Z. Su, P. R. P. R. Mallinson, N. K. Hansen, XD Computer Program Package for Multipolar Refinement and Analysis of Electron Densities from Xray Diffraction Data. Program XDPRO, Free University of Berlin, Berlin, Germany, 1995. .
[239] A. Volkov, P. Macchi, L. J. Farrugia, C.Gatti, P. Mallinson, T. Richter, T. Koritsanszky, XD2006 - A Computer Program Package for Multipole Refinement, Topological Analysis of Charge Densities and Evaluation of Intermolecular Energies from Experimental and Theoretical Structure Factors, 2006. .
[240] M. Barzaghi, PAMoC (Version 2001.0), Online User's Manual, CNR-ISTM, Institute of Molecular Science and Technologies, Milano, Italy, 2002. .
[241] R. F. Stewart, Electron population analysis with generalized x-ray scattering factors: Higher multipoles, J. Chem. Phys. 58 (1973) 1668–1676. .
[242] R. F. Stewart, M. A. Spackman, VALRAY User's Manual, Carnegie-Mellon University, Pittsburgh, USA, 1983. .
[243] S. Noury, X. Krokidis, F. Fuster, B. Silvi, Computational tools for the electron localization function topological analysis., Comput. in Chem. 23 (1999) 597–604. .
[244] D. Kozlowski, J. Pilmé, New insights in quantum chemical topology studies using numerical grid-based analyses, J. Comput. Chem. 32 (2011) 3207–3217. .
[245] J. Contreras-Garcia, P. Mori-Sanchez, B. Silvi, J. M. Recio, A quantum chemical interpretation of compressibility in solids, J. Chem. Theory Comput. 5 (2009) 2108–2114. .
[246] M. Kohout, Program DGrid, version 4.6, Radebeul, 2011. .
[247] H. L. Schmider, A. D. Becke, Chemical content of the kinetic energy density, J. Mol. Struct. (Theochem) 527 (2000) 51–61. .
[248] R. Ponec, Electron pairing and chemical bonds. chemical structure, valences and structural similarities from the analysis of the Fermi holes, J. Math. Chem. 21 (1997) 323–333. .
[249] C. F.-W. Lu Tian, Multiwfn: A multifunctional wavefunction analyzer, J. Comput. Chem. 33 (2012) 580–592. .
[250] E. Francisco, A. Martín Pendás, M. Blanco, EDF: Computing electron number probability distribution functions in real space from molecular wave functions, Comp. Phys. Comm. 178 (2008) 621–634. .
[251] R. Y. de Vries, W. J. Briels, D. Feil, Critical analysis of non-nuclear electron-density maxima and the maximum entropy method, Phys. Rev.

Lett. 77 (1996) 1719–1722. .
[252] D. Jayatilaka, Wave function for beryllium fron x-ray diffraction data, Phys. Rev. Lett. 80 (1998) 798–801. .
[253] A. I. Baranov, M. Kohout, Electron localizability for hexagonal element structures, J. Comput. Chem. 29 (2008) 2161–2171. .
[254] K. Koepernik, H. Eschrig, Full-potential nonorthogonal local-orbital minimum-basis band-structure scheme, Phys. Rev. B 59 (1999) 1743–1757. .
[255] J. K. Dewhurst, S. Sharma, C. Ambrosch-Draxl, Full-potential linearised augmented-planewave code EXCITING for determining the properties of crystalline solids, EXCITING Code Users' Manual version 0.9.114, 2007. .
[256] V. G. Vaks, M. I. Katsnelson, V. G. Koreshkov, A. I. Likhtenstein, O. E. Parfenov, V. F. Skok, V. A. Sukhoparov, A. V. Trefilov, A. A. Chernyshov, An experimental and theoretical study of martensitic phase transitions in Li and Na under pressure, J. Phys. Condens. Matter 1 (1989) 5319–5335. .
[257] C. L. Guillaume, E. Gregoryanz, O. Degtyareva, M. I. McMahon, M. Hanfland, S. Evans, M. Guthrie, S. V. Sinogeikin, H.-K. Mao, Cold melting and solid structures of dense lithium, Nat Phys 7 (2011) 211–214. .
[258] A. I. Baranov, M. Kohout, Electron localization and delocalization indices for solids, J. Comput. Chem. 32 (2011) 2064–2076. .
[259] A. Ormeci, H. Rosner, F. Wagner, M. Kohout, Y. Grin, Electron localization function in full-potential representation for crystalline materials, J. Phys. Chem. A 110 (2006) 1100–1105. .
[260] M. Marqués, G. J. Ackland, L. F. Lundegaard, G. Stinton, R. J. Nelmes, M. I. McMahon, J. Contreras-García, Potassium under pressure: A pseudobinary ionic compound, Phys. Rev. Lett. 103 (2009) 115501. .
[261] M. Marqués, M. I. McMahon, E. Gregoryanz, M. Hanfland, C. L. Guillaume, C. J. Pickard, G. J. Ackland, R. J. Nelmes, Crystal structures of dense lithium: A metal-semiconductor-metal transition, Phys. Rev. Lett. 106 (2011) 095502. .
[262] M. Kohout, A. Savin, atomic shell structure and electron numbers, Int. J. Quant. Chem. 60 (1996) 875–882. .
[263] U. Häussermann, S. Wengert, R. Nesper, Localization of electrons in intermetallic phases containing aluminium., Angew. Chem. Int. Ed. Engl. 33 (1994) 2069–2072. .
[264] R. W. G. Wyckoff, Crystal Structures, Robert E. Krieger, Malabar, 1986. .
[265] R. W. Powell, The electrical resistivity of gallium and some other anisotropic properties of this metal, Proc. R. Soc. A 209 (1951) 525–541. .
[266] Y. Grin, U. Schwarz, W. Steurer, Crystal Structure and Chemical Bonding, Wiley-VCH Verlag GmbH & Co. KGaA, pp. 19–62. .
[267] Y. Grin, 2.13 - crystal structure and bonding in intermetallic compounds, in: J. Reedijk, K. Poeppelmeier (Eds.), Comprehensive Inorganic Chemistry II (Second Edition), Elsevier, Amsterdam, second edition edition, 2013, pp. 359 – 373. .
[268] Y. Grin, F. R. Wagner, M. Armbrüster, M. Kohout, A. Leithe-Jasper, U. Schwarz, U. Wedig, H. G. von Schnering, $CuAl_2$ revisited: Composition, crystal structure, chemical bonding, compressibility and raman spectroscopy, J. of Solid State Chem. 179 (2006) 1707–1719. .
[269] A. I. Baranov, M. Kohout, F. R. Wagner, Y. Grin, W. Bronger, Spatial chemistry of the aluminium–platinum compounds: a quantum chemical approach, Z. Kristallogr. 222 (2007) 527–531. .
[270] A. Ormeci, Y. Grin, Chemical bonding in Al_5Co_2: The electron localizability-electron density approach, Israel Journal of Chemistry 51 (2011) 1349–1354. .
[271] Y. Grin, M. Armbrüster, A. I. Baranov, K. Finzel, M. Kohout, A. Ormeci, H. Rosner, F. R. Wagner, Atomic interactions in the intermetallic catalyst gapd, Mol. Phys. 114 (2016) 1250–1259. .
[272] O. Sichevych, M. Kohout, W. Schnelle, H. Borrmann, R. Cardoso-Gil, M. Schmidt, U. Burkhardt, Y. Grin, $EuTM_2Ga_8$ (TM = Co, Rh, Ir) – a contribution to the chemistry of the $CeFe_2Al_8$-type compounds, Inorg. Chem. 48 (2009) 6261–6270. .
[273] A. Ormeci, A. Simon, Y. Grin, Structural topology and chemical bonding in laves phases, Angew. Chem. Int. Ed. Engl. 49 (2010) 8997–9001. .
[274] D. Bende, F. R. Wagner, Y. Grin, 8 - n rule and chemical bonding in main-group mgagas-type compounds, Inorg. Chem. 54 (2015) 3970–3978. .
[275] R. Llusar, A. Beltrán, J. Andrés, B. Silvi, Pseudopotential periodic hartree fock study of K_8In_{11} and Rb_8In_{11} systems., J. Phys. Chem. 99 (1995) 12483–12487. .
[276] S. Wengert, R. Nesper, Struktur und eigenschaften von $Ba_2Mg_3Si_4$, einer zintl-phase mit planaren Si_6-einheiten, Z. Anorg. Allg. Chem. 624 (1998) 1801–1806. .
[277] T. F. Fassler, The role of non-bonding electron pairs in intermetallic compounds, Chem. Soc. Rev. 32 (2003) 80–86. .
[278] X.-J. Feng, Y. Prots, M. Bobnar, M. P. Schmidt, W. Schnelle, J.-T. Zhao, Y. Grin, Zintl-phase Sr_3LiAs_2H: Crystal structure and chemical bonding analysis by the electron localizability approach, Chem. Eur. J. 21 (2015) 14471–14477. .
[279] D. Bende, Y. Grin, F. R. Wagner, Covalence and ionicity in mgagas-type compounds, Chem. Eur. J. 20 (2014) 9702–9708. .
[280] D. J. Wales, D. M. P. Mingos, T. Slee, Z. Lin, Clusters in inorganic and molecular beam chemistry. some unifying principles, Acc. Chem. Res. 23 (1990) 17–22. .
[281] T. P. Martin, T. Bergmann, H. Goehlich, T. Lange, Shell structure of clusters, J. Phys. Chem. 95 (1991) 6421–6429. .
[282] M. E. Alikhani, S. Shaik, A topological study of the ferromagnetic "no-pair bonding" in maximum-spin lithium clusters: Li-n+1(n)(n=2-6), Theor. Chem. Acc. 116 (2006) 390–397. .
[283] V. Bezugly, P. Wielgus, M. Kohout, F. R. Wagner, Electron localizability indicators ELI-D and ELIA for highly correlated wavefunctions of homonuclear dimers. I. Li_2, Be_2, B_2, and C_2, J. Comput. Chem. 31 (2010) 1504–1519. .
[284] S. Berski, P. Durlak, Nature of the mg-mg and ca-ca bonding in model metalo-organic compounds. the topological analysis of ELF function., Polyhedron (2017) paper submitted. .
[285] F. R. Wagner, A. Noor, R. Kempe, Ultrashort metal-metal distances and extreme bond orders, Nat Chem 1 (2009) 529–536. .
[286] A. Falceto, K. H. Theopold, S. Alvarez, Cr−Cr quintuple bonds: Ligand topology and interplay between metal-metal and metal-ligand bonding, Inorg. Chem. 54 (2015) 10966–10977. ; A. Falceto, S. Alvarez, Comparison of the Cr−Cr quadruple and quintuple bonding mechanisms, in: P. D. M. Mingos (Ed.), The Chemical Bond - 100 years old and getting stronger., Springer Berlin Heidelberg, Berlin, Heidelberg, 2016, pp. 249–264. .

[287] F. A. Cotton, W. T. Hall, Reactions of niobium(III) and tantalum(III) compounds with acetylenes. 2. preparation and structure of $Ta_2Cl_4(\mu{-}Cl)_2(\mu{-}Me_3CC{\equiv}CCMe_3)(THF)_2$ the shortest known tantalum-tantalum bond, Inorg. Chem. 19 (1980) 2354–2356. .

[288] S. M. Beshouri, I. P. Rothwell, K. Folting, J. C. Huffman, W. E. Streib, Synthesis and structure of hexabenzyl-dimolybdenum (Mo≡Mo), Polyhedron 5 (1986) 1191 – 1195. .

[289] F. A. Cotton, T. Inglis, M. Kilner, T. R. Webb, Quadruply bonded pairs of metal atoms bridged by amidines. I. preparation and structure of tetrakis-(N,N'-diphenylbenzamidianto)dimolybdenum(II), Inorg. Chem. 14 (1975) 2023–2026. .

[290] L. Gagliardi, 7, in: G. Frenking, S. Shaik (Eds.), The Chemical Bond : Chemical Bonding Across the Periodic Table, Wiley-VCH Verlag GmbH & Co. KGaA, Weinheim, Germany., 2014, pp. 253–268. .

[291] R. Llusar, A. Beltrán, J. Andrés, F. Fuster, B. Silvi, Topological analysis of multiple metal-metal bonds in dimers of the $M_2(formamidinate)_4$ type with M=Nb, Mo, Tc, Ru, Rh and Pd., J. Phys. Chem. A 105 (2001) 9460–9466. .

[292] S. S. Shaik, D. Danovich, B. Silvi, D. Lauvergnat, P. Hiberty, Charge-shift bonding–a class of electron pair bonds emerges from valence bond theory and supported by electron localization function approach, Chem. Eur. J. 21 (2005) 6358–6371. .

[293] G. La Macchia, F. Aquilante, V. Veryazov, B. O. Roos, L. Gagliardi, Bond length and bond order in one of the shortest Cr−Cr bonds, Inorg. Chem. 47 (2008) 11455–11457. .

[294] A. Noor, F. Wagner, R. Kempe, Metal-metal distances at the limit: A coordination compound with an ultrashort chromium-chromium bond, Angew. Chem. Int. Ed. Engl. 47 (2008) 7246–7249. .

[295] D. B. DuPré, Multiple bonding in the chromium dimer supported by two diazadiene ligands, J. Phys. Chem. A 113 (2009) 1559–1563. .

[296] M. Brynda, L. Gagliardi, P.-O. Widmark, P. P. Power, B. O. Roos, A quantum chemical study of the quintuple bond between two chromium centers in [phcrcrph]: trans-bent versus linear geometry, Angew. Chem. Int. Ed. Engl. 45 (2006) 3804–3807. .

[297] J. Utko, S. Przybylak, L. B. Jerzykiewicz, K. Mierzwicki, Z. Latajka, P. Sobota, The first structurally characterized nonorganometallic titanium(iii) alkoxo-bridged dinuclear complexes, Inorg. Chem. 42 (2003) 267–269. .

[298] S. Hao, K. Feghali, S. Gambarotta, Preparation and characterization of a diamagnetic and dinuclear titanium(iii) formamidinate complex. evidence for the existence of a Ti−Ti bond?, Inorg. Chem. 36 (1997) 1745–1748. .

[299] R. Bianchi, G. Gervasio, D. Marabello, The experimental charge density in transition metal compounds, C. R. Chim. 8 (2005) 1392 – 1399. .

[300] X. Li, S. Huo, Y. Zeng, Z. Sun, S. Zheng, L. Meng, Metal-metal and metal-ligand bonds in $(\eta_5{-}C_5H_5)_2M_2$ (M = BeMgCaNiCuZn), Organometallics 32 (2013) 1060–1066. .

[301] M. R. Philpott, Y. Kawazoe, The electronic structure of the dizincocene core, Chem. Phys. 327 (2006) 283–290. ; M. R. Philpott, Y. Kawazoe, Electronic structure of dimetallocene molecules: Dizincocene $Zn_2(\eta_5{-}C_5Me_5)_2$, J. Mol. Struct. (Theochem) 773 (2006) 43–52. ; M. R. Philpott, Y. Kawazoe, Ab initio study of the change from η_5- to η_1-coordination in group 12 dimetallocenes $MM'(C_5H_5)_2$ with M, M'=Zn, Cd, Hg, Chem. Phys. 333 (2007) 201–207. .

[302] C. Foroutan-Nejad, J. Vicha, R. Marek, M. Patzschke, M. Straka, Unwilling u-u bonding in $U_2@C_{80}$: cage-driven metal-metal bonds in di-uranium fullerenes, Phys. Chem. Chem. Phys. 17 (2015) 24182–24192. .

[303] A. A. Popov, S. M. Avdoshenko, A. M. Pendas, L. Dunsch, Bonding between strongly repulsive metal atoms: an oxymoron made real in a confined space of endohedral metallofullerenes, Chem. Commun. 48 (2012) 8031–8050. .

[304] Y.-C. Liu, S.-X. Wu, Y.-H. Kan, H.-Y. Zhang, Z.-M. Su, Structural and bonding analyses on a homologous metalÃćÂĂÂŞmetal bond guestÃćÂĂÂŞhost series $M_2@C_{50}X_{10}$ (M = Zn, Cd, Hg; X = CH, N, B), Eur. J. Inorg. Chem. 2013 (2013) 2220–2230. .

[305] H.-S. Hu, N. Kaltsoyannis, The shortest th-th distance from a new type of quadruple bond, Phys. Chem. Chem. Phys. (2017) –. .

[306] F. Estevan, S. Ibáñez, A. Ofori, P. Hirva, M. Sanaú, M. A. Úbeda, Benzoato and thiobenzoato ligands in the synthesis of dinuclear palladium(iii) and -(ii) compounds: Stability and catalytic applications, Eur. J. Inorg. Chem. 2015 (2015) 2822–2832. ; F. Estevan, P. Hirva, A. Ofori, M. Sanaú, T. Špec, M. Úbeda, Pyrazole and pyrazolate as ligands in the synthesis and stabilization of new palladium(ii) and (iii) compounds, Inorg. Chem. 55 (2016) 2101–2113. .

[307] A. Ofori, S. Suvanto, S. Jääskeläinen, L. Koskinen, I. O. Koshevoy, P. Hirva, Versatile coordination modes in silver-imidazolecarbaldehyde oxime complexes: Structural and computational analysis, Crystal Growth & Design 16 (2016) 255–264. .

[308] P. Pyykko, Strong closed-shell interactions in inorganic chemistry, Chem. Rev. 97 (1997) 597–636. .

[309] E. O'Grady, N. Kaltsoyannis, Does metallophilicity increase or decrease down group 11? computational investigations of $[Cl{-}M{-}PH_3]_2$ (M = Cu, Ag, Au, [111]), Phys. Chem. Chem.Phys. 6 (2004) 680–687. .

[310] K.-C. Wong, V.-M. Au, V.-W. Yam, 8.03 - noncovalent metal-metal interactions, in: J. Reedijk, K. Poeppelmeier (Eds.), Comprehensive Inorganic Chemistry II (Second Edition), Elsevier, Amsterdam, second edition edition, 2013, pp. 59 – 130. .

[311] L. Ray, M. M. Shaikh, P. Ghosh, Shorter argentophilic interaction than aurophilic interaction in a pair of dimeric $[(NHC)MCl]_2$ (m = ag, au) complexes supported over a N/O-functionalized N-heterocyclic carbene (NHC) ligand, Inorg. Chem. 47 (2008) 230–240. .

[312] J.-P. Zhang, Y.-B. Wang, X.-C. Huang, Y.-Y. Lin, X.-M. Chen, Metallophilicity versus $\pi-\pi$ interactions: Ligand-unsupported argentophilicity/cuprophilicity in oligomers-of-dimers $[M_2L_2]$n (M=CuI or AgI, L=tridentate ligand), Chem. Eur. J. 11 (2005) 552–561. .

[313] J.-M. Poblet, M. Benard, Cuprophilicity, a still elusive concept: a theoretical analysis of the ligand-unsupported cui-cui interaction in two recently reported complexes, Chem. Commun. (1998) 1179–1180. .

[314] H. L. Hermann, G. Boche, P. Schwerdtfeger, Metallophilic interactions in closed-shell copper(i) compounds-a theoretical study, Chemistry - A European Journal 7 (2001) 5333–5342. .

[315] X. Jiang, J. C. Bollinger, M.-H. Baik, D. Lee, Copper clusters built on bulky amidinate ligands: spin delocalization via superexchange rather than direct metal-metal bonding, Chem. Commun. (2005) 1043–1045. .

[316] A. C. Lane, C. L. Barnes, W. E. Antholine, D. Wang, A. T. Fiedler, J. R. Walensky, Di- and trinuclear mixed-valence copper amidinate complexes from reduction of iodine, Inorg. Chem. 54 (2015) 8509–8517. .

[317] S. Dinda, A. G. Samuelson, The nature of bond critical points in dinuclear copper(i) complexes, Chem. Eur. J. 18 (2012) 3032–3042. .

[318] C. Barriere, K. Piettre, V. Latour, O. Margeat, C.-O. Turrin, B. Chaudret, P. Fau, Ligand effects on the air stability of copper nanoparticles obtained from organometallic synthesis, J. Mater. Chem. 22 (2012) 2279–2285. ; C. Barriere, G. Alcaraz, O. Margeat, P. Fau, J. B. Quoirin, C. Anceau, B. Chaudret, Copper nanoparticles and organometallic chemical liquid deposition (OMCLD) for substrate metallization, J.

Mater. Chem. 18 (2008) 3084–3086. ; A. Glaria, J. Cure, K. Piettre, Y. Coppel, C. Turrin, B. Chaudret, P. Fau, Deciphering ligands' interaction with cu and Cu_2O nanocrystal surfaces by nmr solution tools, Chem. Eur. J. 21 (2015) 1169–1178. ; J. Cure, Y. Coppel, T. Dammak, P. F. Fazzini, A. Mlayah, B. Chaudret, P. Fau, Monitoring the coordination of amine ligands on silver nanoparticles using nmr and sers, Langmuir 31 (2015) 1362–1367. ; J. Cure, K. Piettre, Y. Coppel, E. Beche, J. Esvan, V. Collière, B. Chaudret, P. Fau, Solution layer deposition: A technique for the growth of ultra-pure manganese oxides on silica at room temperature, Angew. Chem. Int. Ed. Engl. 55 (2016) 3027–3030. .

[319] B. S. Lim, A. Rahtu, J.-S. Park, R. G. Gordon, Synthesis and characterization of volatile, thermally stable, reactive transition metal amidinates, Inorg. Chem. 42 (2003) 7951–7958. .

[320] B. de Courcy, J.-P. Dognon, C. Clavaguéra, N. Gresh, J.-P. Piquemal, Interactions within the alcohol dehydrogenase zn(ii)-metalloenzyme active site: Interplay between subvalence, electron correlation/dispersion, and charge transfer/induction effects, Int. J. Quant. Chem. 111 (2011) 1213–1221. .

[321] E. Espinosa, E. Molins, C. Lecomte, Hydrogen bond strengths revealed by topological analyses of experimentally observed electron densities, Chem. Phys. Lett. 285 (1998) 170 – 173. ; E. Espinosa, I. Alkorta, I. Rozas, J. Elguero, E. Molins, About the evaluation of the local kinetic, potential and total energy densities in closed-shell interactions, Chem. Phys. Lett. 336 (2001) 457 – 461. .

[322] M. Boukallaba, B. Kerkeni, C. Lepetit, D. Berthomieu, Coordination complexes of 4-methylimidazole with znii and cuii in gas phase and in water: A dft study., J. Mol. Model. (2017) in press. .

[323] J. E. Bercaw, A. C. Durrell, H. B. Gray, J. C. Green, N. Hazari, J. A. Labinger, J. R. Winkler, Electronic structures of pdii dimers, Inorg. Chem. 49 (2010) 1801–1810. .

[324] N. Nebra, N. Saffon, L. Maron, B. Martin-Vaca, D. Bourissou, 1,3-bis(thiophosphinoyl)indene: A unique and versatile scaffold fora original polymetallic complexes, Inorg. Chem. 50 (2011) 6378–6383. .

[325] S. Grimme, J.-P. Djukic, Cation-cation "attraction": When london dispersion attraction wins over coulomb repulsion, Inorg. Chem. 50 (2011) 2619–2628. .

[326] G. Jansen, M. Schubart, B. Findeis, L. H. Gade, I. J. Scowen, M. McPartlin, Unsupported ti-co and zr-co bonds in heterobimetallic complexes: A theoretical description of metal-metal bond polarity, J. Am. Chem. Soc. 120 (1998) 7239–7251. .

[327] M. Green, A new approach to the formal classification of covalent compounds of the elements, Journal of Organometallic Chemistry 500 (1995) 127 – 148. .

[328] R. A. Jones, A. L. Stuart, J. L. Atwood, W. E. Hunter, Substitution reactions of di-tert-butylphosphido complexes of nickel(i). crystal structures of $Ni_2[\mu-(Me_3C)_2P]_2(CO)_2(PMe_3)$(Ni−Ni)and$Ni_2[\mu-(Me_3C)_2P]_2(CO)_3$ (ni-ni), Organometallics 2 (1983) 874–878. .

[329] W. Zhu, A. C. Marr, Q. Wang, F. Neese, D. J. E. Spencer, A. J. Blake, P. A. Cooke, C. Wilson, , M. Schröder, Modulation of the electronic structure and the ni-fe distance in heterobimetallic models for the active site in [NiFe] hydrogenase, Proc. Nat. Acad. Sci. 102 (2005) 18280–18285. .

[330] D. Schilter, V. Pelmenschikov, H. Wang, F. Meier, L. B. Gee, Y. Yoda, M. Kaupp, T. B. Rauchfuss, S. P. Cramer, Synthesis and vibrational spectroscopy of 57fe-labeled models of [nife] hydrogenase: first direct observation of a nickel-iron interaction, Chem. Commun. 50 (2014) 13469–13472. .

[331] M. T. Huynh, D. Schilter, S. Hammes-Schiffer, T. B. Rauchfuss, Protonation of nickel-iron hydrogenase models proceeds after isomerization at nickel, J. Am. Chem. Soc. 136 (2014) 12385–12395. .

[332] D. Schilter, M. J. Nilges, M. Chakrabarti, P. A. Lindahl, T. B. Rauchfuss, M. Stein, Mixed-valence nickel–iron dithiolate models of the [NiFe]-hydrogenase active site, Inorg. Chem. 51 (2012) 2338–2348. .

[333] A. Krapp, G. Frenking, Chemical bonding in "early–late" transition metal complexes $[(H_2N)_3M\cdots M'(CO)_4]$ (M=Ti, Zr, Hf; M′= Co, Rh, Ir), Theor. Chem. Acc. 127 (2010) 141–148. .

[334] M. P. Blake, N. Kaltsoyannis, P. Mountford, Heterobimetallic complexes containing Ca-Fe or Yb-Fe bonds: Synthesis and molecular and electronic structures of $[M\{CpFe(CO)_2\}_2(THF)_3]_2$ (M = Ca or Yb), J. Am. Chem. Soc. 133 (2011) 15358–15361. .

[335] C. Werlé, M. Hamdaoui, C. Bailly, X.-F. Le Goff, L. Brelot, J.-P. Djukic, Electron-deficient η_1-indenyl,η_3-allylpalladium(ii) complexes stabilized by fluxional non-covalent interactions, J. Am. Chem. Soc. 135 (2013) 1715–1718. .

[336] C. Werlé, C. Bailly, L. Karmazin-Brelot, X.-F. Le Goff, M. Pfeffer, J.-P. Djukic, First stabilization of 14-electron rhodium(i) complexes by hemichelation, Angew. Chem. Int. Ed. Engl. 53 (2014) 9827–9831. .

[337] C. Werle, D. M. Anstine, L. Karmazin, C. Bailly, L. Ricard, J.-P. Djukic, New pd(ii) hemichelates devoid of incipient bridging CO···Pd interactions, Dalton Trans. 45 (2016) 607–617. .

[338] B. L. Blass, R. Hernández Sánchez, V. A. Decker, M. J. Robinson, N. A. Piro, W. S. Kassel, P. L. Diaconescu, C. Nataro, Structural, computational, and spectroscopic investigation of $[Pd(\kappa_3-1'_1-bis(di-tert-butylphosphino)ferrocenediyl)X]^+$ (X = Cl, Br, I) compounds, Organometallics 35 (2016) 462–470. .

[339] L. J. Farrugia, C. Evans, Metal-metal bonding in bridged ligand systems: experimental and theoretical charge densities in $Co_3(\mu_3-CX)(CO)_9$ (X = H, Cl), C. R. Chim. 8 (2005) 1566 – 1583. .

[340] L. J. Farrugia, P. Macchi, Bond orders in metal–metal interactions through electron density analysis, in: D. Stalke (Ed.), Electron Density and Chemical Bonding I: Experimental Charge Density Studies, Springer Berlin Heidelberg, Berlin, Heidelberg, 2012, pp. 127–158. .

[341] D. Chopra, Advances in understanding of chemical bonding: Inputs from experimental and theoretical charge density analysis, J. Phys. Chem. A 116 (2012) 9791–9801. .

[342] J. Andrés, S. Berski, M. Feliz, R. Llusar, F. Sensato, B. Silvi, The nature of chemical bonds in di and polynuclear metal cluster complexes as depicted by the analysis of the electron localization function, C. R. Chim. 8 (2005) 1400–1212. .

[343] E. Matito, M. Solà, The role of electronic delocalization in transition metal complexes from the electron localization function and the quantum theory of atoms in molecules viewpoints, Coord. Chem. Rev. 253 (2009) 647 – 665. .

[344] A. D. Becke, Density-functional thermochemistry. iii. the role of exact exchange, J. Chem. Phys. 98 (1993) 5648–5652. .

[345] C. Lee, Y. Yang, R. G. Parr, Development of the colle-salvetti correlation-energy formula into a functional of the electron density, Phys. Rev. B37 (1988) 785. .

[346] J. P. Perdew, Y. Wang, Accurate and simple analytic representation of the electron-gas correlation energy, Phys. Rev. B 45 (1992) 13244–

13249. .
[347] S. Berski, G. L. Gutsev, M. D. Mochena, J. Andrés, Toward understanding the electron density distribution in magnetic clusters: Insight from the ELF and AIM analyses of ground-state Fe_4, J. Phys. Chem. A 108 (2004) 6025–6031. .
[348] H. Lavanant, C. Fressigné, C. Simonnet-Jégat, R. Dessapt, A. Mallard, F. Sćheresse, N. Sellier, Mass spectral and theoretical characterisation of non-symmetric Mo(V) dithiolene complexes, Int. J. Mass Spectr. 243 (2005) 205 – 214. .
[349] L. J. Farrugia, C. Evans, H. M. Senn, M. M. Hänninen, R. Sillanpää, QTAIM view of metal-metal bonding in di- and trinuclear disulfido carbonyl clusters, Organometallics 31 (2012) 2559–2570. .
[350] L. J. Farrugia, H. M. Senn, Metal-metal and metal-ligand bonding at a QTAIM catastrophe: A combined experimental and theoretical charge density study on the alkylidyne cluster $Fe_3(\mu{-}H)(\mu{-}COMe)(CO)_{10}$, J. Phys. Chem. A 114 (2010) 13418–13433. .
[351] B. K. Rao, P. Jena, S. Burkart, G. Ganteför, G. Seifert, AlH_3 and Al_2H_6: Magic clusters with unmagical properties, Phys. Rev. Lett. 86 (2001) 692–695. .
[352] J. F. Van der Maelen, J. A. Cabeza, A topological analysis of the bonding in $[M_2(CO)_{10}]$ and $[M_3(\mu{-}H)_3(CO)_{12}]$ complexes (M = Mn, Tc, Re), Theor. Chem. Acc. 135 (2016) 64. .
[353] J. S. Jones, B. Pan, F. P. Gabbaï, Group 15 metal-metal bonds, in: S. T. Liddle (Ed.), Molecular Metal-Metal Bonds, Wiley-VCH Verlag GmbH & Co. KGaA, 2015, pp. 519–558.
.